Funded by
the European Union

SEVENTH FRAMEWORK PROGRAMME

IAQSense
Air Quality in Closed Environments

IAQSense

Work package 2 – Final report

Date	**27/10/1016**
Project	**IAQSense – FP7 - 604325**
Starting date and duration	**01/09/2013 – 36 months**
Author, company	**Mathias Holz, nano analytik GmbH**

Objectives – The Goals of nanoanalytik GmbH

The duty of nano analytik GmbH was the development of three technologies from TRL4 to TRL6 with actions to design the manufacturing processes.
The development process was focused on the manufacturing technology of the sensors and test structures for technology verification. It required development of manufacturing sub-processes of: spectrometer-FET-transistor, tip-FET-transistor and piezo-resistive cantilever beam functionalized with nanotubes. Subsequently these sub-processes have been integrated into technological blocks for final product manufacturing. Cantilever and Spectrometer on chip sensors were delivered to the partners concerned in characterization process concurrently with characterization platforms issued from WP3.

The key specifications of the sensors

• sensitivity <100ppb for the spectrometer and selectivity between the molecules of the reference set;
• sensitivity to 1ppb with a set of 4 functionalization layers for the transistor on tip,
• sensitivity to ppt with a set of 2 functionalization layers for the cantilever with nanorods;
• 70eV ionizer with controlled plasma sample reaching the sensing layer;

Design of building blocks (Design for Manufacturing oriented)

Sensor blocks were designed according to functional specifications (T1.1.), considering the functionality, performances, life time expectancy by combining sensing elements (FETsensing, cantilever, porous metal gate, self-aligned nanorods, nanoparticles or nanotubes) and pre-conditioning blocks (ionizer, hot plate).
During the development process all definition of the sensor, production and testing procedures were established**,** all dimensioning parameters identified and distribution defined. In particular, the definition of the sensor geometry and sensor interface.
Testing and characterization equipment for MOSFET Spectrometer was realized and delivered by FACET, in line with the sensor design and sensor geometry. Sensors were developed and produced by NANO in cooperation with Efficience Marketing and FACET.
The functionalization technology for active cantilevers with piezo-resistive readout was developed in close cooperation with ISL.

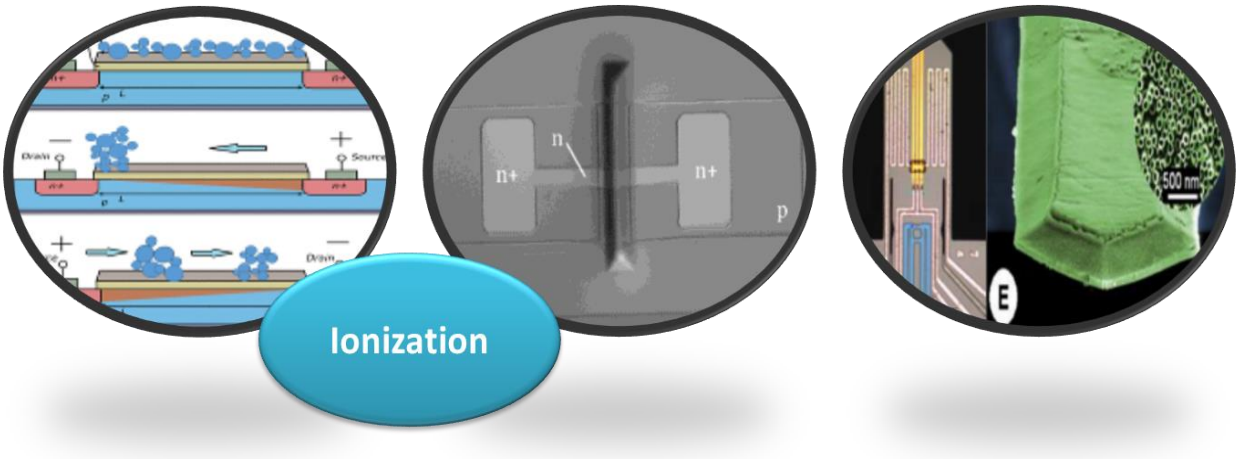

Figure 1 The 3 groundbreaking sensor concepts of IAQSense.

In the following section, the three sensor types (figure 1), and their critical parameters, dimensions, manufacturing process flow and design are explained.

Technology-Type 1: Integrated Mobility Spectrometer

MOSFET with porous gate sensor system is based on mobility, dynamics of ions and operates as spectrometer on chip. The spectrometer sensor has high technological 3D-manufacturing steps and highest complexity within the project.

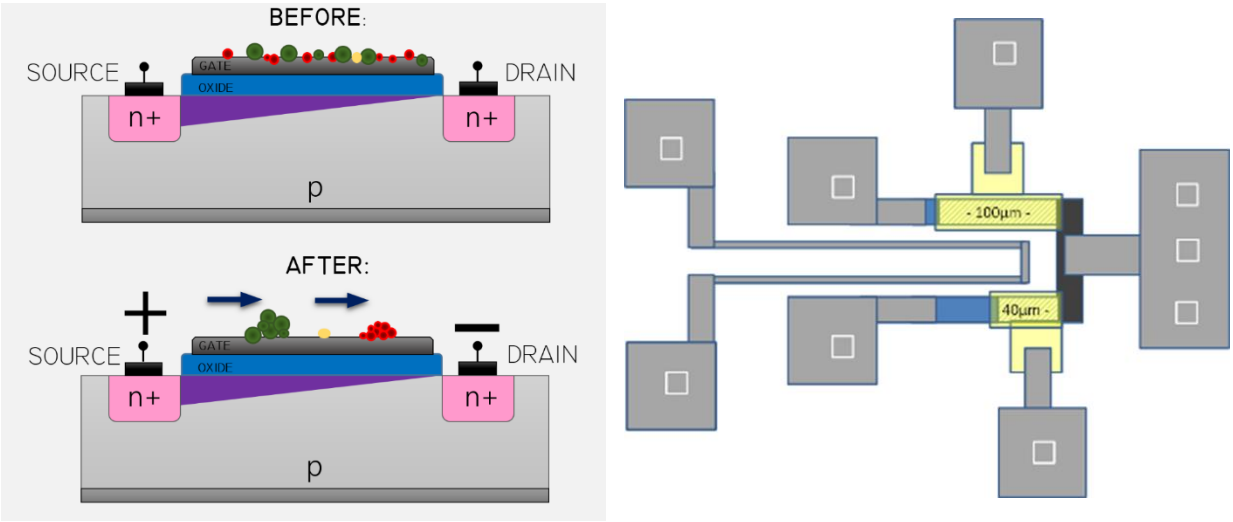

Figure 2 2D model of the MOSFET spectrometer sensor.

A 2D model of the senor including the various components and illustrating the principle of operation of the sensor technology is given in figure 2. The sensing transistor is symmetrical, it means that drain and source are identical and perfectly exchangeable. This property is used to dynamically change the drain/source polarity at high frequency (up to 100 kHz). Ionized molecules adsorbed on the surface of the porous gate are then moved in one direction, accumulating near one electrode and then moved in other direction at different velocities depending on their surface mobility. The surface velocity is 2 order of magnitudes than the speed of vertical adsorption from the ambient environment which is not accelerated by any field. In total molecules of different types are creating dynamic signals (current through the channel) due to their different time of arrival (time of flight) at the sensitive point of the channel (situated near the source). The length of the channel (100µm) creates reasonable timings in the range of 100ms to 1s depending on the molecule. The electrical pattern coming from the sensing transistor contains signatures of different molecules which have been adsorbed on the surface on the gate. The molecules on the surface create an additional potential to the gate voltage which is trimmed to determine the detection threshold.

The example is given with N-channel MOSFET and Ions with three different colours. The porous gate allows the Ions to reach a collective layer of SnO_2. N-channel FET is modulated with alternate voltage applied between the leads of symmetric Source and Drain regions. In result the attached to the Gate Ions are concentrated to a certain section of the Gate, locally changing the conductivity of the channel bellow.

The initial design of the Integrated Mobility Spectrometer sensor is based on a standard CMOS technology and 3D-µ-integration of 5 MEMS ingredients. The components are: (1)

ionizer-filament, (2) collective layer, (3) field-effect transistor, (4) heater, and (5) temperature sensor.

Development:

In the beginning of the project the technology was at TRL4 level with proven working principle and the set goal was to reach TRL6 at the end of the project.

The main objective of the first process step was amassing better knowledge of the technology's intrinsic capability starting as follows:

- to define the structure able to reach the performance (all technical partners);
- to proceed with device simulation (MICRO);
- to prepare variants for DOE plan including intrinsic parameters and environmental ones;

Initial assessment for the key parameters were the dimensions of (a) collection layer, (b) FET dimensions, (c) ionizer dimensions and accelerating electrode place, (d) the overall device cavity).

The relationship between target specifications and key parameter variation was planned to be analysed with the characterization platform prepared by FACET at the established specialized laboratory in Sofia - SOFIA LAB and ISL for analysis in a gas chamber.

First step of the development process was establishing the design of the transistor. To define the structure of the sensor, able to meet the requirements, 8 different configurations were approved and realized.

First layout was a transistor with narrow rectangular gate with dimensions 40μm length and 4μm width. The design of the mask is shown in figure 3.

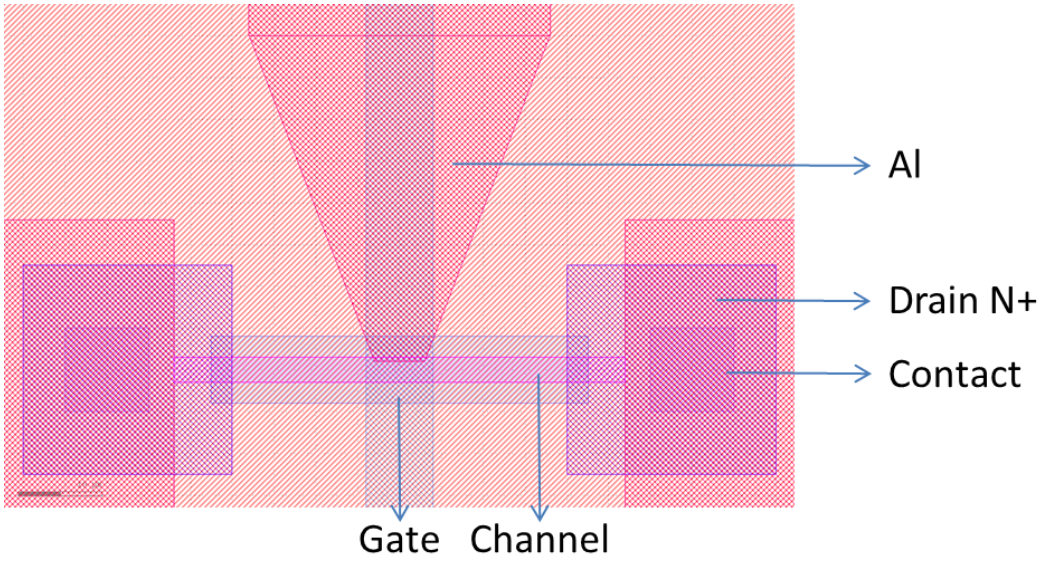

Figure 3 Batch 1 – layout 1, 100x10.

Second transistor designed with layout 1 was with gate dimensions 100μm length and 10μm width. The design of the mask is shown in figure 4. The gate length/width ratio for "layout 1" is chosen 10.

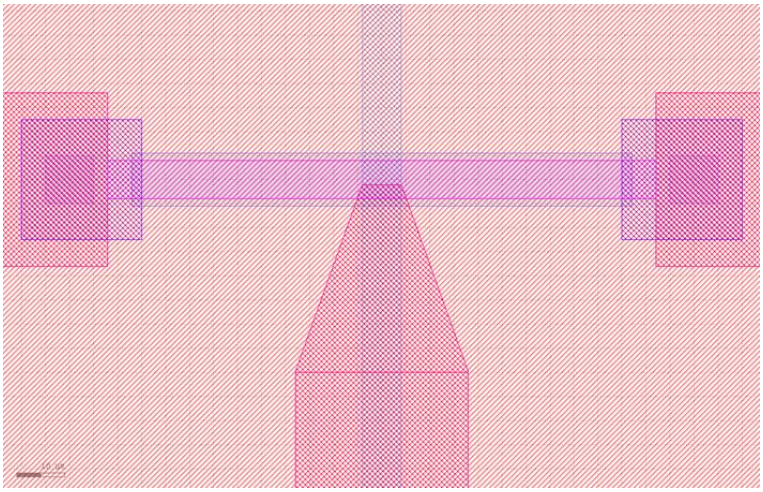

Figure 4 Batch 1 – layout 1, 40x4.

"Layout 2" is diamond shape gate with dimensions 40µm length and 4µm width (figure 5) and 100µm length and 10µm width (figure 6).

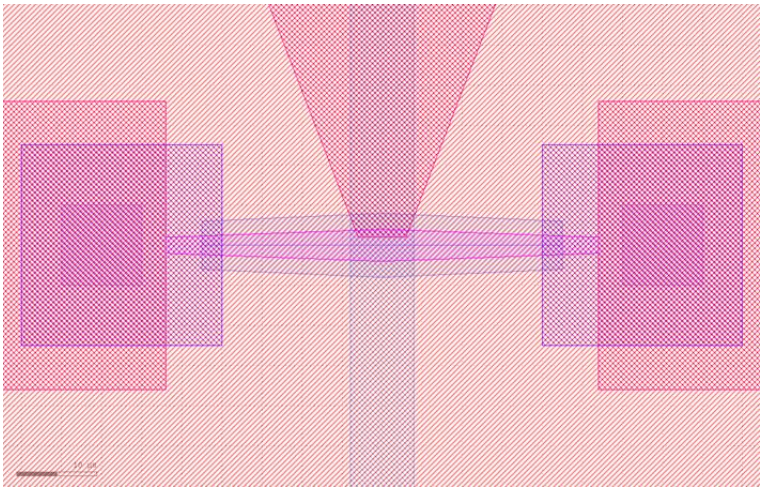

Figure 5 Batch 1 - layout 2, 40x4.

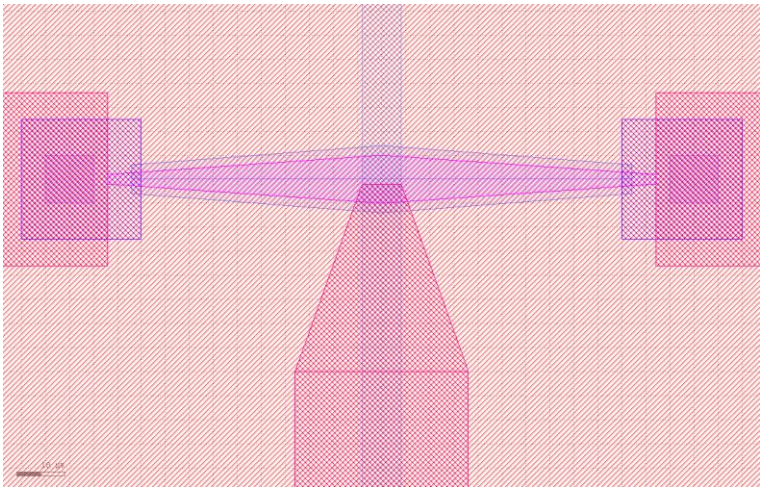

Figure 6 Batch1 - layout 2, 100x10.

"Layout 3" is designed with rectangular shape of the gate as for "Layout 1", but with different gate length/width ratio. The transistor with the small gate is with dimensions 40µm length and 10µm width (figure 7). The transistor with big gate is with dimensions 100µm length and 25µm width (figure 8). The ratio for this layout is 4.

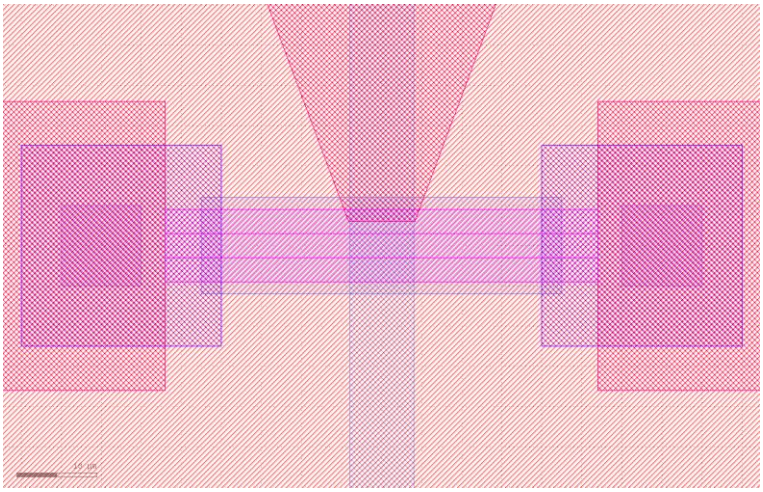

Figure 7 Batch 1 - layout 3, 40x10.

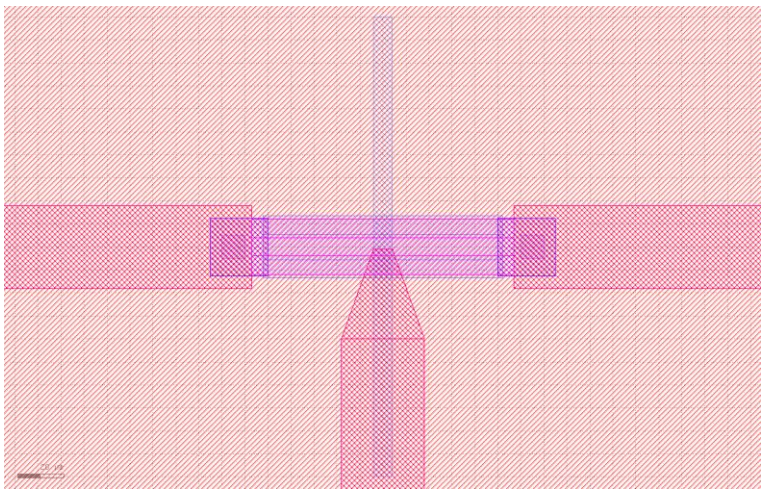

Figure 8 Batch 1 - layout 3, 100x25.

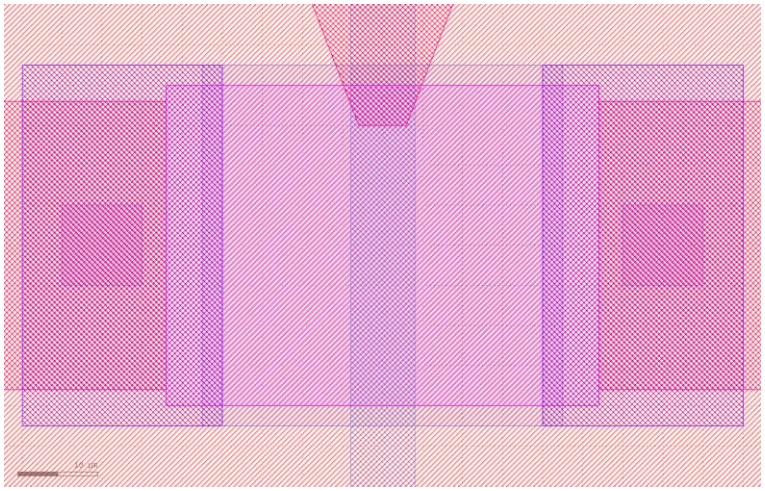

Figure 9 Batch 1 - layout 4, 40x40.

The last "Layout 4" is a design with square shape of the gate. For this layout, again we have 2 sizes of the channel, one small 40x40μm (figure 9), and one big 100x100μm (figure 10).

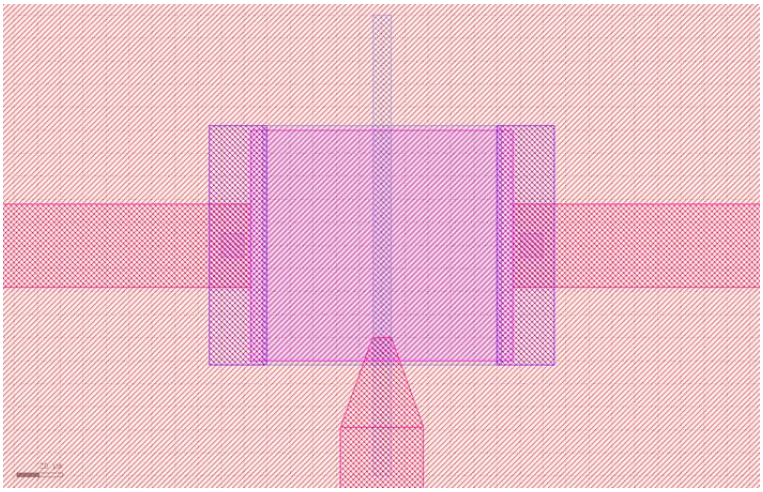

Figure 10 Batch 1 - layout 4, 100x100.

All mask designs had to be modified because of an issue that came out during the discussions of the layout. The "Al" line that connects the gate of the transistor with the bonding pad was overlapping the gate itself, which is a standard layout technique for all conventional transistors. Unlike the case with transistors with passivated gate, the gate layer of the spectrometer transistor is fabricated from porous material and overlapping the gate region with "Al" would cause interference with adsorption and dynamics on the porous layer. Aluminum layer would passivate the region of overlapping. For this reason, the layout design was modified as it is shown in figure 11.

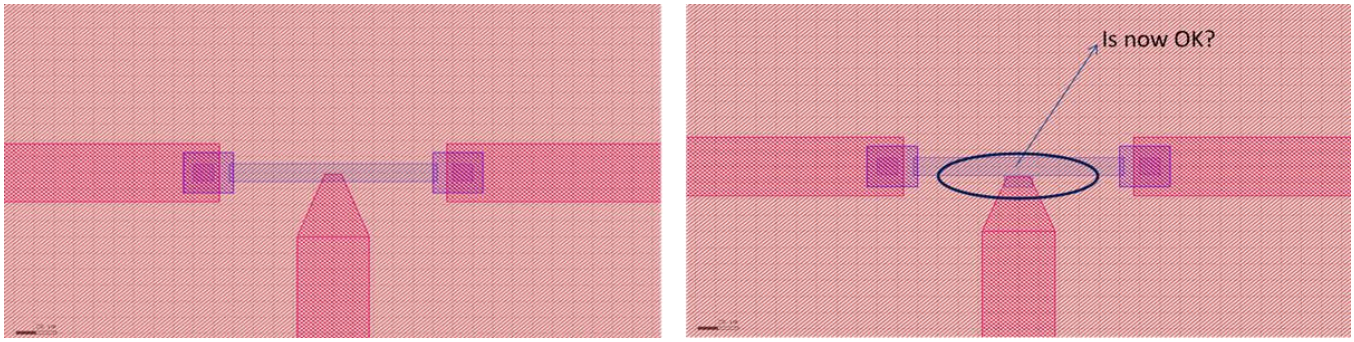

Figure 11 Batch 1 - layout modification.

The gate shape has additional sector on the side, where it is realized the aluminum-gate connection. This allows the connection of the gate layer to the aluminum bonding pad to be secured without influencing the adsorption properties of the porous gate.

Batch 1.

First batch of spectrometer transistors was started on 13/11/2013.

General block diagram of the chip:

The general block diagram of the sensor is illustrating the realization of ESD protection of the sensor, using diodes connected to the gate of the spectrometer.

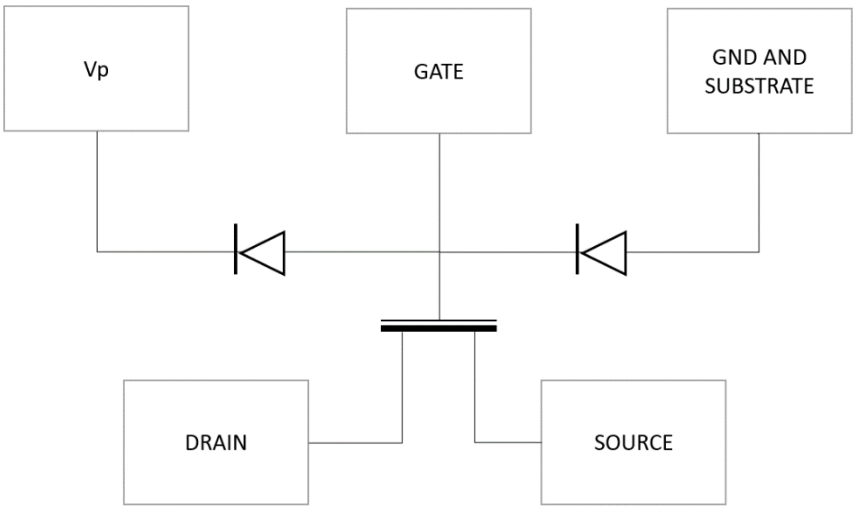

Figure 12 Batch 1 - Chip block diagram.

General description: Spectrometer on chip (naSe001A) designed for the purposes of the IAQSense project consist of two N-channel field-effect transistors with Tin oxide porous layer (SnO_2). They were delivered in TO12 package with build-in heater and temperature sensing diode. The design includes ESD protection.

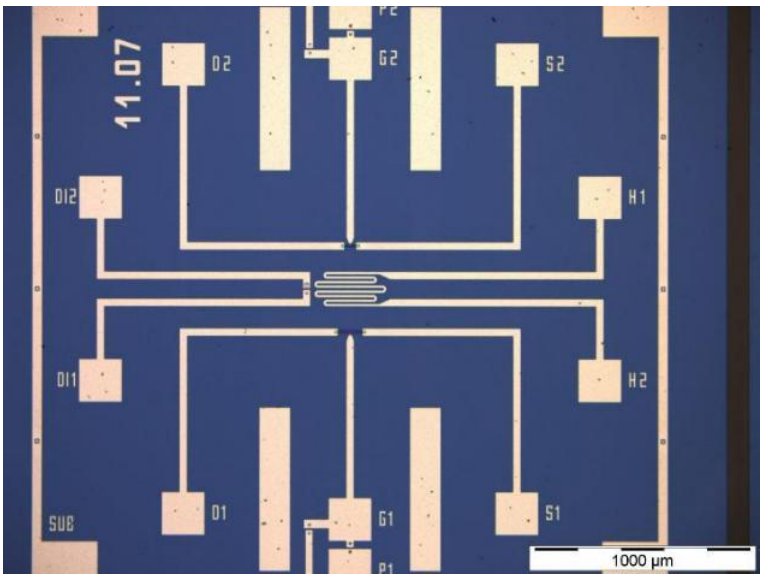

Figure 13 Batch 1 - Chip layout with ESD protection.

Chip layout is shown in figure 13. All chips have unique number which allows tracing each chip to specific coordinates on the wafer(figure14).

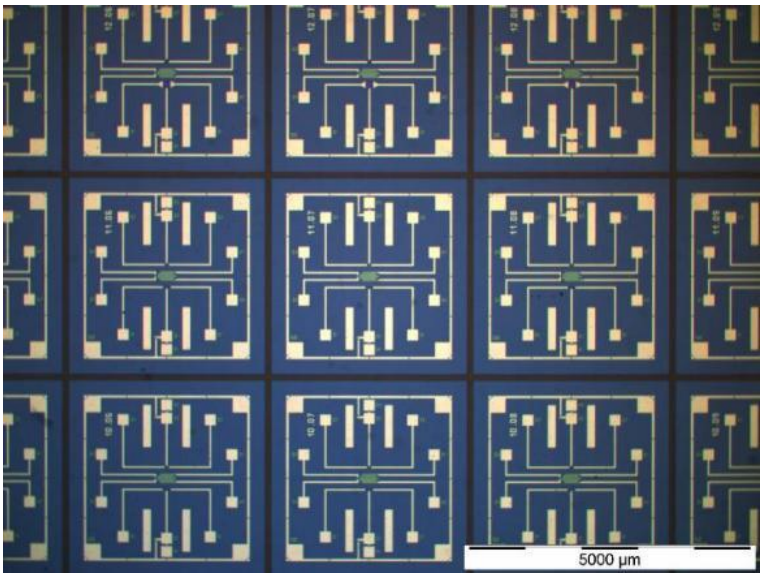

Figure 14 Batch 1 - Chip layout with addresses.

Device features:

- Chip dimensions 5x5 mm;
- Two MOSFETs on each chip with different channel dimensions;
  (1)T1: L=40µm, W=4µm T2: L=100µm, W=10µm (RECTANGULAR);
  (2)T1: L=40µm, W=4µm T2: L=100µm, W=10µm (DIMOND);
  (3)T1: L=40µm, W=10µm T2: L=100µm, W=25µm (RECTANGULAR);
  (4)T1: L=40µm, W=40µm T2: L=100µm, W=100µm (SQUARE);
- Interchangeability of transistor's drain and source connections;
- Two substitutable substrate (body) connections;
- Consist of resistive structure H1 for providing heating to the die during cleaning of the porous surface;
- Consist of TSENS1 – diode based temperature sensor for temperature measurement and control;

Housing:

Fabricated silicon chip is glued with insulating glue to the package and certain contact pads are wire – bonded to the corresponding leads of the TO 12-pin metal can package. Because of the developmental and measuring purposes the housing cover is not permanently attached to the package, and can be easily removed by removing thin strips of paper-adhesive tape. Because of the wire-bonding needs and to ease shipping, leads were bent to become flat (parallel) relative to the package.

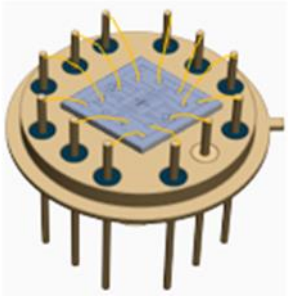

Figure 15 TO12 package.

PIN	DESCRIPTION	SIGNAL TYPE	SIMPLIFIED OUTLINE	REALIZATION
1	G2 – T2 (40 µm) gate	AI*	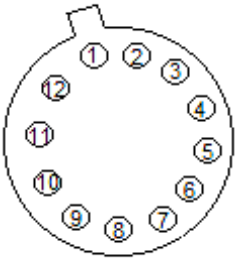	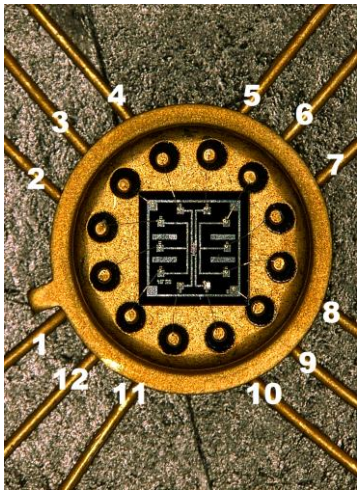
2	S2 – T2 (40 µm) source	AIO*		
3	SUB- substrate connection			
4	H1 - heater contacts	AI		
5	H2- heater contacts	AI		
6	S1 – T1 (100 µm) source	AIO		
7	G1 – T1 (100 µm) gate	AI		
8	D1 – T1 (100 µm) drain	AIO		
9	SUB- substrate connection			
10	DI1- temperature measurement diode-anode	AIO		
11	DI2- temperature measurement diode-cathode	AIO		
12	D2 – T2 (40 µm) drain	AIO		

AI- analog input, AIO*- analog input/output*

After gluing the chip in the TO12 package and bonding the connection pins to the die pads, each sample was covered with protection metal cap and additionally placed in a plastic box for storage. In this way samples were ready for shipment to the project partners.

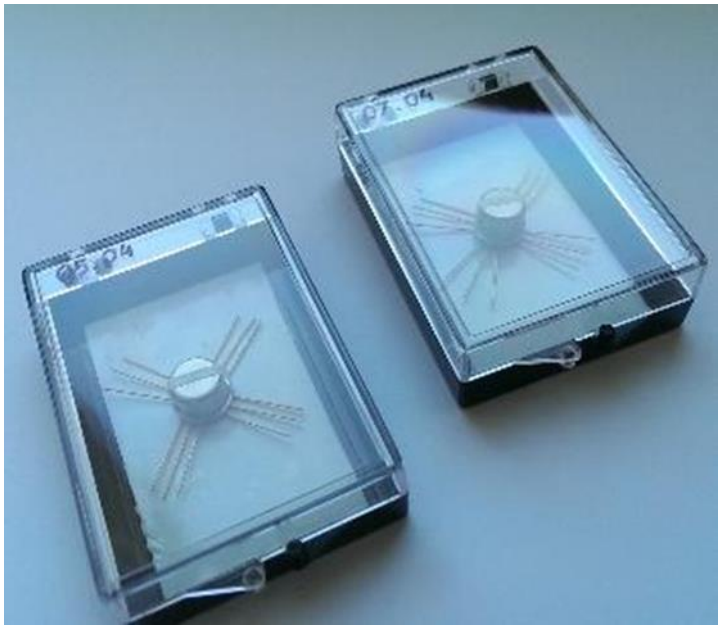

Figure 16 Spectrometer sensors, bonded in TO12 packages.

In figure 15 are shown all 8 designs of MOSFET spectrometer on chip manufactured in the first production run. After production of Batch 1 finished in month 10, NANO started inspection of the sensors using digital microscope, scanning electron microscope(SEM) and electrical characterisation of the chips.

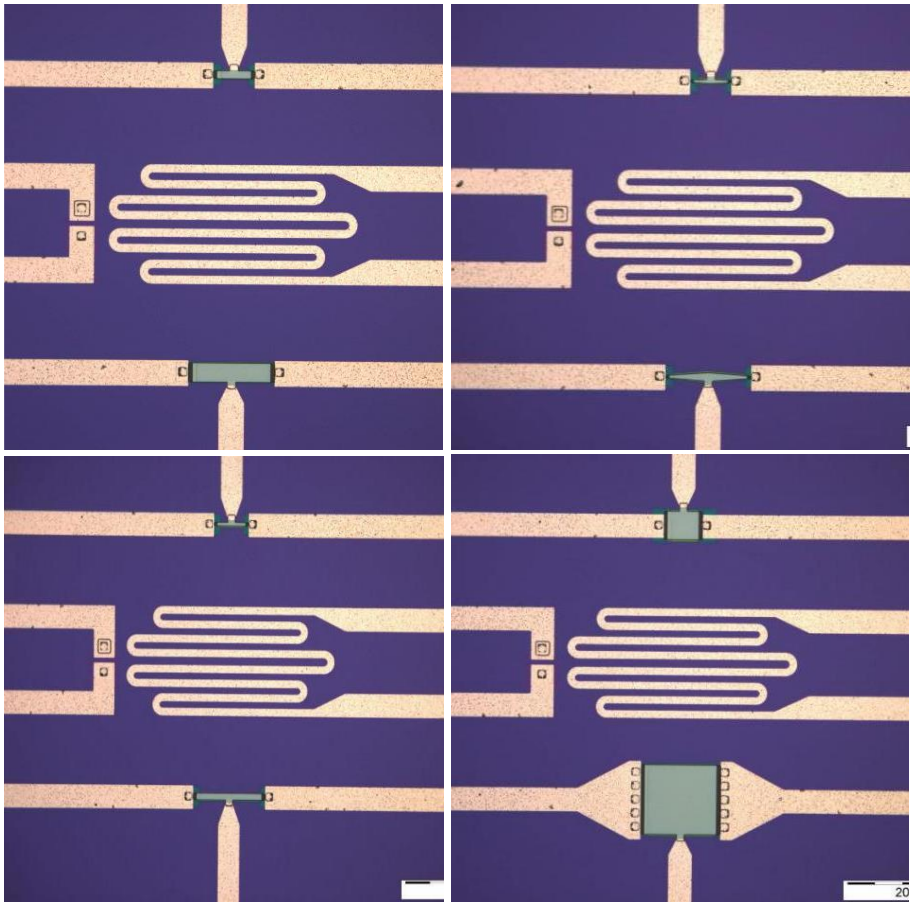

Figure 17 Batch 1 - all 8 designs realized on 4" wafer.

Batch 1 – Analysis.

SEM-control

First measurements made after manufacturing the samples was the inspection with scanning electron microscope. These measurements showed the lateral structure of the SnO_2 material deposited as a gate layer.

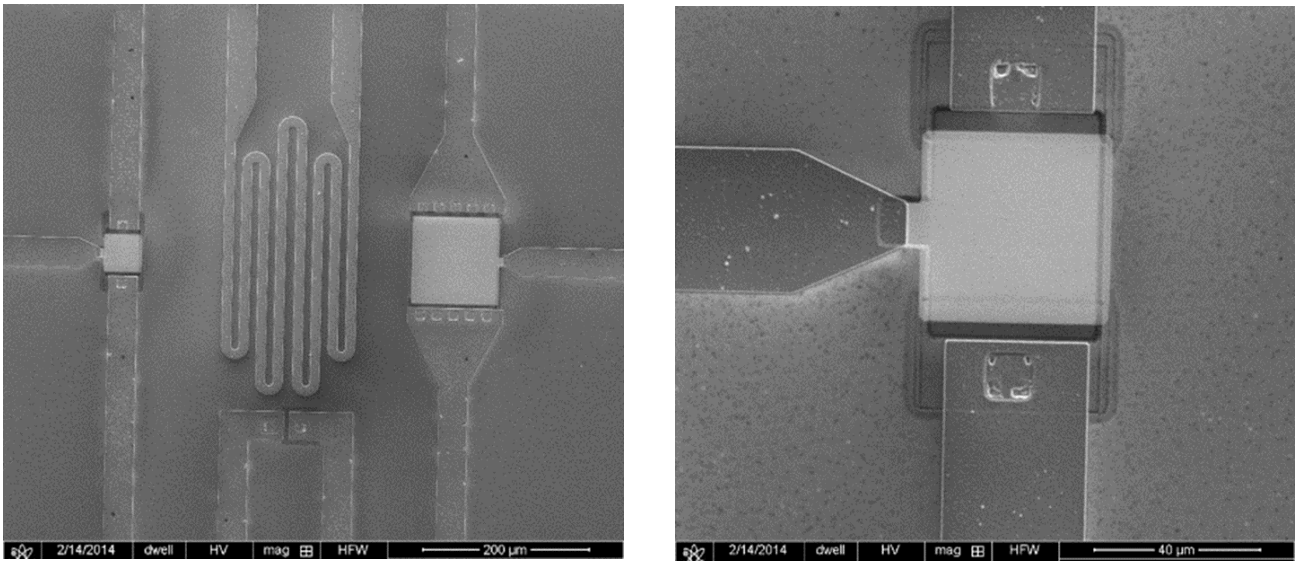

Figure 18 SEM images of MOSFET spectrometer T1:40x40, T2:100x100.

Development of SnO_2 Gate technology.

Unforeseen the deposition of proper Tin oxide layer was a big challenge.

- Too high porosity;
- Too high granulation during deposition;
- Presence of micro cracks leads to impaired conductivity.

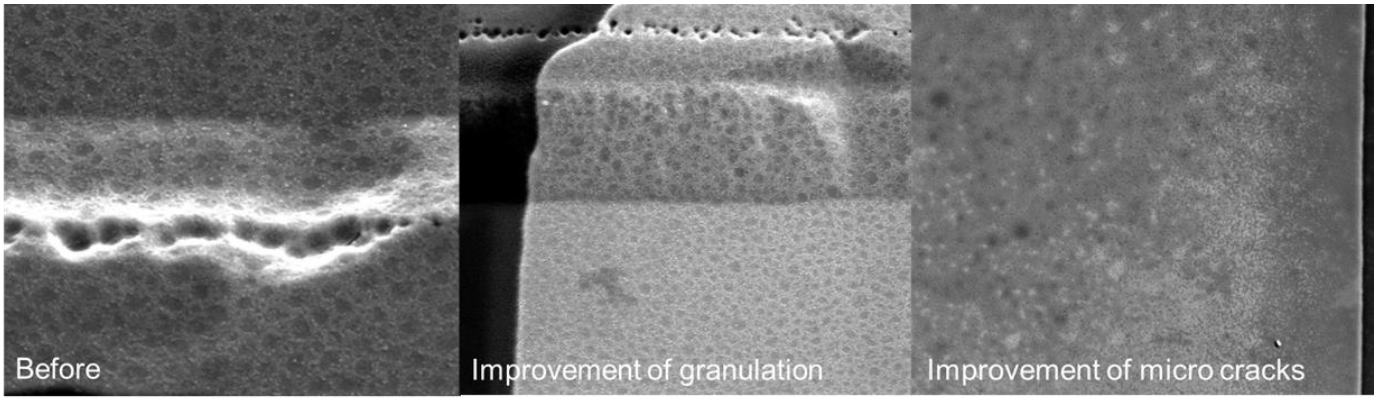

Figure 19 SEM images of the Tin oxide layer.

The key to best sensor performance is the quality of the collective layer of the sensor. A few test runs were performed to establish the proper parameters for SnO_2 deposition. In figure 18 are presented 3 SEM images of the Tin oxide layer. In the early runs, granulation and micro cracks are observed. These issues were solved and the technology of deposition was improved.

After performing of the first electrical characterisation measurements, a problem with the ESD-protection circuit was figured out. Design failure caused short-cut in the pull-up/down diodes.

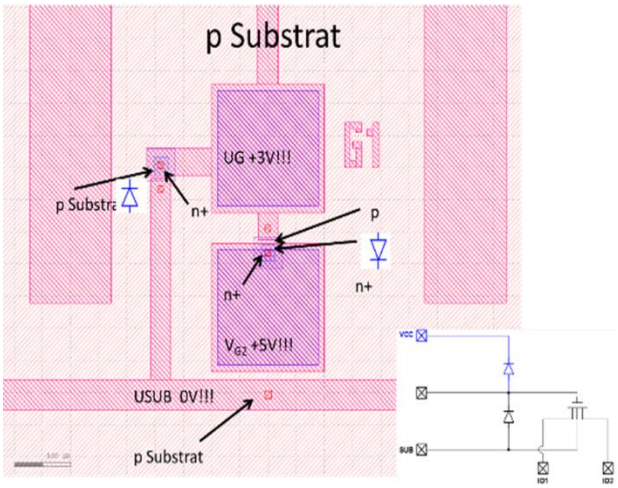

Figure 20 Batch 1 - ESD layout.

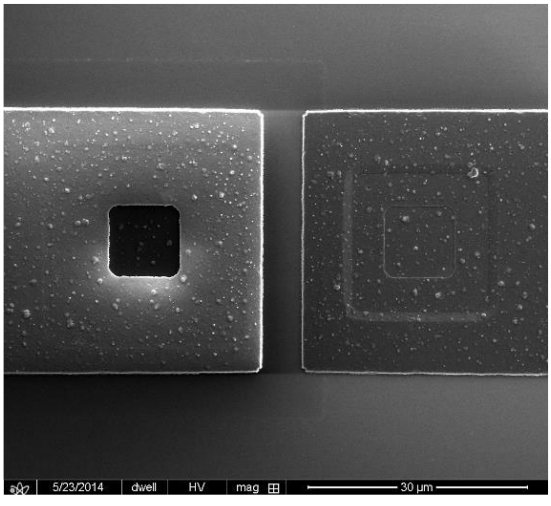

Figure 21 SEM image of the ESD diode.

After SEM investigation, it was reviled that problem in the design of the mask causes short-circuit. Immediately NANO started redesign of the chip corresponding to the second redesign phase for lunching second batch of sensors which was approved by the project partners.

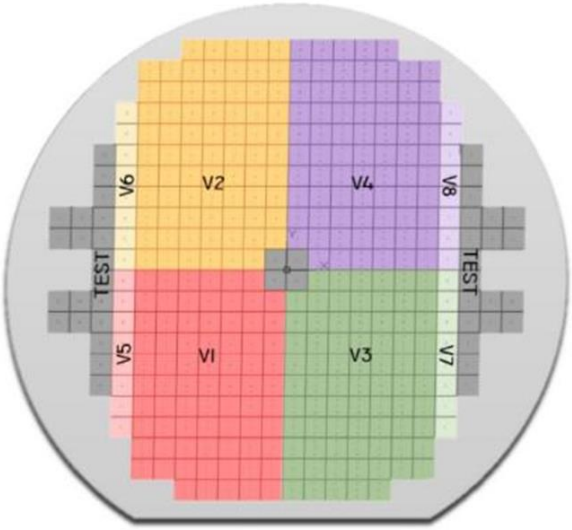

Figure 22 Batch 1 - wafer map.

In parallel to these steps, as a backup plan, sensors from the peripheral dies were used for further characterisation experiments.

In general, single wafer consists of 372 chips, of which 44 are test devices, 32 are the chips without ESD protection (4 groups of 8 pieces), and 296 main devices (also divided into 4 groups of 74).

Test chips are located on the sides and in the center of wafer to enable topographical comparison of parameters across the wafer. MOSFET sensor from the peripheral regions of the wafers V5, V6, V7 and V8 were usable for further experiment. In figure 22 is shown the wafer map of the different chips position.

Electrical characterisation of the sensor devices.

The main tool used for electrical characterisation of the spectrometer sensors was dual channel system source meter *Keithley 2602A* (Figure 23).

Figure 23 Dual Channel System Source Meter Keithley 2602A

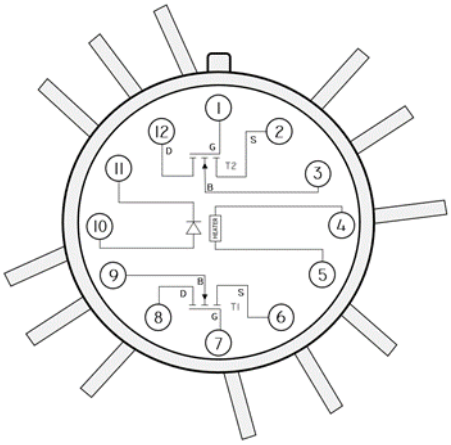

Figure 24 Sample pinout with electrical schematics of structures within

In figure 24 is illustrated the pinout diagram of all structures inside the package of the sample. In every packed it is possible to be bonded just one die. Therefore, every sample consist of 2 transistors with different designs, a diode for temperature measurement

and control and “Al” heater for cleaning the sensor from any molecules and Ions of different substances attached to the sensing layer of the transistors.

In figure 25 is described the equivalent setup for measuring MOSFET output and transfer characteristics.

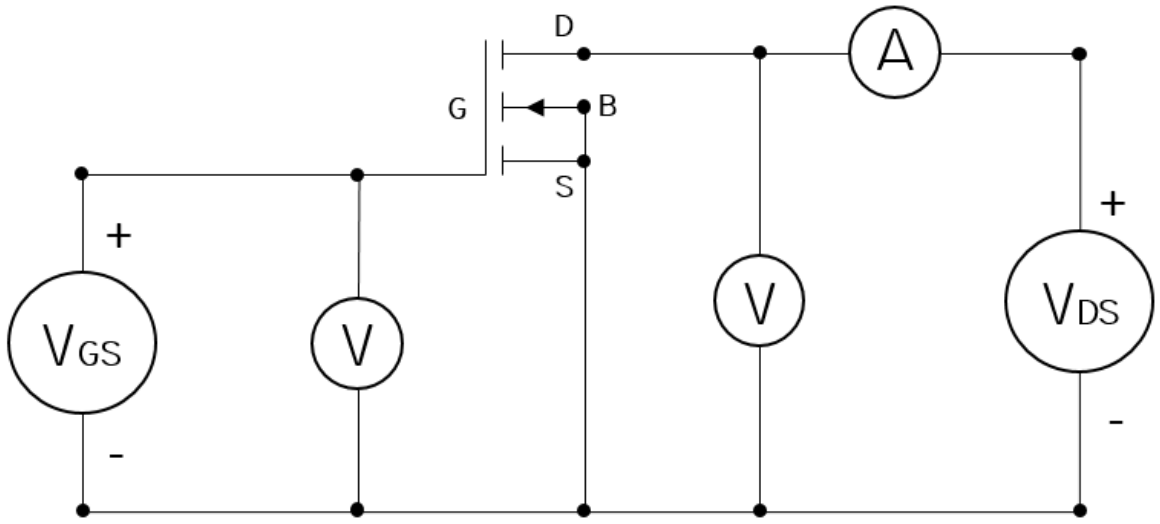

Figure 25 MOSFET output and transfer characteristics equivalent measurement setup.

Batch 1 - MOSFET spectrometer output characteristics.

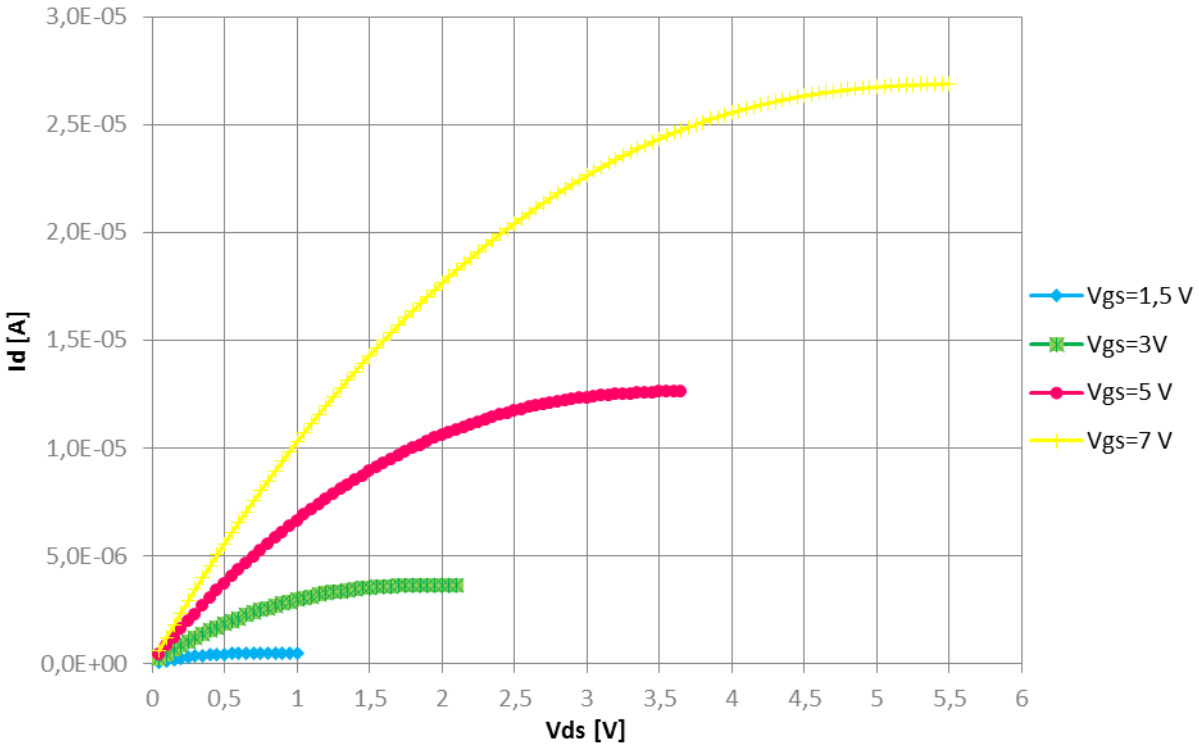

Figure 26 Output characteristics – Chip 05.04 T1(100 µm).

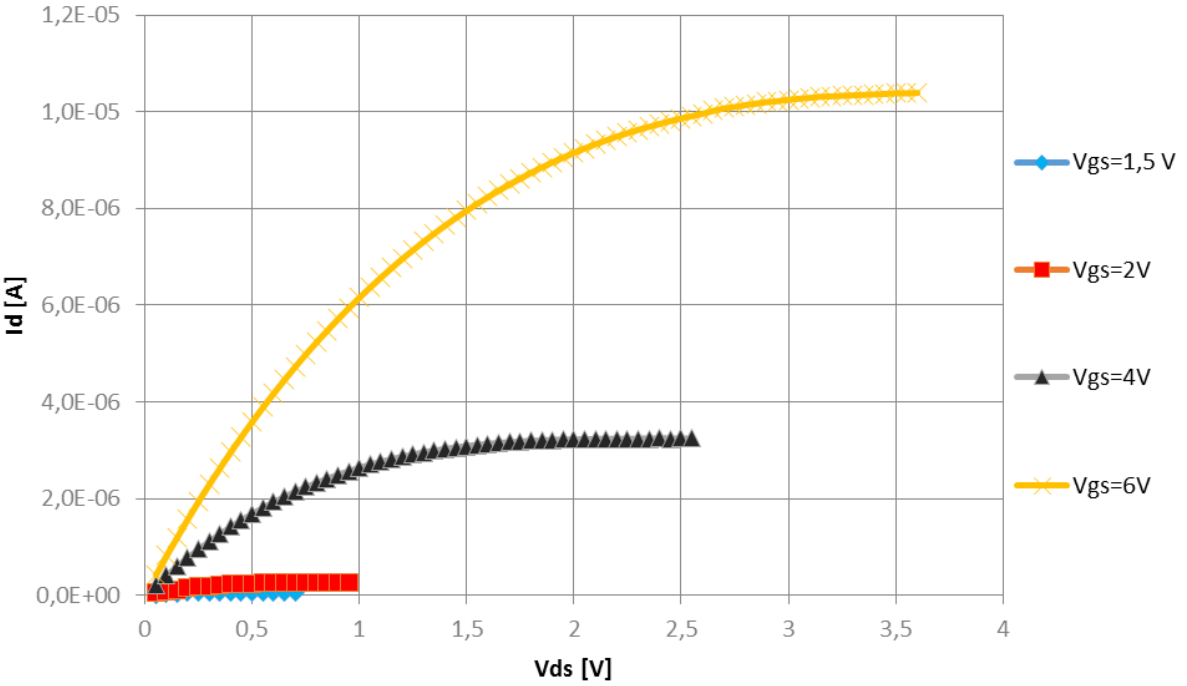

Figure 27 Output characteristics – Chip 05.04 T2(40 µm).

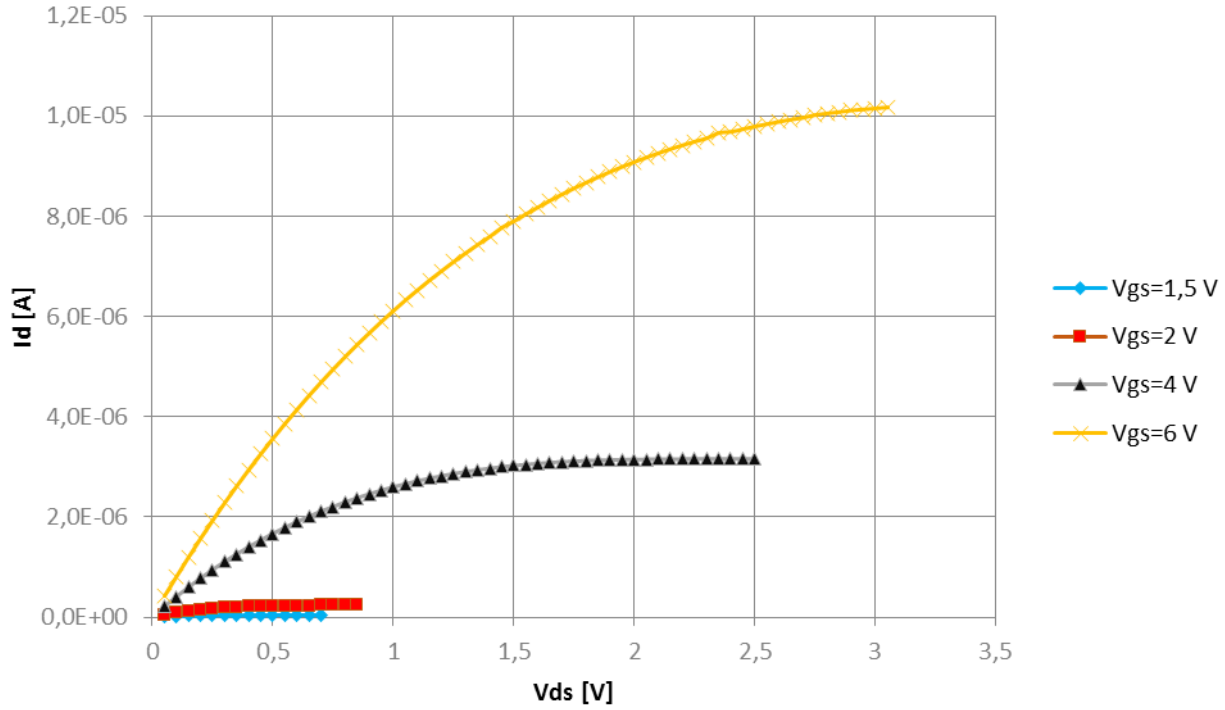

Figure 28 Output characteristics – Chip 07.04 T2(40 µm).

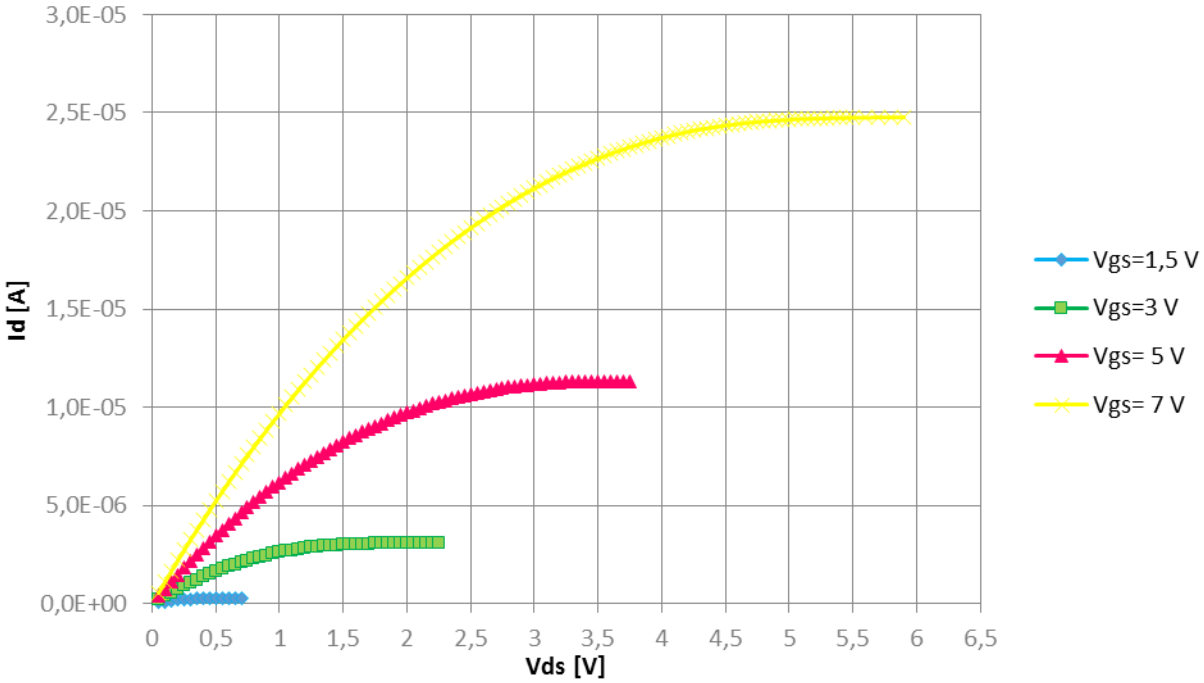

Figure 29 Output characteristics – Chip 07.04 T1(100 µm).

Batch 1 - MOSFET spectrometer transfer characteristics.

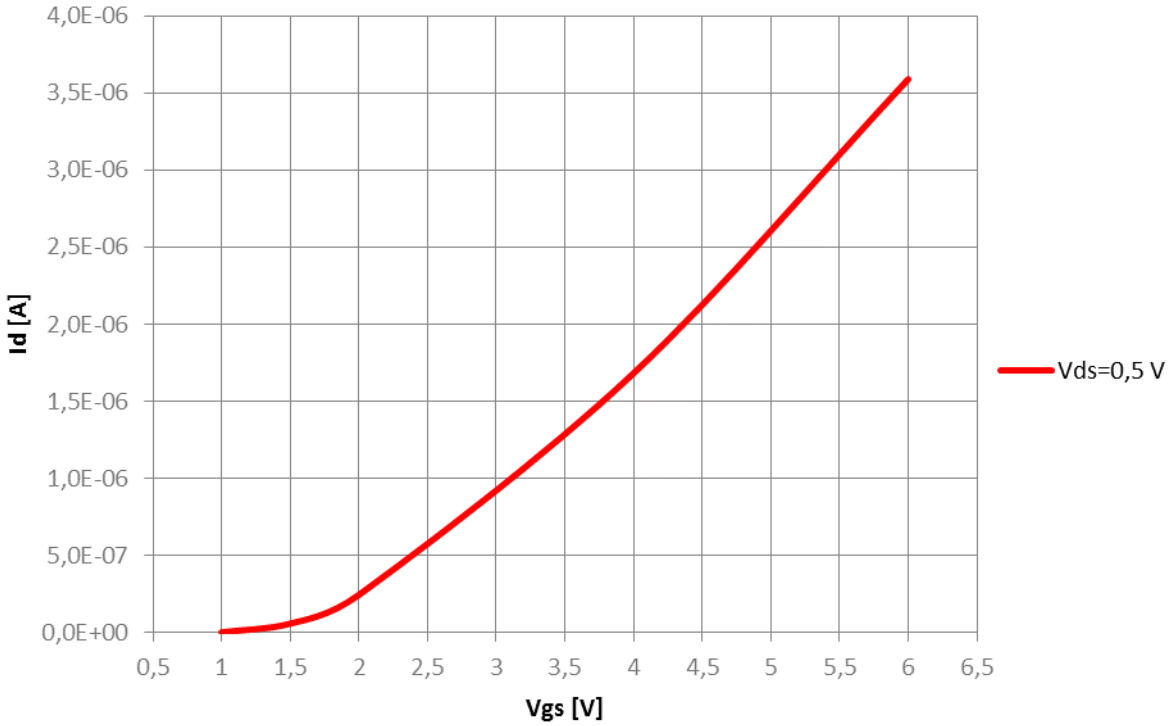

Figure 30 Transfer characteristics – Chip 05.04 T2(40 µm).

The transfer characteristic relates MOSFET drain current (Id) response to the gate-source voltage (Vgs). Since the gate terminal is electrically isolated from the remaining terminals (drain, source and bulk), the gate current is essentially zero, so that gate current is not part of the device characteristics. The transfer characteristic curve can locate the gate voltage at which the transistor passes current and leaves the OFF-state. This is the device threshold voltage (Vth). As it is visible from graphs shown in figures

30,31,32 and 33, the threshold voltage varies for the different transistors between 0,5V (Chip 05.04 T1) up to 1,3V (Chip 07.04 T1).

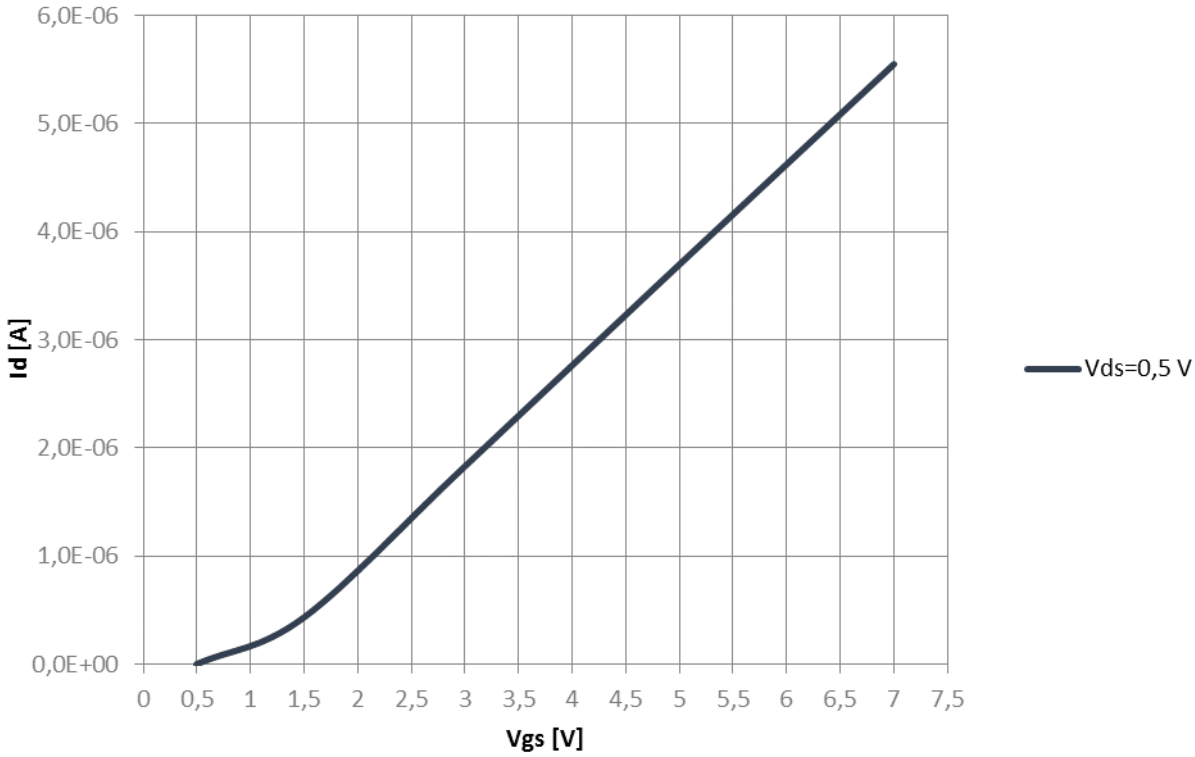

Figure 31 Transfer characteristics – Chip 05.04 T1(100 µm).

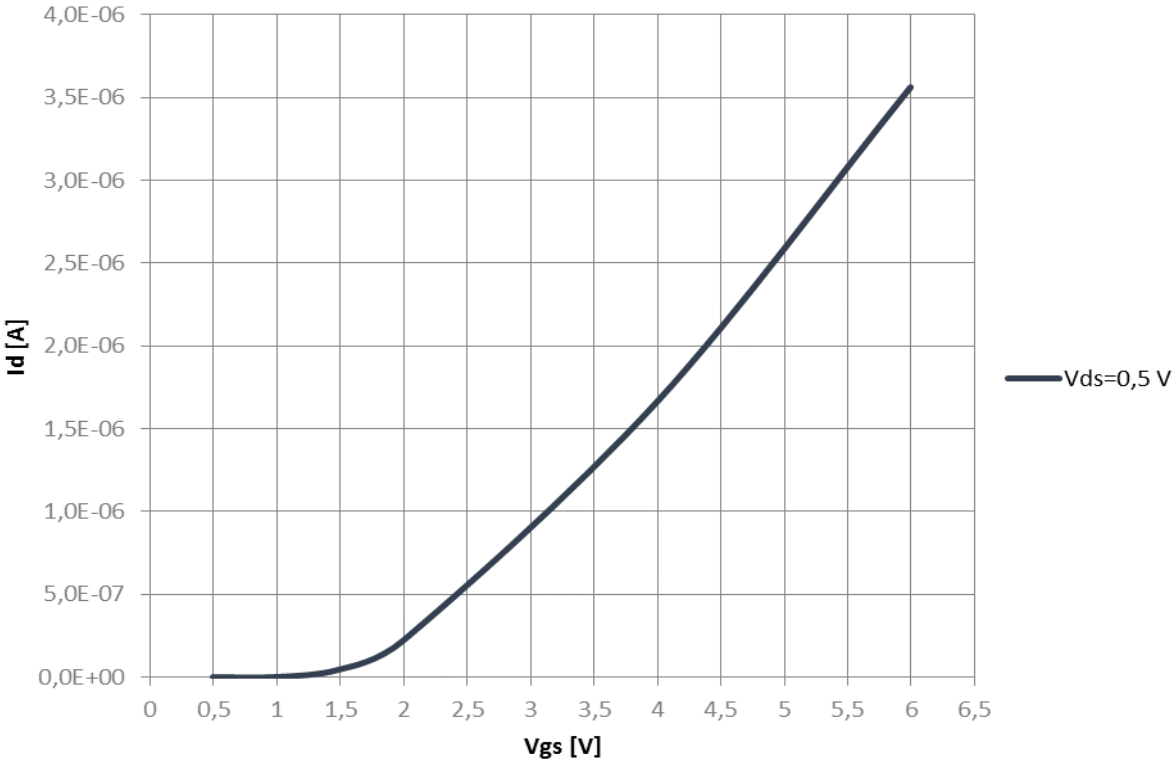

Figure 32 Transfer characteristics – Chip 07.04 T1(100 µm).

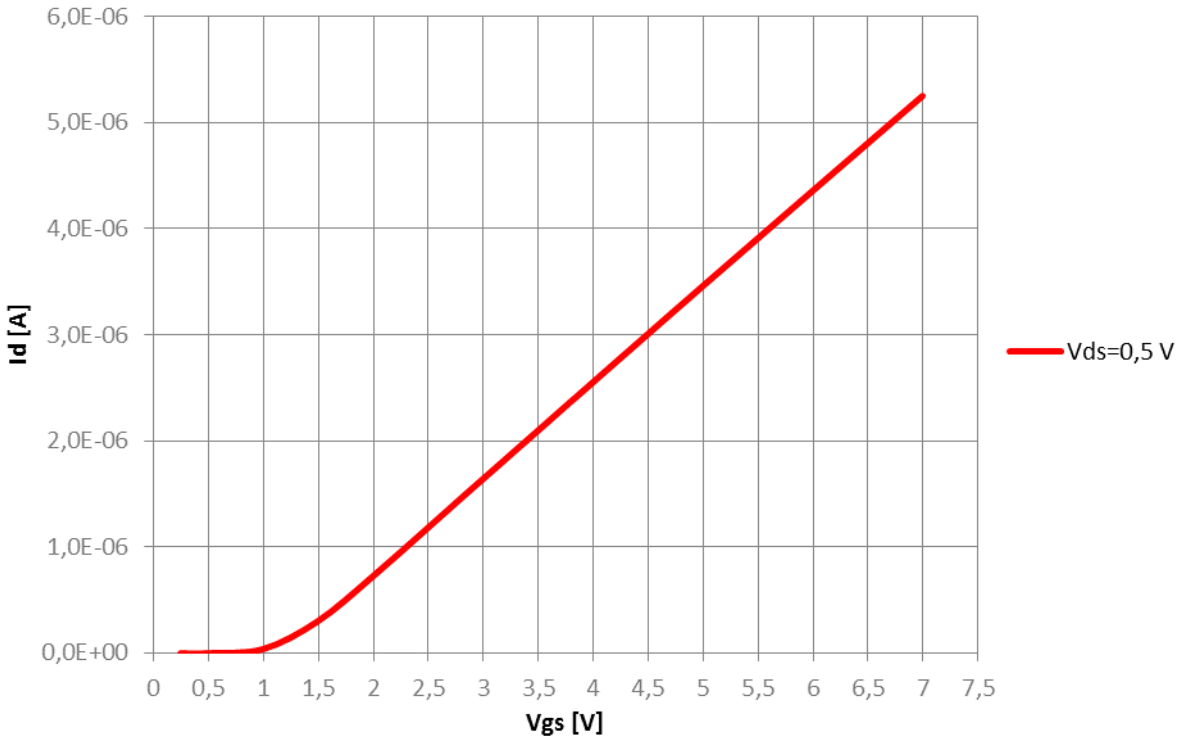

Figure 33 Transfer characteristics – Chip 07.04 T2(40 µm).

Batch 1 - MOSFET spectrometer breakdown voltage.

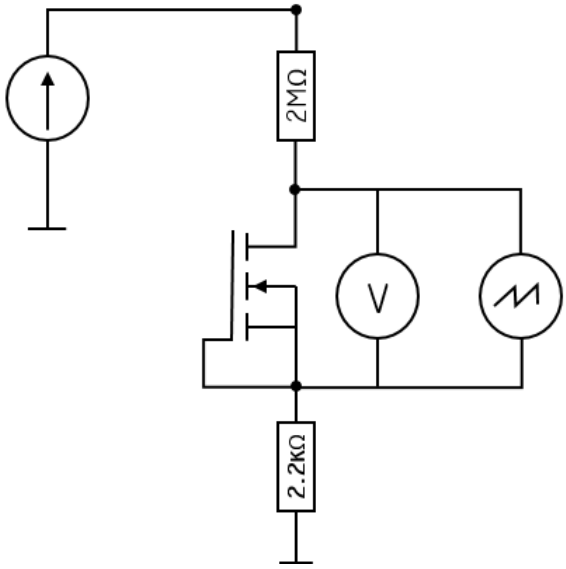

Figure 34 Test setup for MOSFET breakdown voltage measurements.

In figure 34 is presented the test circuit for measuring of the breakdown voltage for MOSFET spectrometer on chip sensors. This setup includes current source realized with *Agilent Technologies E3648A* DC Power Supply, a few passive components, *Agilent Technologies DSO1024A* oscilloscope and digital multimeter *FLUKE 179.*

The measurement of allowable breakdown voltage was performed in a way allowing to saturate transistor with maximal values without destroying it. Ramp signal of varied amplitude and known frequency is applied between source and drain, while keeping transistor closed (no gate voltage applied). The voltage at which signal ramp stops rising is the transistor's breakdown value. Because of using a circuit with a large serial resistor connected to the drain terminal of the transistor, no damage to the sample is done.

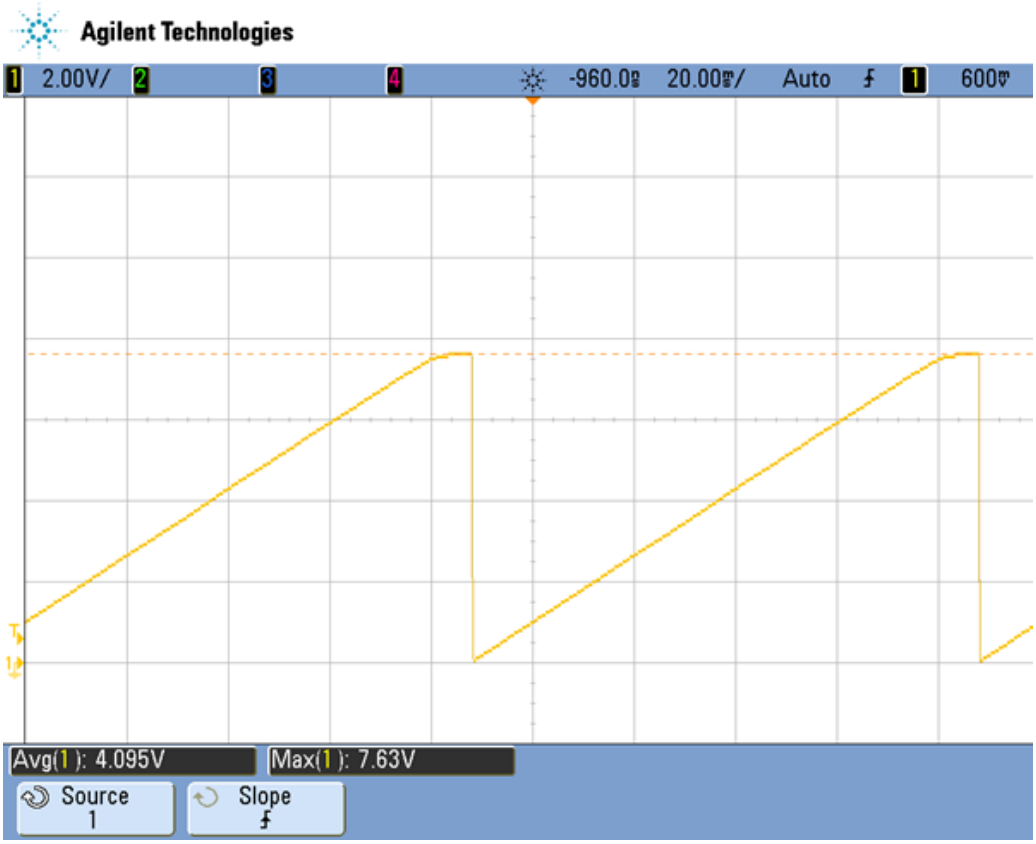

Figure 35 Batch 1 - Breakdown voltage measurement result.

As it is visible from the oscillogram in figure 35, the breakdown voltage for the measured sample from Batch 1 is about 7.7V, which is showing a critical problem in the production of the Batch, because the breakdown voltage is too low and is not in acceptable range.

One of the suspected reasons for the failure is due to the use of wet oxidation, the field oxide is for technical reasons produced as wet oxide and the influence on the Gate-oxide is unlikely but still unknown.

Experiment with dry oxidation of the Gate oxide was performed, to secure the quality-management, we processed the Gate oxide of 2 final wafers, externally in traditional foundry, but the comparison with the wet oxide isn't showing any differences. According to the quality management there is no irregularities or variances in the internal processes. Due to this experiment the only remaining untestable parameter is the wafer implantation made externally.

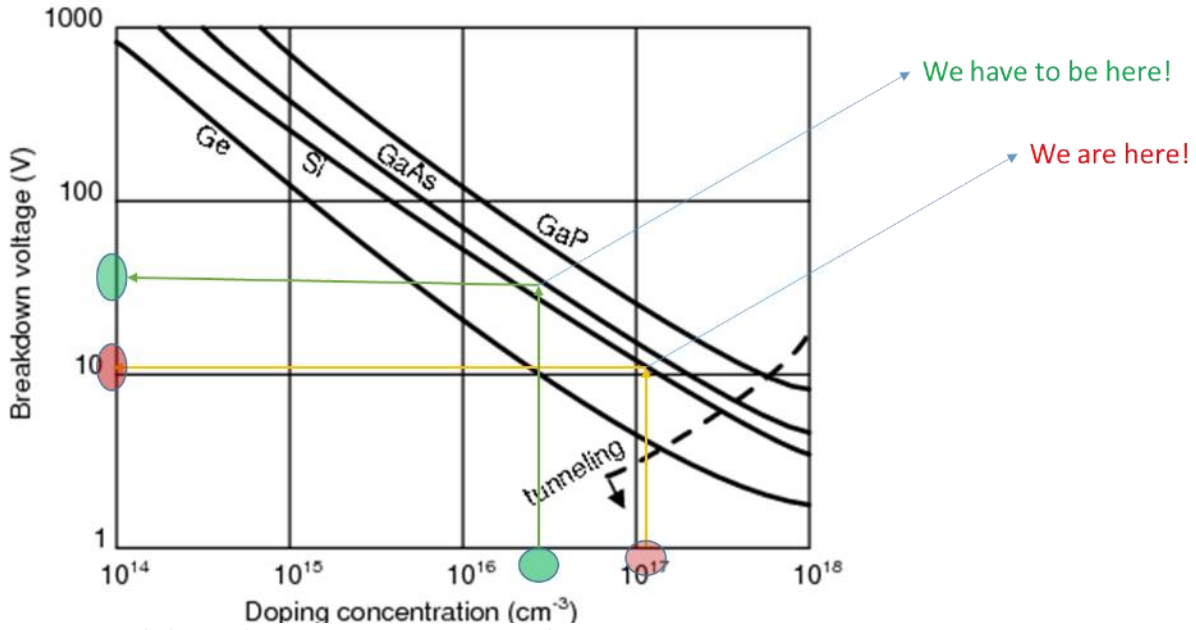

Figure 36 Break-down voltage - Doping concentration relation.

The graphic shown in figure 36 presents the relation between the doping concentration and the Break-down voltage which illustrates the problem with the transistor sensors from Batch 1.

Key point after launching Batch 1:

- Changing implantation company;
- Improving the ESD-protection design – new mask;
- Launching second Batch with MOSFET spectrometer sensors;
- No ESD-protection for the new design;

ESD-protection – modification in the technology steps:

Regarding to the issue with the short-cut in the ESD-protection circuit, new set of technological steps were tested and established.

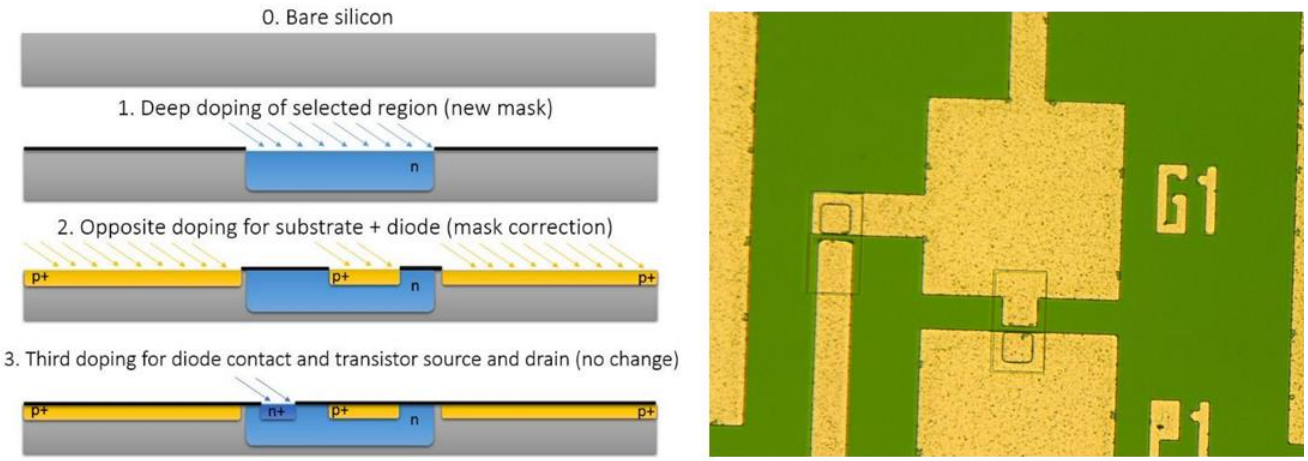

Figure 37 Left: New set of manufacturing steps for ESD-protection. Right: image of the ESD-protection diode taken with digital microscope.

After identification of the problem in the design, using a new mask there was introduced an additional N-doped region in the bare silicon wafer. Just after this step opposite doping is performed to create the substrate layer and the ESD diode with a modified mask. At last N+ doping is performed for creation of transistor source and drain regions, together with the other ESD diode.

Batch 2.

Batch 2 was launched in month 14 of the IAQSense project. The focus of the second batch of sensors was solving the critical issues reviled during the analysis of the sensors from Batch 1.

Spectrometer on chip (SoC) wafers were produced by Nano Analytik in the Ilmenau facility of nano analytik GmbH on a 4" line inside cleanroom of class 100/1000. Characterization included static and dynamic electrical tests with biggest focus on sample's detection capability.
The measurements were performed on naSE002A SoC samples manufactured according to „Tentative Product Specifications (TPS) - Spectrometer on chip for VOC detection & Tip based polar ionization detector of biomolecules - Test structure (Test)" and „Process Specifications - Custom Process for Spectrometer on chip And Tip based detection". The samples are based on N-channel MOSFET produced without ESD protection and with different doping/implantation parameters resulting in adjusted breakdown voltage values. Sensors are realized on a die with dimensions 5 mm by 5 mm.
Measurements were performed solely on V2.1-type transistors on membrane, which are characterized by 100 µm square symmetrical channel and tin oxide gate material, glued and wire-bonded to 12-pin TO-package housing.

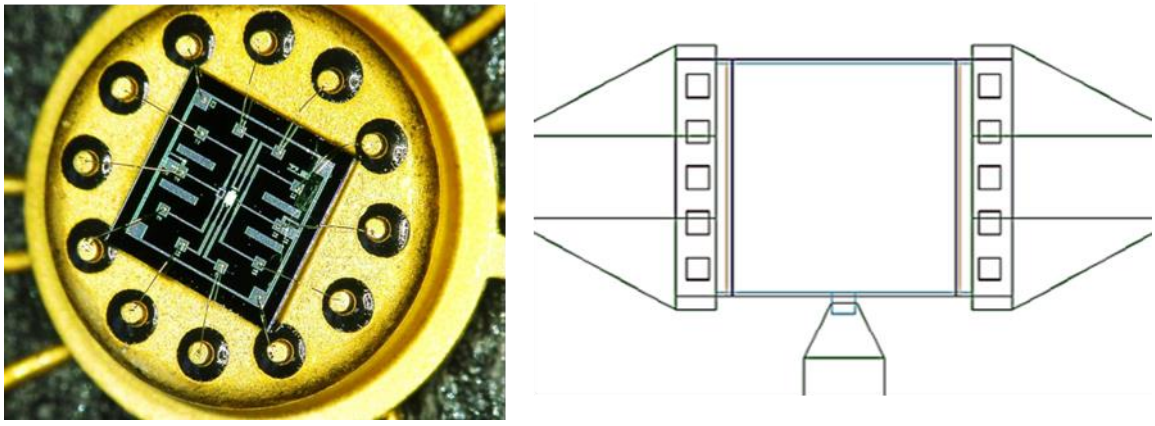

Figure 38 Left: The picture of SoC sample bonded to TO-housing (no cap), Right: Geometry of measured transistor with square geometry of the channel.

Second batch of spectrometer transistors were built within the membrane in order to get a better thermal insulation. The power of the build in heater is not enough to heat the regain with transistors to the needed temperature ratings to clean the surface of the collective layer when transistors are not thermally insulated. That is why usage of a membrane technology is necessary.

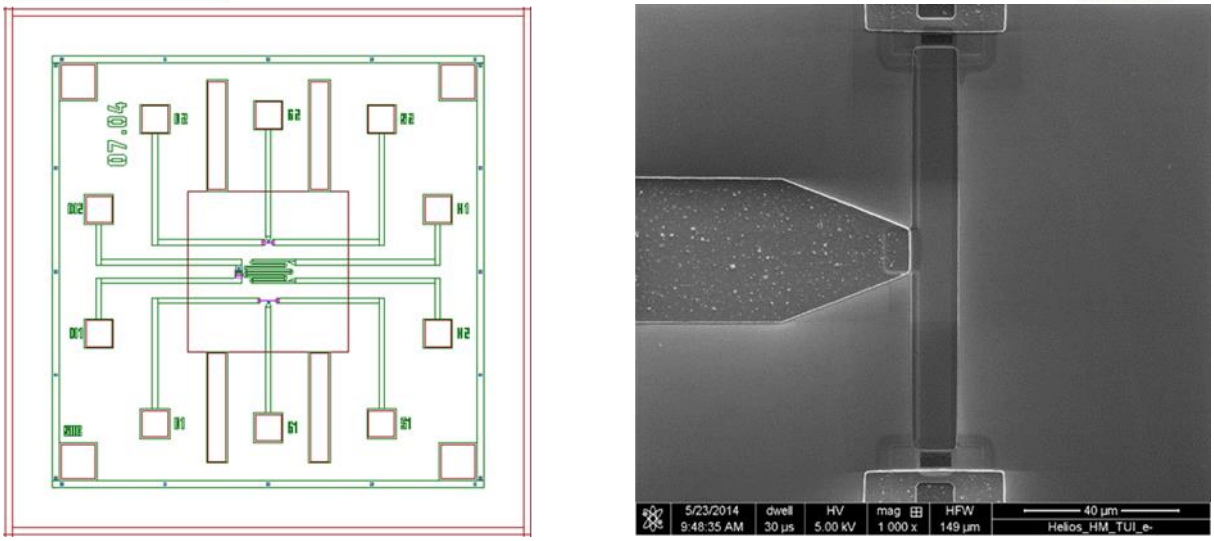

Figure 39 Left: The layout of the mask for N-channel MOSFET spectrometer on membrane (Batch 2), Right: SEM image of a MOSFET is rectangular geometry.

Batch 2 - MOSFET spectrometer output and transfer characterization.

Characteristics collected have shown that transistors can conduct the drain current in the range of milliamps without any damage for the sample. For the purpose of testing maximum chosen gate voltage applied was 15V and drain source voltage 18 V, however, for future use values to apply can be bigger if needed.
Observed V_{Th} value is fluctuating near 0÷1V depending on sample.

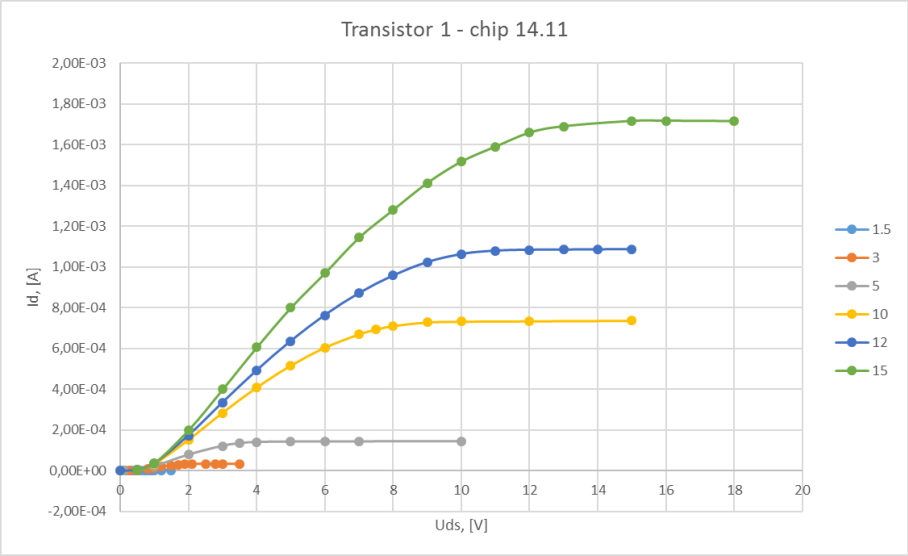

Figure 40 Batch 2, output characteristics – Chip 14.11 T1(100 µm).

Short comparison between the output charts of transistors manufactured in Batch 1 and these produced in Batch 2 shows essential difference in the performance. The drain current and drain-source voltage ratings are much higher for the transistors from Batch 2. The result from Batch 2 goes much closer to the calculated values, which is evident for improvement of the wafer implantation manufacturing process.

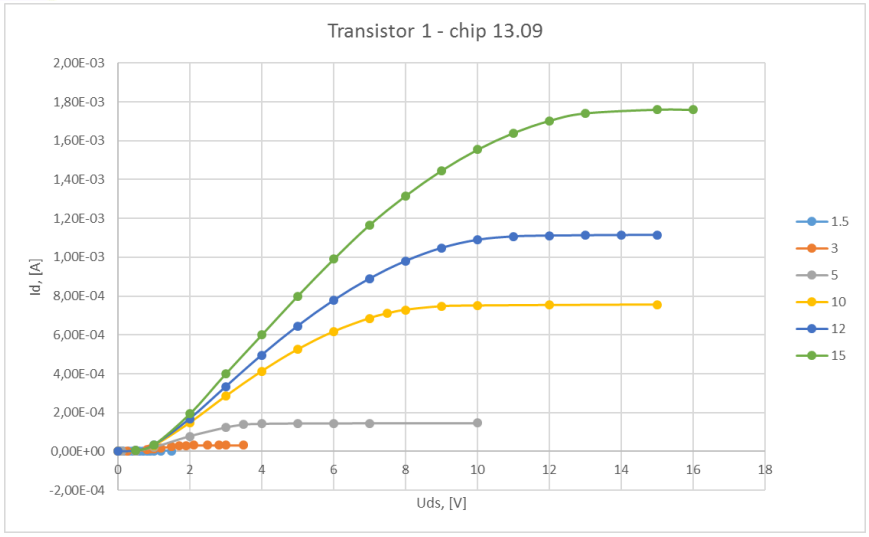

Figure 41 Batch 2, output characteristics – Chip 13.09 T1(100 µm).

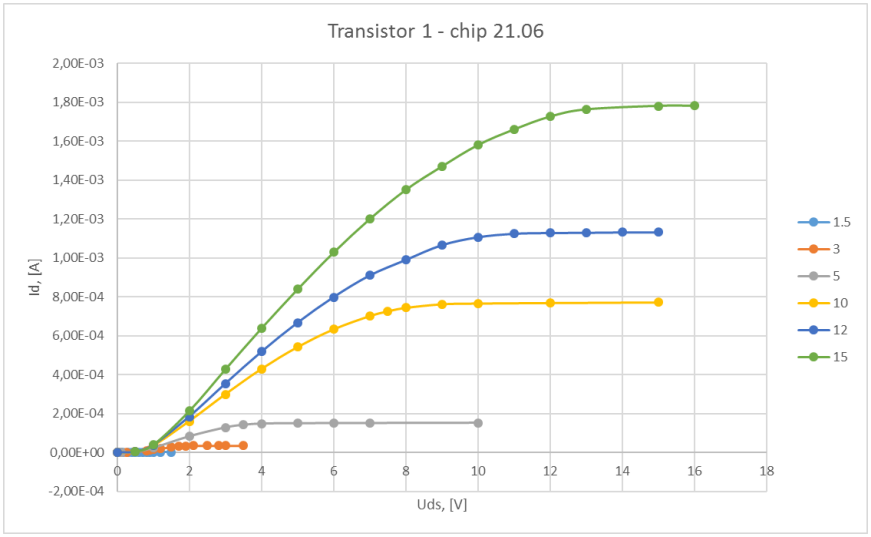

Figure 42 Batch 2, output characteristics – Chip 21.06 T1(100 µm).

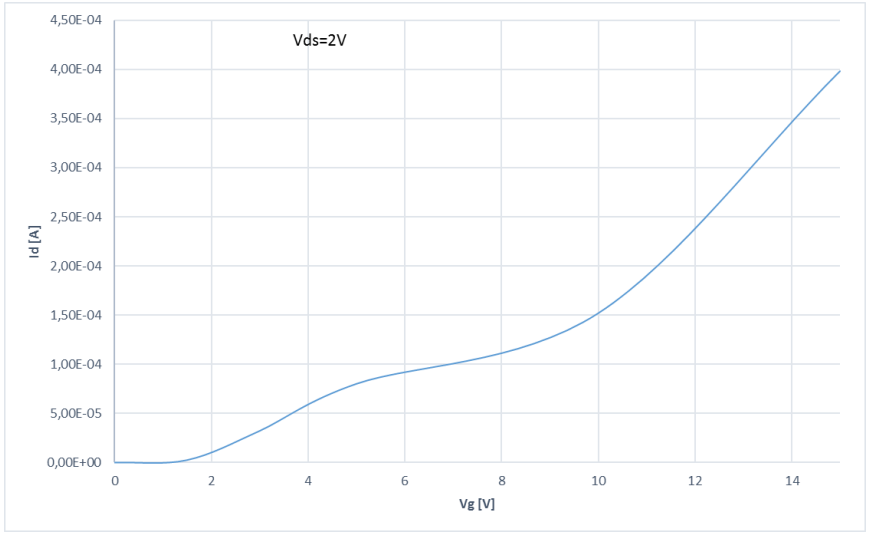

Figure 43 Averaged transfer characteristics of 25% of total amount of V2.2 transistors.

Batch 2 - MOSFET spectrometer symmetry test.

To check the symmetry of source/drain work of the transistor, measurements with interchanged source/drain pins were conducted. In that case the lead which normally was used as a source was connected to work as a drain; and typical drain was connected to the substrate and worked as a source. All measurements have shown slight change in the signal, but generally difference observed was not bigger than 20%. Exemplary output characteristics comparing S/D-D/S behavior and showing typical size of response variance are given below.

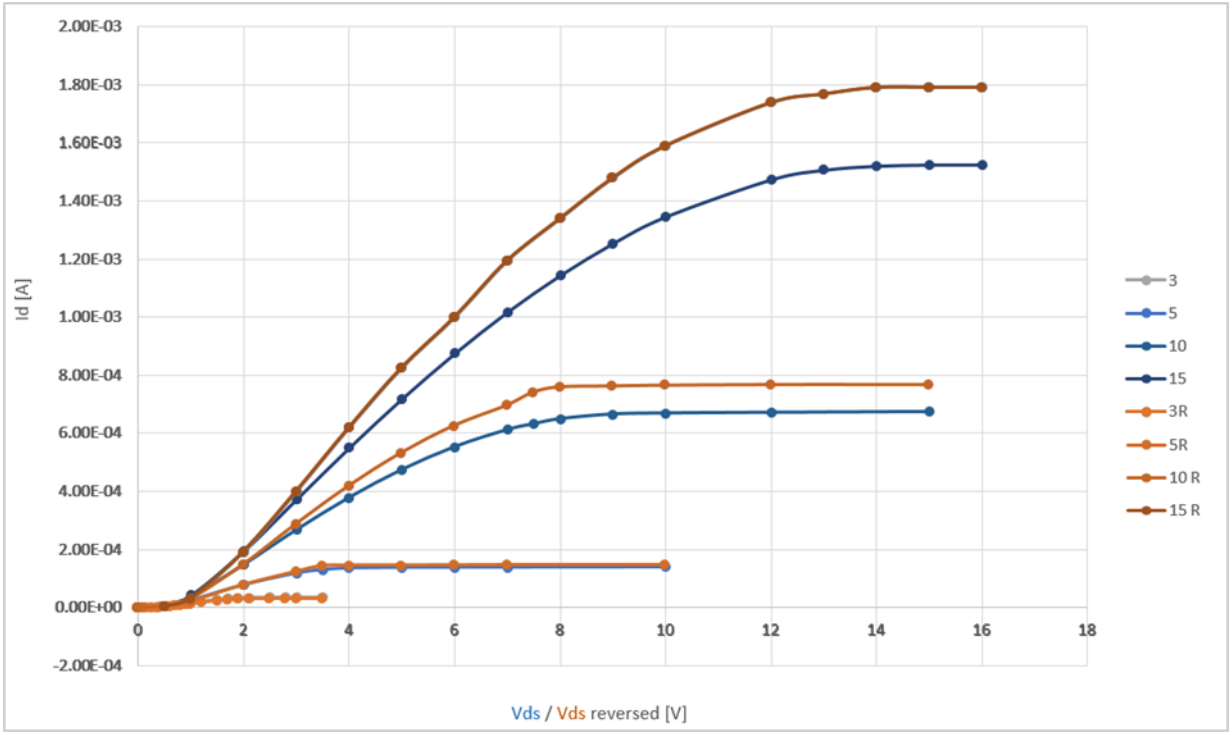

Figure 44 Output characteristics symmetry test.

Batch 2 - MOSFET spectrometer breakdown voltage.

Measurements carried out according to the description provided in figure 34 have revealed that basing on measurement of 25% of V2.1 transistors, the breakdown voltage is estimated at the level of 37.5 V with standard deviation of σ=4.46 V. Some of the measurement results are listed below:

- *Break-down voltage for chip 13.09 – Transistor 100µx100µ: 35V*
- *Break-down voltage for chip 14.11 – Transistor 100µx100µ: 34V*
- *Break-down voltage for chip 21.06 – Transistor 100µx100µ: 37V*

Batch 2 - MOSFET spectrometer – dynamic electrical response.

First dynamic measurements were performed with the samples from second batch. Transistor used in this experiment is shown in figure 39 (right). The measurement setup block diagram is shown in figure 45.

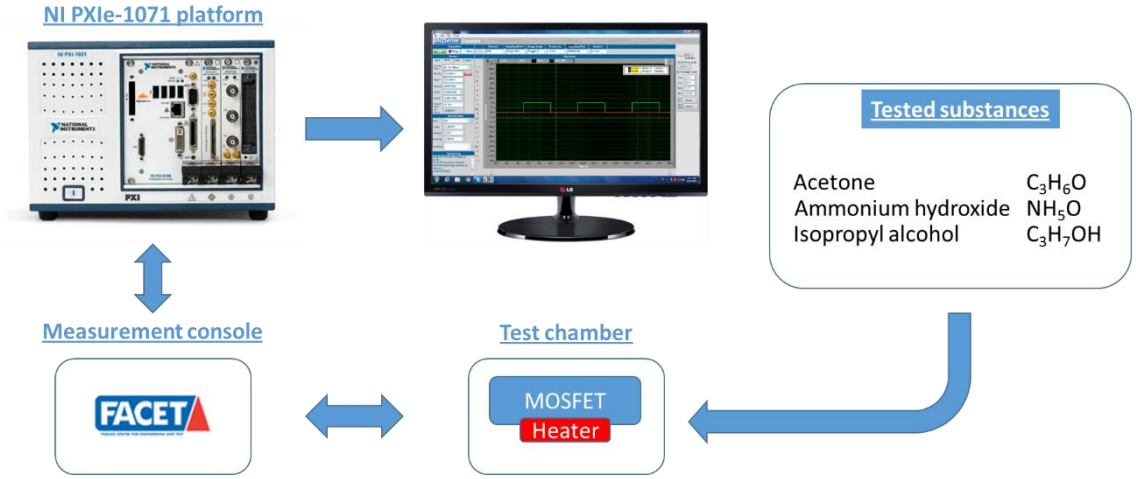

Figure 45 Test setup with NI platform and measurement realized by FACET and delivered on 7th July 2015 for dynamic characterization of spectrometer on chip sensors.

The setup shown on the figure above consist of Measurement console, developed by FACET, the NI platform with the software application developed for the needs of IAQSense project for characterization of spectrometer transistors, a display monitor, a test chamber where is placed the sensor itself. The chamber is supplied with different substances via capsule filled with micropipette. The NI platform plays the role of a process controller with integrated computer device that records the amplitude and the shape of the current signal floating through the drain-source electrodes of the sample. The FACET measurement platform plays the role of the transistor driver, connecting the sensor in a diagonal of a Wheatstone bridge giving the possibility to switch the polarity of the drain-source terminals. In addition, a heater is present inside the test chamber to give flexibility of the measurement setup. In case of saturation of the MOSFET spectrometer (that could happen when sensor is overdosed), heating up the whole chip prevents a surface effect issues caused by the environmental reasons.

The parameters used in this measurement are listed below:

- Bridge voltage – 5V;
- Gate voltage – 4V;
- Rsense – 3000Ω;
- System overall gain – 6,35;
- Sampling mode – Continuous;
- Bridge mode – Toggle0;
- Switching frequency – 1Hz;
- Sampling rate – 20kHz;
- Number of samples – 64000;
- Temperature – 25°C;

The aim of this first chemical experiment with spectrometer MOSFET was to observe if there is any change in sensor response. The principle of operation of the technology includes set of parameters for driving the transistor itself. These parameters are the applied voltage on the drain-source terminals, the frequency for switching the voltage

and the gate potential. The other two parameters involved in regime of operation of the spectrometer are the sampling mode and the bridge mode.

The second group of parameters are influencing the readout system, and this includes the hardware resistor for conversion the drain current into voltage. Rsense is hardware component that can't be modified via the software console but must be considered for further understanding of the spectrometer operation. The next parameters of this group are the gain factor, sampling rate and the number of samples.

Apart of this two major groups, the temperature must be taken in to account when the measurements are conducted.

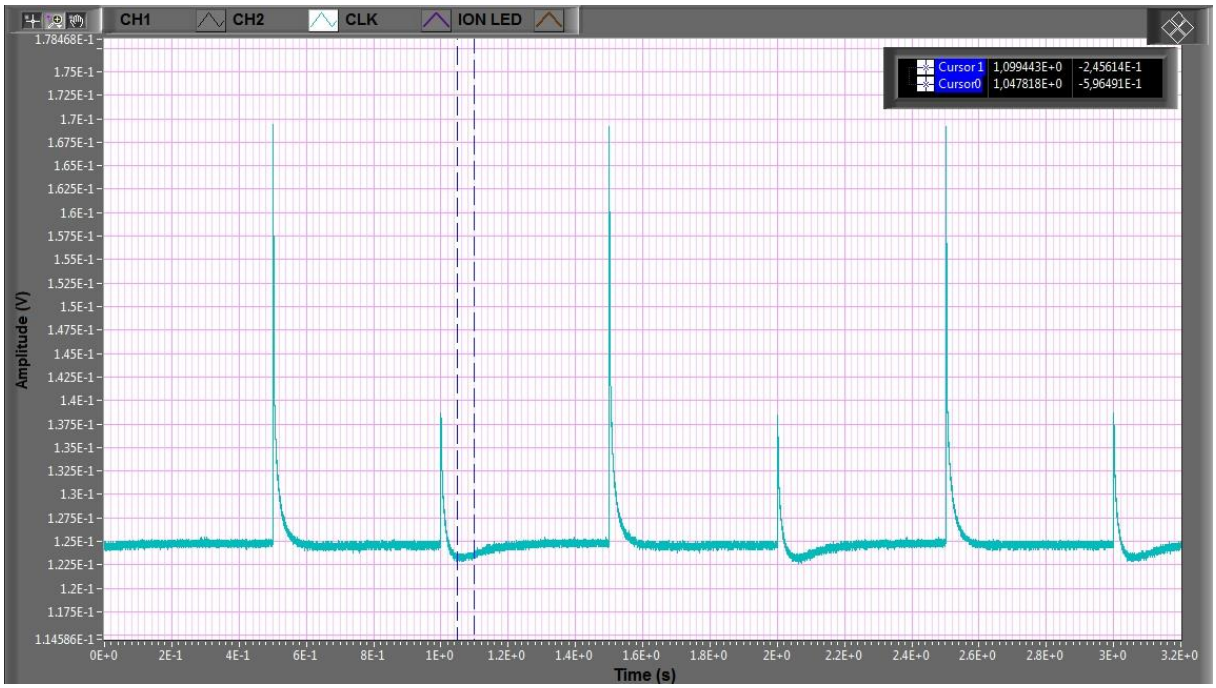

Figure 46 Spectrometer chip 9.08 N-channel MOSFET, L:100 W:10 – response in air.

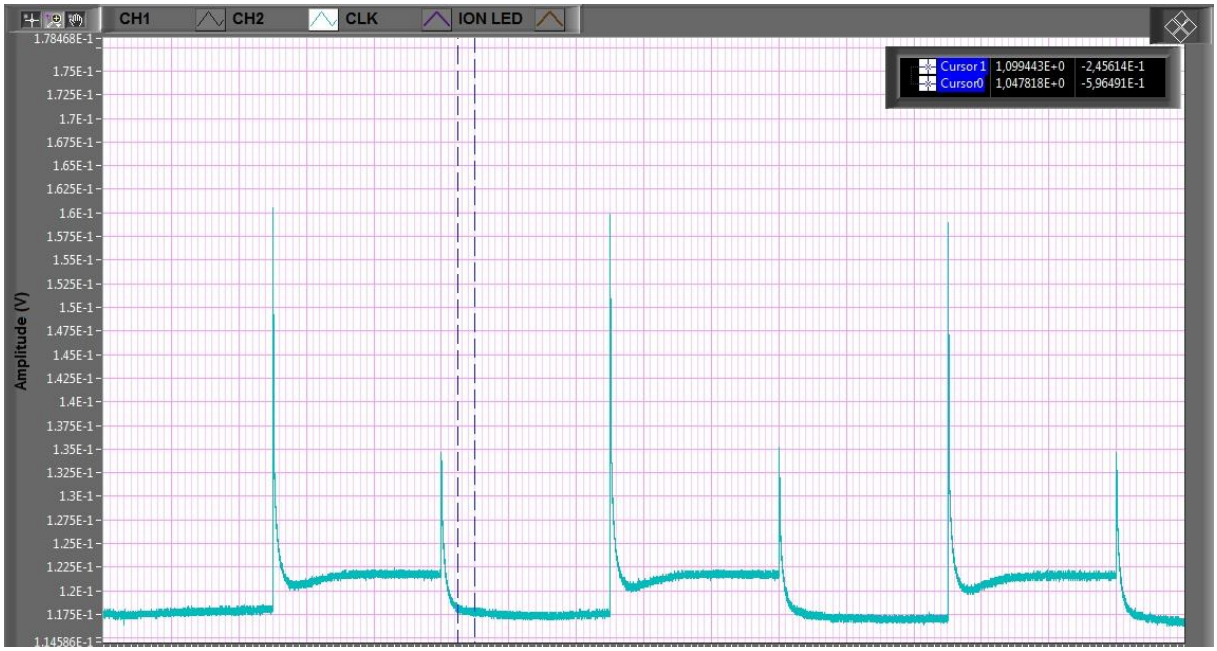

Figure 47 Spectrometer chip 9.08 N-channel MOSFET, L:100 W:10 – response in acetone vapours in progress.

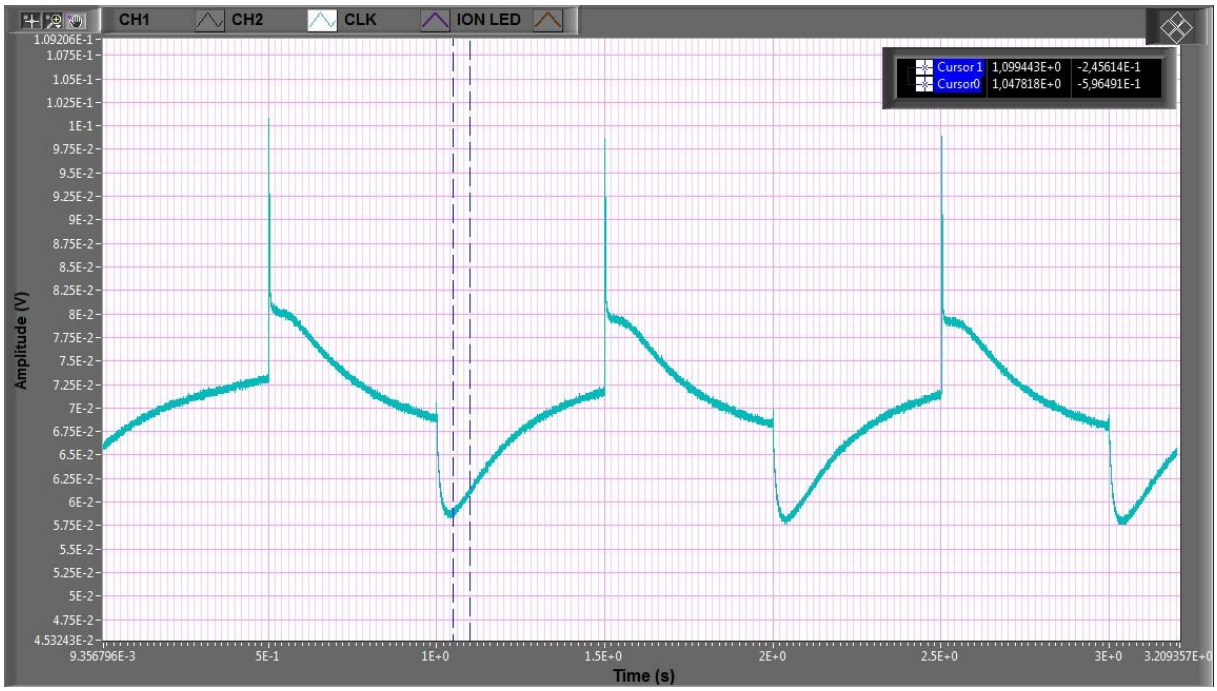

Figure 49 Spectrometer chip 9.08 N-channel MOSFET, L:100 W:10 – response in acetone vapours.

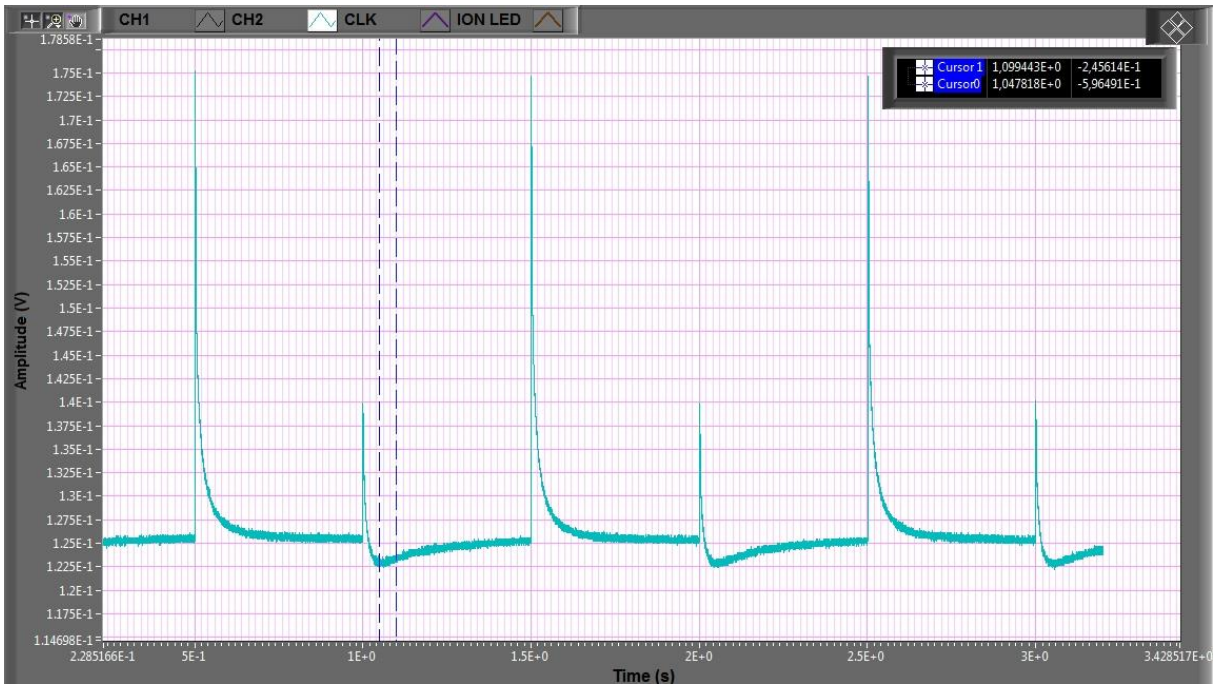

Figure 48 Spectrometer chip 9.08 N-channel MOSFET, L:100 W:10 – response in air after acetone.

N-channel spectrometer MOSFET response in room air conditions, in environment of acetone vapours and isopropyl alcohol vapours is presented in figures 46, 47, 48, 49 and 50. The oscillogram shown in these figures represents the current floating true the channel of the transistor. As it was expected the sensor reacted and we observe significant change in the amplitude and the shape of the signal. The exact concentration inside the chamber during the chemical characterisation experiments was unknown, but the significant difference in acetone and isopropyl alcohol vapours response is evident.

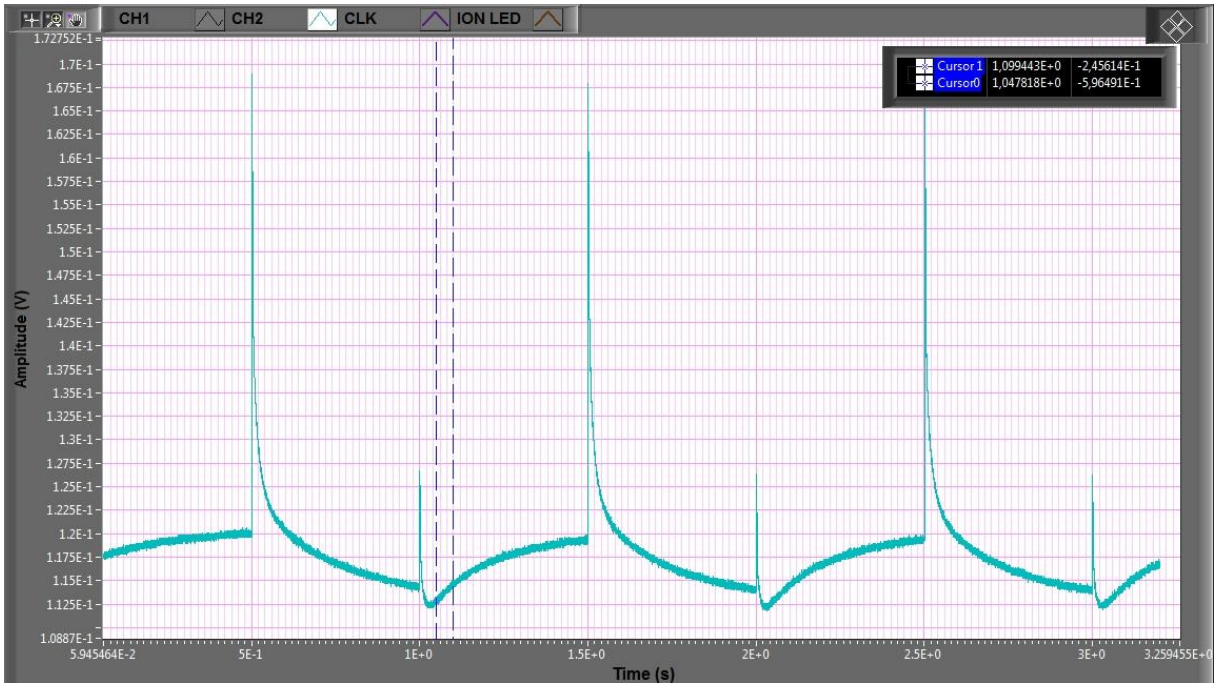

Figure 50 Spectrometer chip 9.08 N-channel MOSFET, L:100 W:10 – response in isopropyl alcohol vapours.

To understand the real current value, it is needed to be considered the gain of the front-end amplifier and the sensing resistor from the current to voltage converter.

$$Id = \left(\frac{Uout}{Gain}\right)\Big/_{Rsense} \quad [A]$$

Batch 3.

Batch 3 was launched in month 18 of the IAQSense project. The sensors manufactured in this batch are P-channel based, realized on a die with dimensions 1 mm by 1 mm.

Spectrometer on chip (SoC) wafers were produced by Nano Analytik in the Ilmenau facility of nano analytik GmbH on a 4" line inside cleanroom of class 100/1000. Characterization included static and dynamic electrical tests with biggest focus on sample's detection capability. The measurements were performed on naSE001P SoC samples manufactured according to „Tentative Product Specifications (TPS) - Spectrometer on chip for VOC detection & Tip based polar ionization detector of biomolecules - Test structure (Test)" and „Process Specifications - Custom Process for Spectrometer on chip And Tip based detection". The samples are produced without ESD protection, without integrated heater and temperature control sensor.

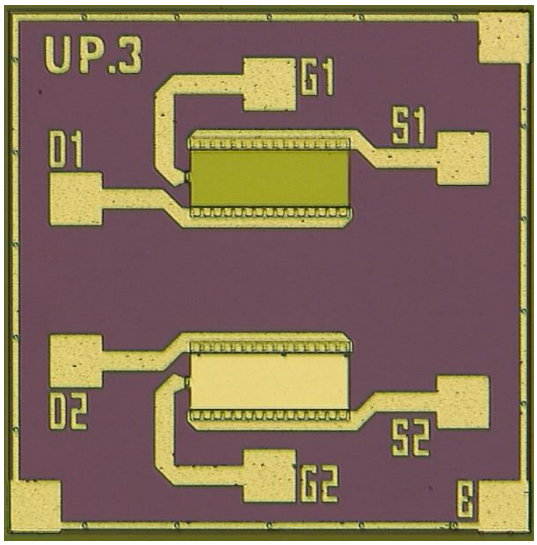

Figure 51 P-channel spectrometer MOSFET, batch 3.

Sensors manufactured in the third batch are P-channel MOSFETs, the charge carriers mobility difference is 3 times smaller than the one for N-channel MOSFETs. This leads to increasing of the transistor channel to keep the same output characteristics of the N-channel sensors and the P-channel sensors. In figure 51 is shown the design of a P-channel MOSFET sensor. There are 2 transistors on each chip. Transistor 1 is with Tin oxide gate, but the second transistor on the chip is with "Al" gate, which purpose is to be used as a reference transistor. Gate dimensions of the transistor are 100µm by 300µm. The thickness of the Tin oxide layer is 80nm. The sheet resistance of the SnO_2 layer is in range of few hundreds of kiloohms.

Batch 3 – P-channel MOSFET spectrometer output characteristic:

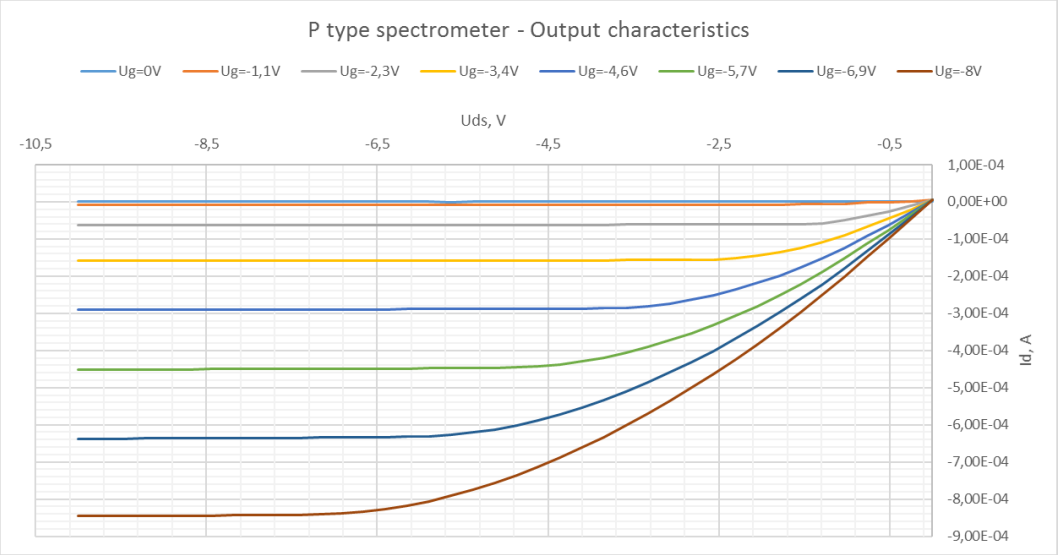

Figure 52 Batch 3 - P-channel MOSFET spectrometer output characteristics.

Typical output characteristic measured for a P-channel MOSFET spectrometer is shown on figure 52. This type of spectrometer sensor has been delivered to three of the project partners and the measurement of the transistor output characteristic was established as a part of a standard procedure of testing the bonded sensors.

Batch 3 – P-channel MOSFET spectrometer – dynamic electrical response:

This type of sensors was used in chemical parallel characterization test of a N-channel spectrometer and P-channel spectrometer.

The aim of the parallel characterization test was to investigate the response behavior of different sensor samples for different substances.

The parameters used in this measurement are listed below:

- Bridge voltage – 5V;
- Gate voltage – 1,5V;
- Rsense – 3000Ω;
- System overall gain – 6,35;
- Sampling mode – Continuous;
- Bridge mode – Toggle0;
- Switching frequency – 0,5Hz;
- Sampling rate – 8kHz;
- Number of samples – 64000;
- Temperature – 25°C;

Tested substances:

Xylene	Chlorbenzol	Toluene	Butyl acetate	Methyl isobutyl ketone
C_8H_{10}	C_6H_5Cl	C_7H_8	$C_6H_{12}O_2$	$C_6H_{12}O$
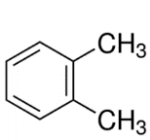	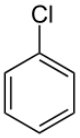	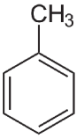	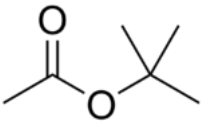	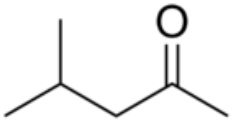
	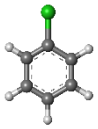	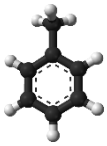	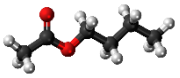	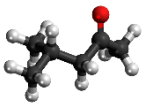

Figure 53 Tested substances.

The measurement sequences consisted of reference measurement in room air. The following measurements were done after injection of 100µl. of substance inside the measurement chamber with volume of 0,75l. All rules of the safety measures are followed strictly during the experiment. Spectrometer sensor board with the MOSFET chips were in gas ventilation hood with constant airflow to prevent inhalation of the measurement substances. Presented measurement result shows one period of the whole measurement sequence.

Xylene measurement.

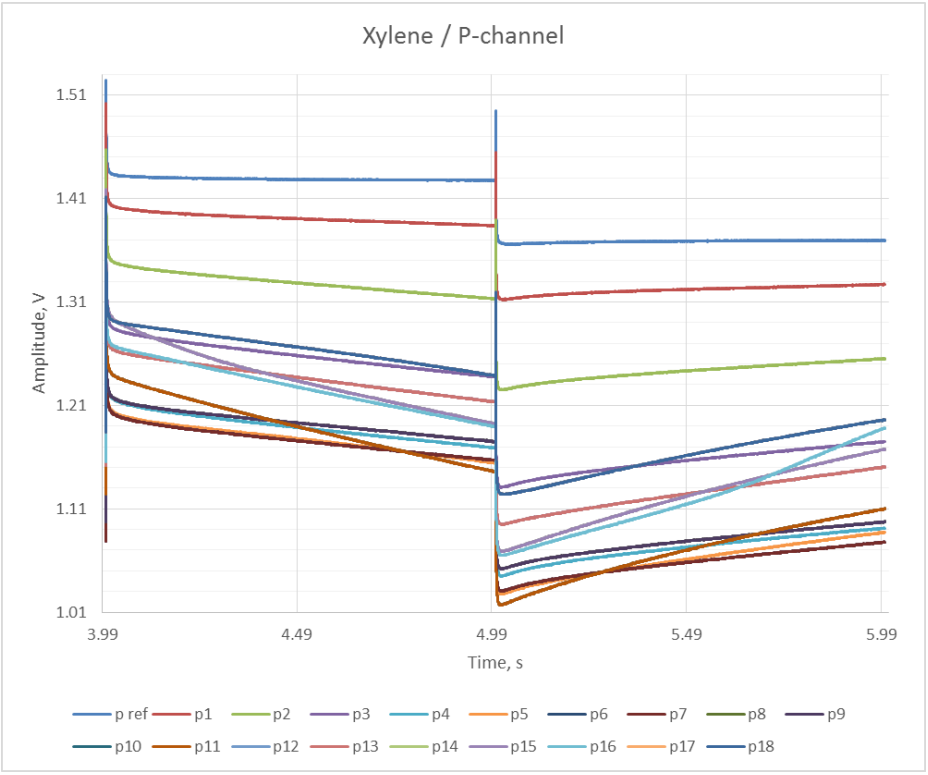

Figure 54 Full chart – Xylene measurement with P-channel MOSFET spectrometer.

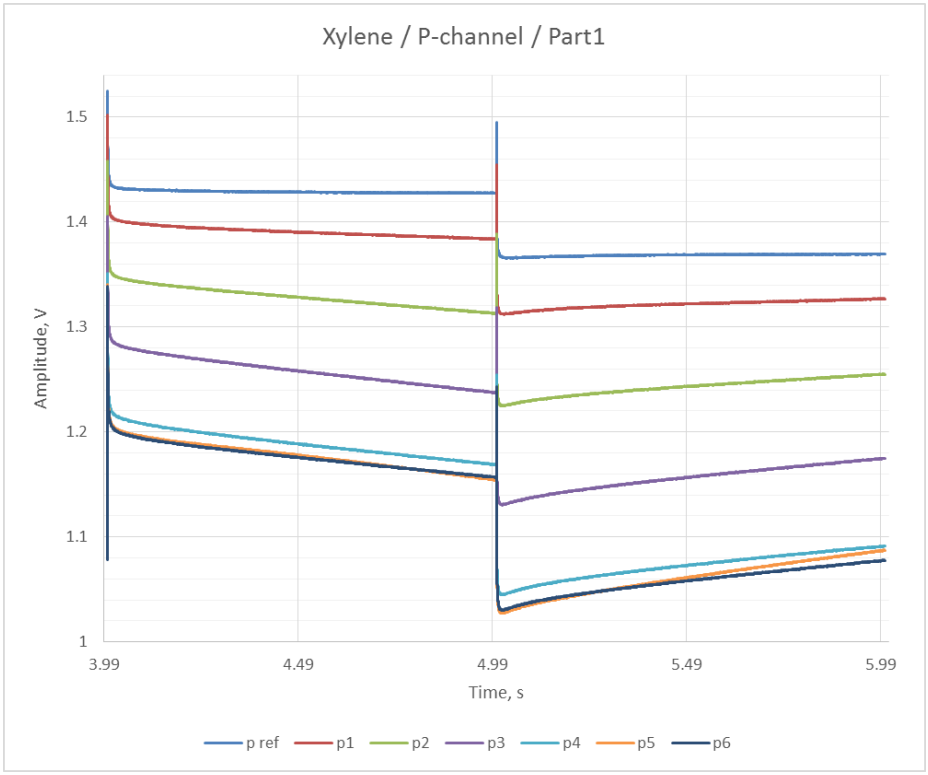

Figure 56 Xylene measurement with P-channel MOSFET spectrometer - part 1.

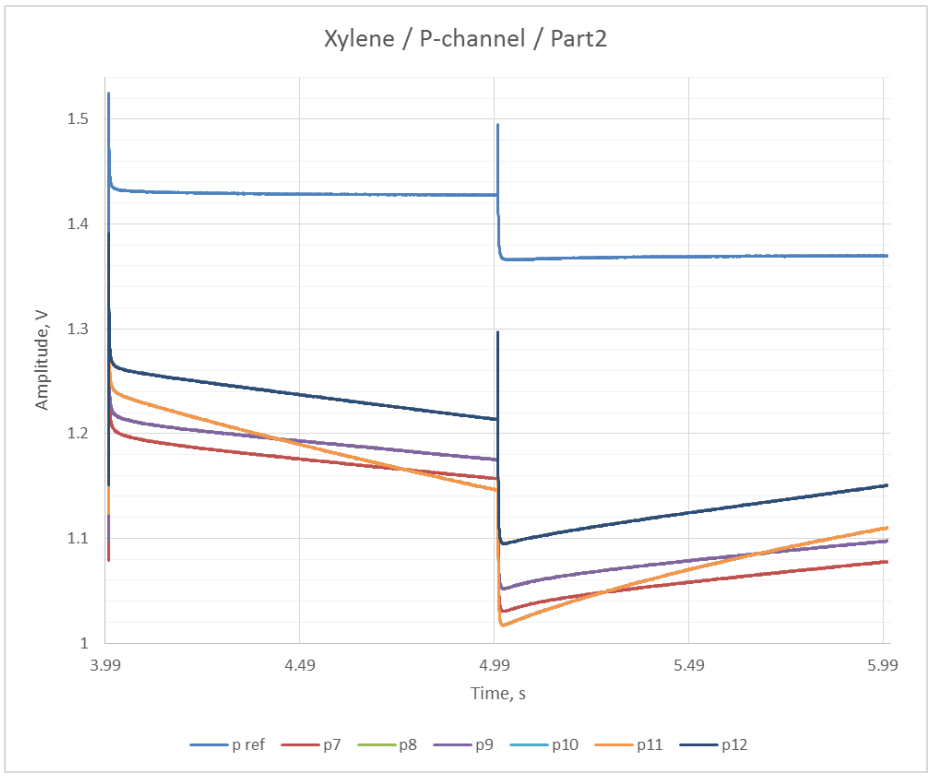

Figure 55 Xylene measurement with P-channel MOSFET spectrometer - part 2.

For all charts, the reference measurement is present, so it is easy to evaluate the sensor response. The separation of the graphs per parts makes the difference significant. There is offset of the sensor signal in respect to the reference, aside of this fact amplitude shape has changed in the process of environmental changes inside the chamber.

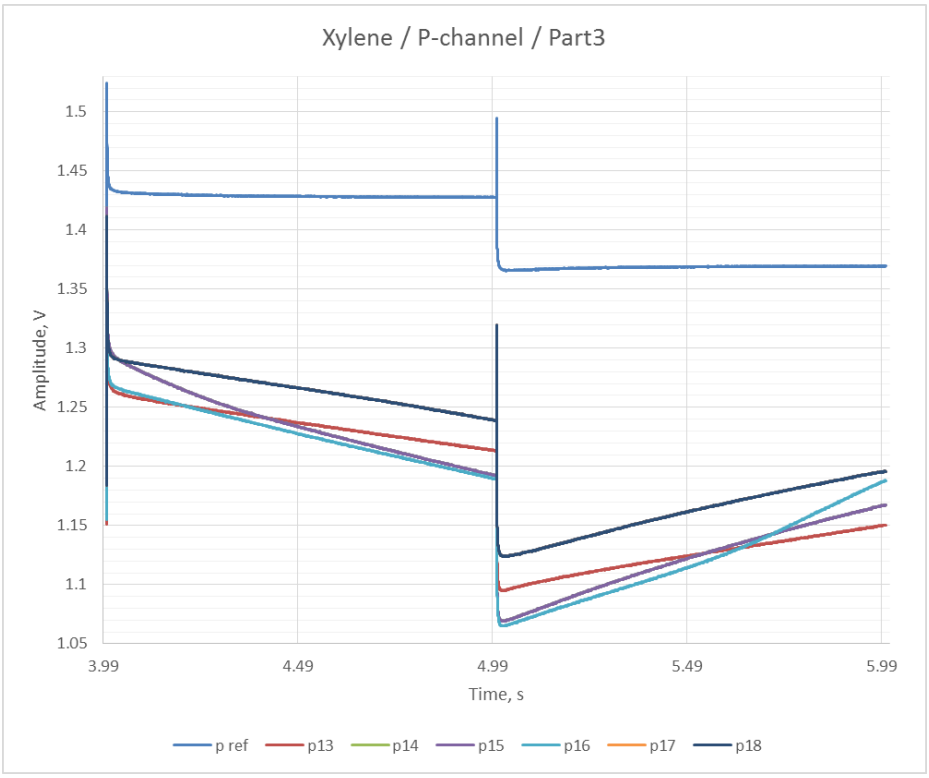

Figure 57 Xylene measurement with P-channel MOSFET spectrometer - part 3.

Chlorbenzol measurement.

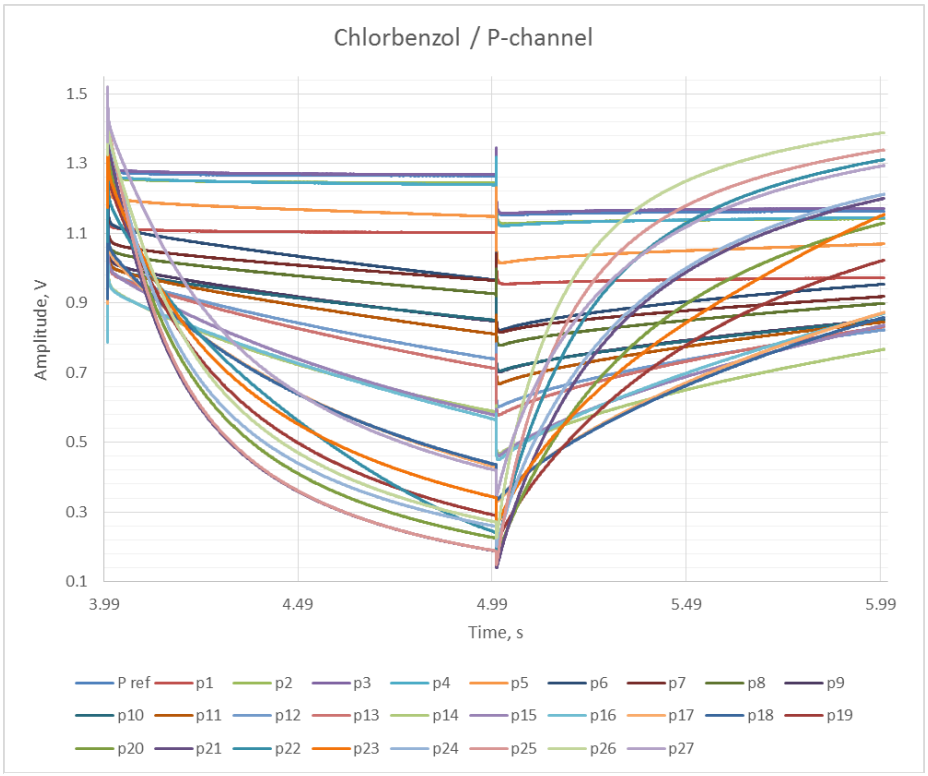

Figure 58 Chlorbenzol measured with P-channel MOSFET spectrometer.

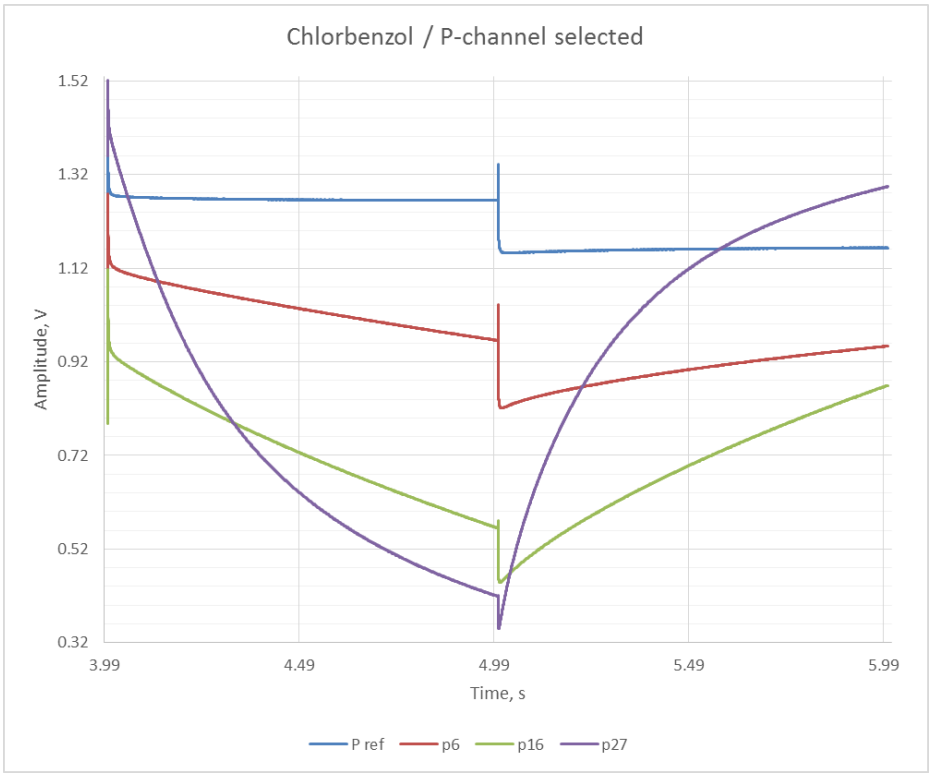

Figure 59 Selected signal – Chlorbenzol measurement with P-channel MOSFET spectrometer.

Toluene measurement.

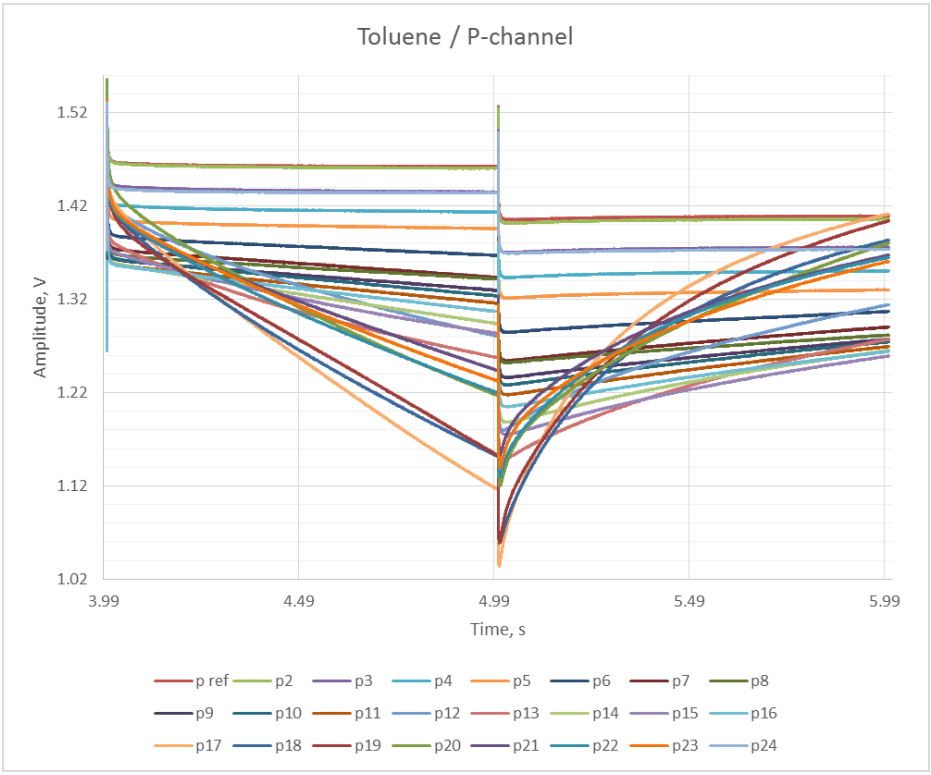

Figure 60 Full chart – Toluene measurement with P-channel MOSFET spectrometer.

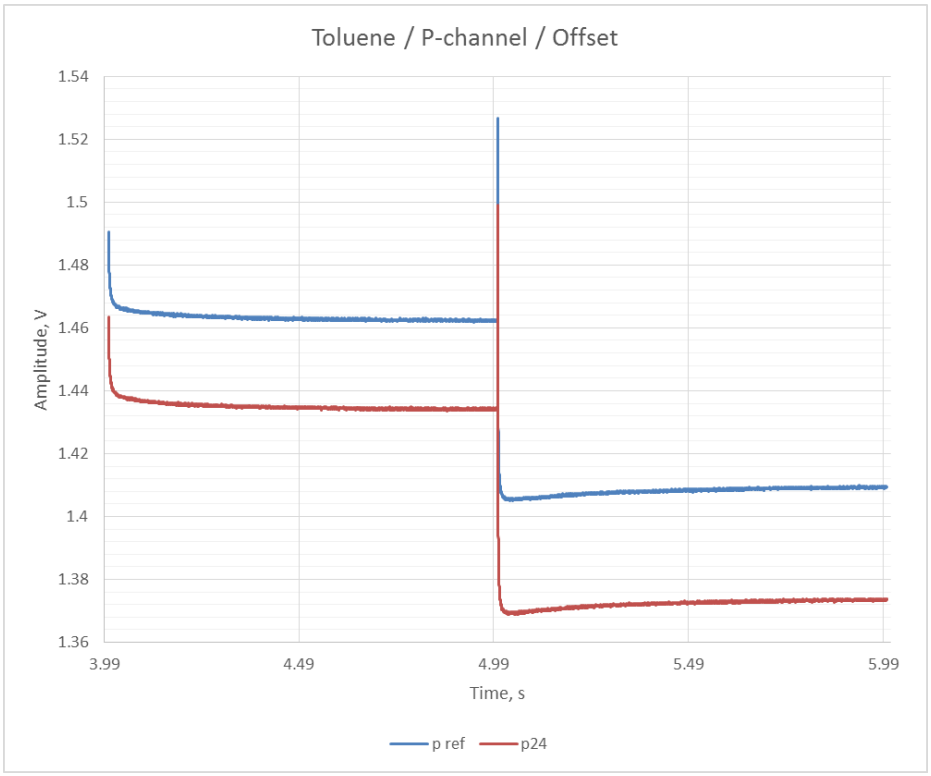

Figure 61 Toluene measurement – P-channel MOSFET Offset.

Butyl acetate measurement.

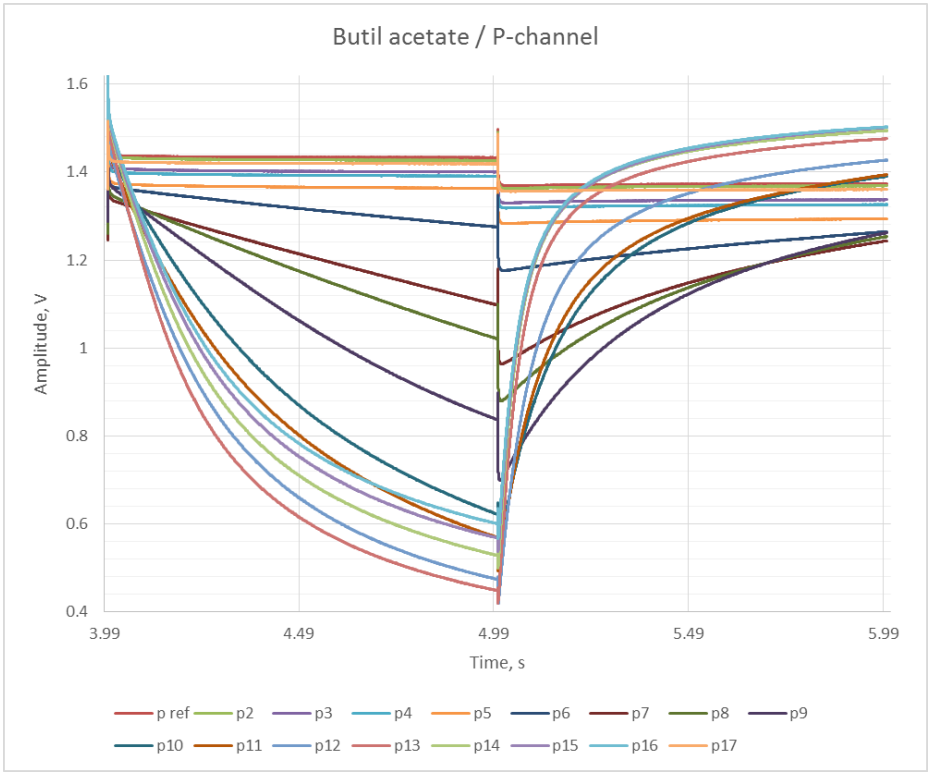

Figure 63 Full chart – Butyl acetate measurement with P-channel MOSFET spectrometer.

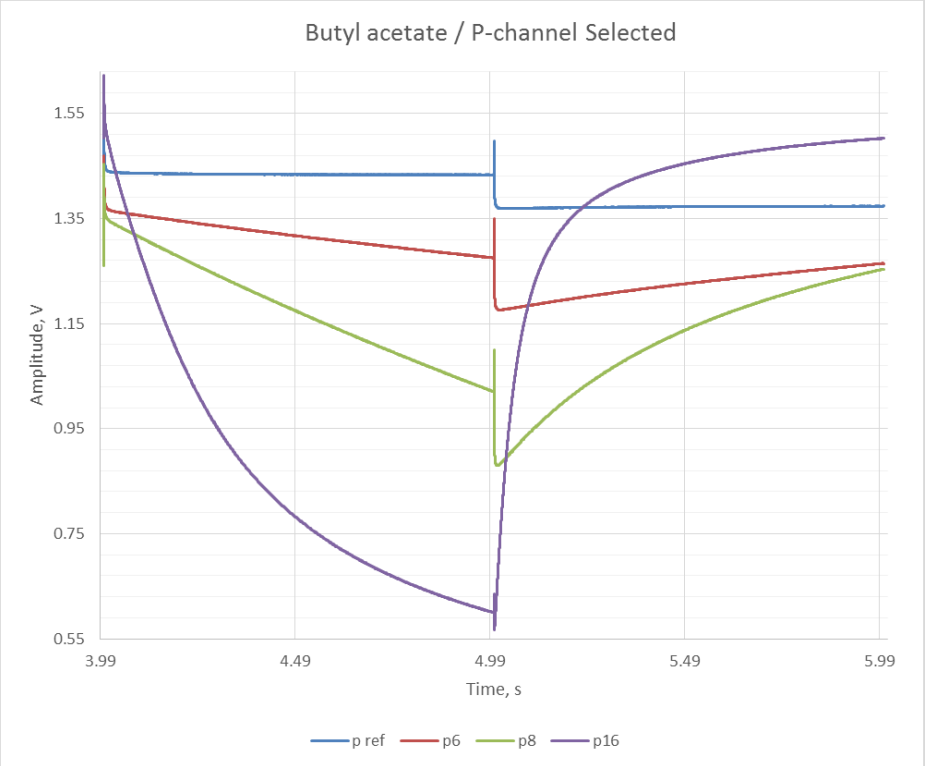

Figure 64 Selected signal – Butyl acetate measurement with P-channel MOSFET spectrometer.

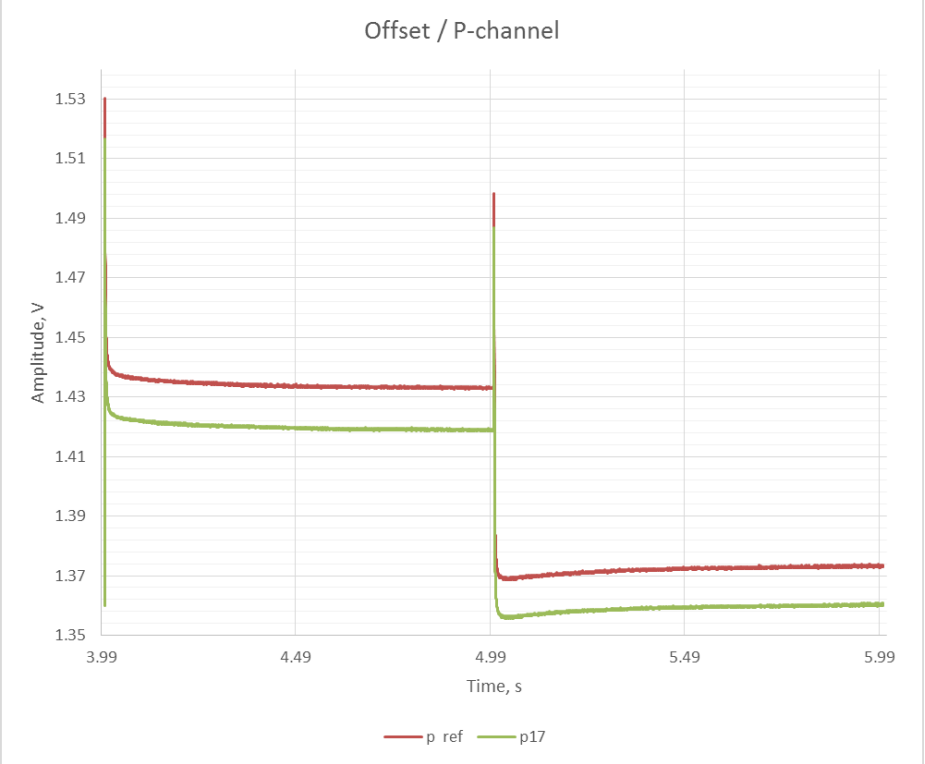

Figure 65 Butyl acetate measurement – P-channel MOSFET Offset.

Results of the measurement illustrated in the Batch 3 section are commented in the section of Batch 4, where is made parallel between the performance of both spectrometer sensors.

Methyl isobutyl ketone measurement.

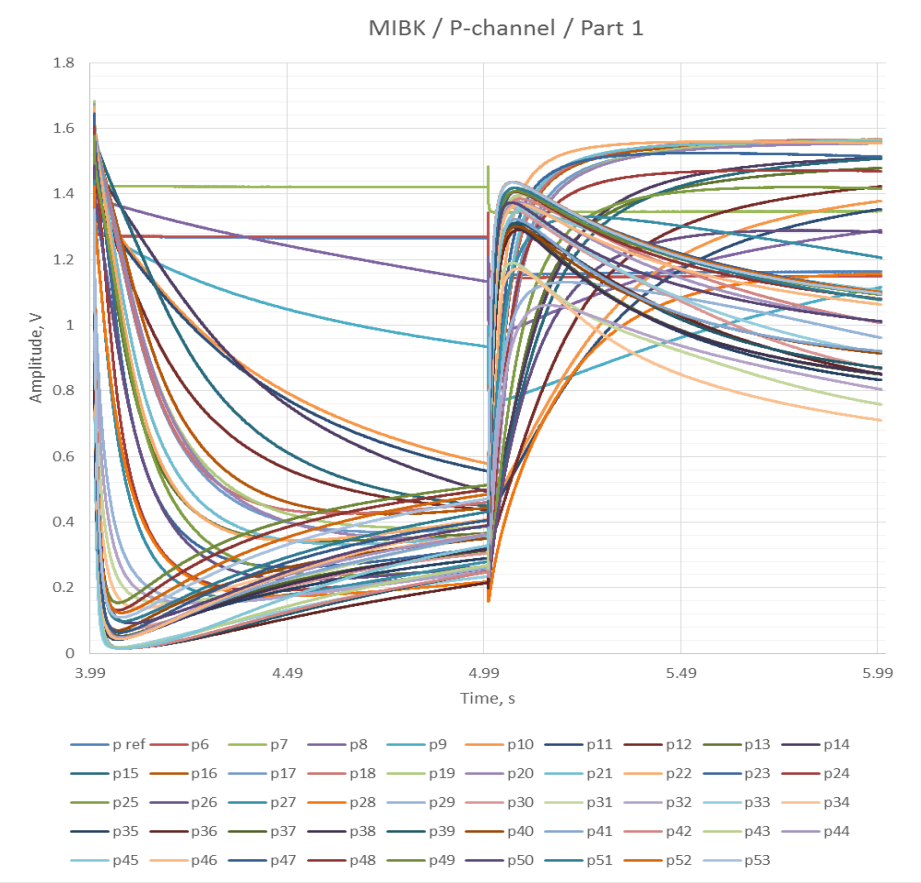

Figure 66 MIBK measurement with P-channel MOSFET spectrometer.

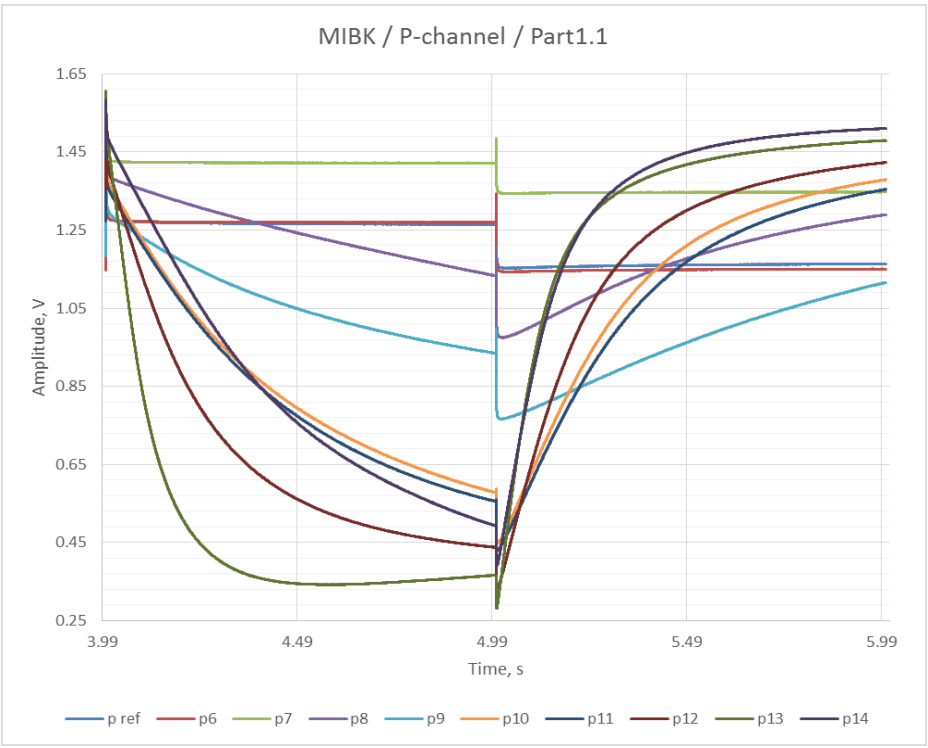

Figure 67 MIBK measurement with P-channel MOSFET spectrometer - part 1.

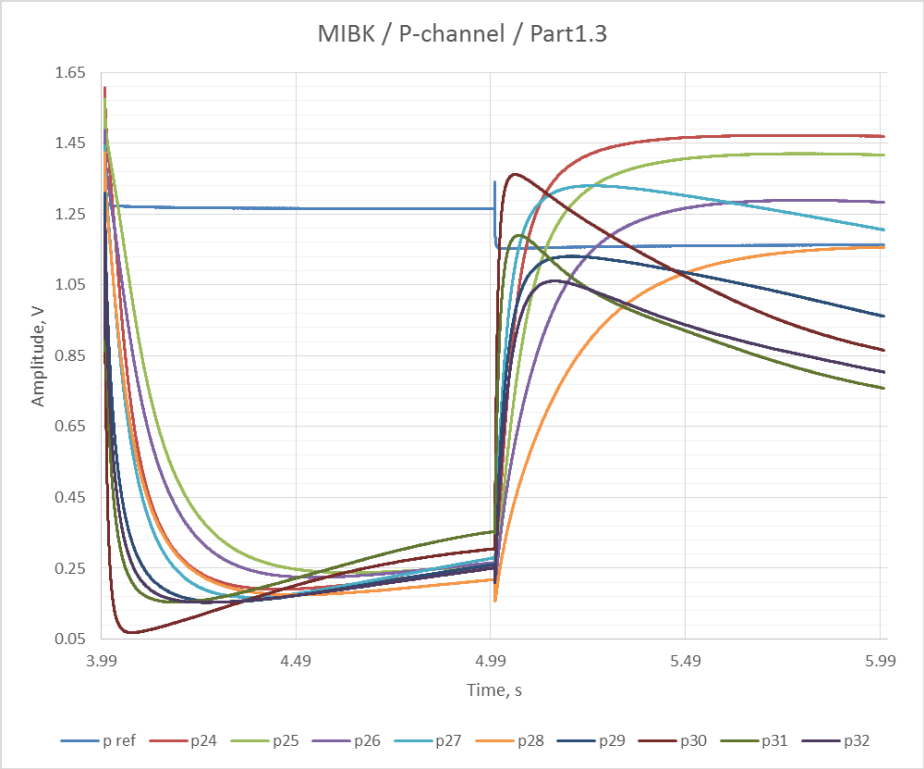

Figure 68 MIBK measurement with P-channel MOSFET spectrometer - part 3.

Batch 4.

Batch 4 was launched in month 28 of the IAQSense project. Spectrometer on chip (SoC) wafers were produced by Nano Analytik in the Ilmenau facility of nano analytik GmbH on a 4" line inside cleanroom of class 100/1000. Characterization included static and dynamic electrical tests focused on sample's detection capability.

The measurements were performed on naSE005A SoC samples manufactured according to „Tentative Product Specifications (TPS) - Spectrometer on chip for VOC detection & Tip based polar ionization detector of biomolecules - Test structure (Test)" and „Process Specifications - Custom Process for Spectrometer on chip And Tip based detection". The samples are based on N-channel MOSFET produced without ESD protection. Sensors are realized on a die with dimensions 1 mm by 1 mm. The spectrometer sensor manufactured in Batch 4 are with two different thickness of the gate layer. For each chip, there is a transistor with 80nm gate layer and 40nm gate layer. This has been done to answer the **Debye length** objective.

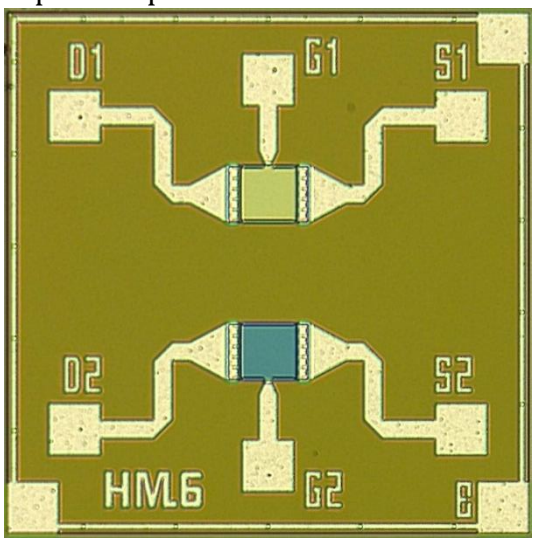

Figure 69 N-channel spectrometer MOSFET, batch 4.

Batch 4 – N-channel MOSFET spectrometer output characteristic:

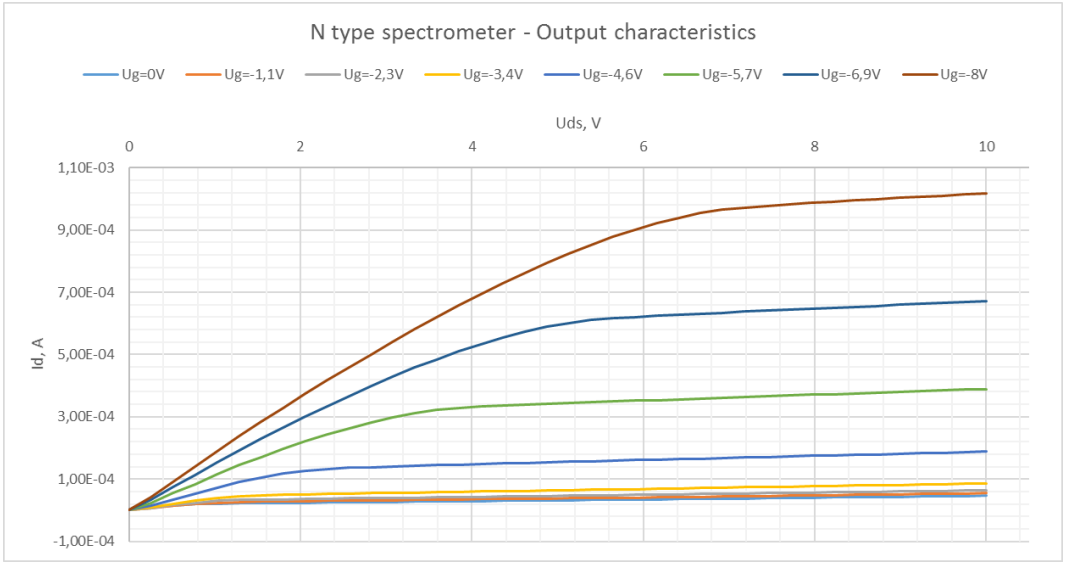

Figure 70 Batch 4 - N-channel MOSFET spectrometer output characteristics.

All sensors that were manufactured by NANO and provided to the project partners from batch 4 are electrically characterised. The output characteristic of a sensor produced in the fourth batch is shown in figure 70. The characteristics of N-channel transistor from batch 4 and the characteristics of the P-channel transistors from the previous batch are covering the expectations of the initially calculated values for the sensors. This is an evidence that all CMOS processes were performed successful.

Batch 4 – N-channel MOSFET spectrometer AFM investigation:

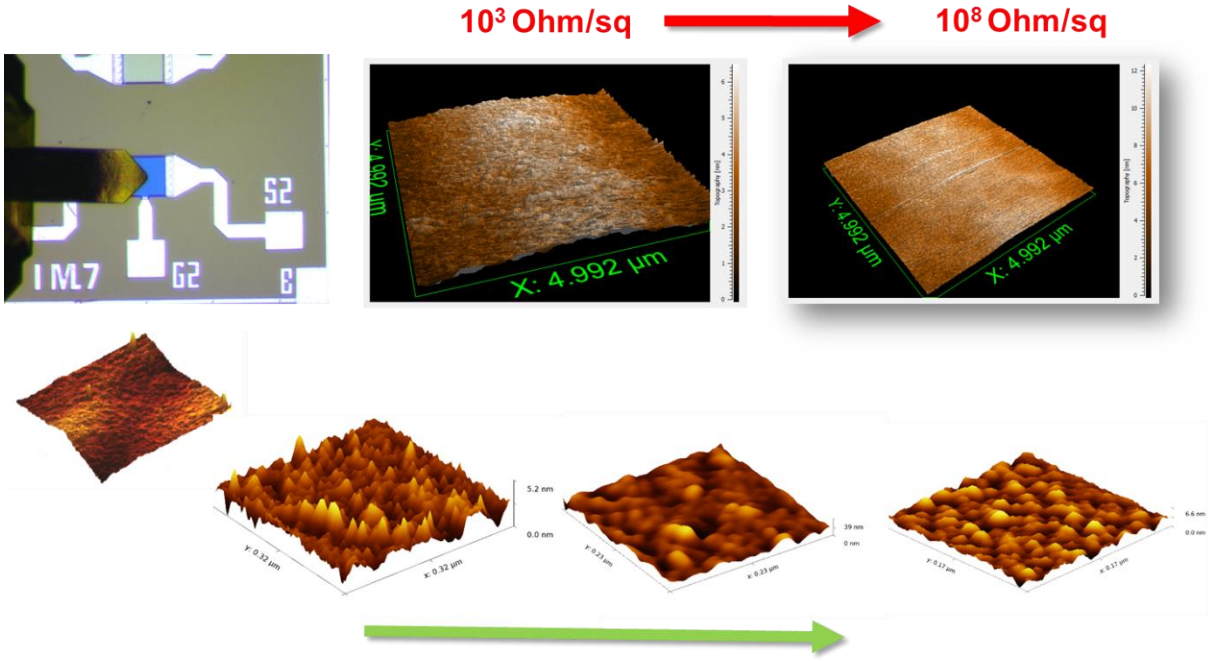

Figure 71 Tin oxide gate layer of the MOSFET spectrometer investigated with Atomic-Force Microscope.

The roughness of the gate layer of the N-channel MOSFET spectrometer has been investigated with Atomic-Force Microscope. This measurement was performed in order to get better understanding for the physical properties of the layer. The size of the Tin oxide grains represents the material sheet resistance. The sheet resistance of the collective layer plays important role in the performance of the whole sensor device. The Debye length is the distance over which a charge Q is shielded by the surrounded charges. When the conductivity of the collective layer is big, this means that in the Tin oxide layer there are many free electrons that can shield the charge attached to the collective layer surface and in this way, to prevents sensing of the charge (Ion) from the sensor. This is the reason why the collective layer sheet resistance was investigated and improved during this project.

Batch 4 – N-channel MOSFET spectrometer – dynamic electrical response:

This N type of sensors was used in chemical parallel characterization test of a N-channel spectrometer and P-channel spectrometer.

The measurements were performed under the same conditions as the described for the measurement of P-channel spectrometer sensors.

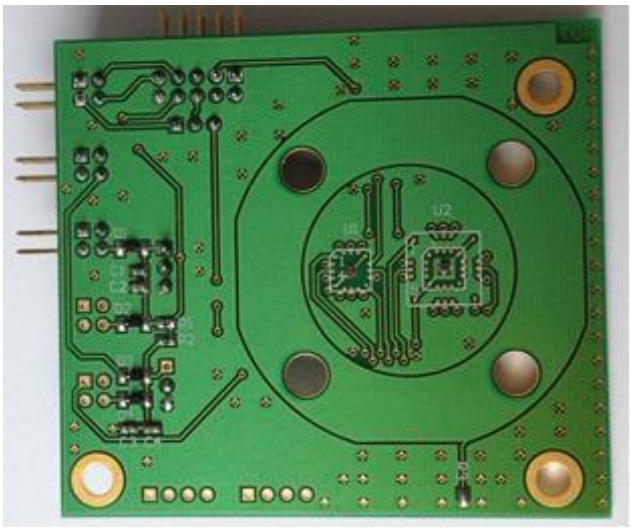

In figure 72 is shown the interface spectrometer PCB for parallel characterisation test of the spectrometer MOSFET sensors. The layout of the board allows attaching the sensors to the flange of a gas chamber and easy handling. On each PCB are glued and bonded 2 spectrometer chips, one N-channel and one P-channel MOSFET.

Sensors used in the current experiment, imaged with digital microscope are shown in figure 73.

Figure 72 The interface spectrometer PCB for gas measurements.

Substances used for the characterisation of the chemical characterisation of the Batch 4 spectrometers are the same as in figure 53.

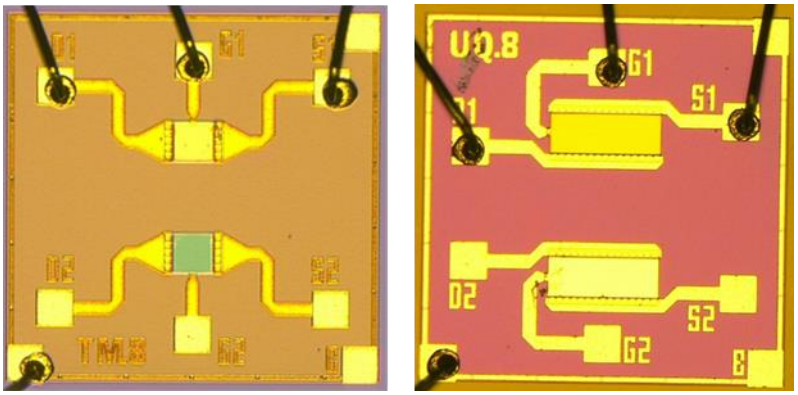

Figure 73 Microscope image of N-channel spectrometer Batch 4(on the left)) and P channel-spectrometer Batch 3 (on the right).

Figure 74 Image of the IAQSense software console developed by FACET.

Set of parameters used for the characterisation measurement can be seen in figure 73. The green signal of the oscillogram represents the switching drive signal of the spectrometer. The white (N-channel MOSFET spectrometer) and the red (P-channel MOSFET spectrometer) signals are the current true the drain-source terminals. The application allows having both signals plotted on the oscillogram window simultaneously and observation of the changes in the sensor behaviour. All rules of the safety measures are followed strictly during the experiment. Spectrometer sensor board with the MOSFET chips was in gas ventilation hood with constant airflow to prevent inhalation of the measurement substances.

Xylene measurement.

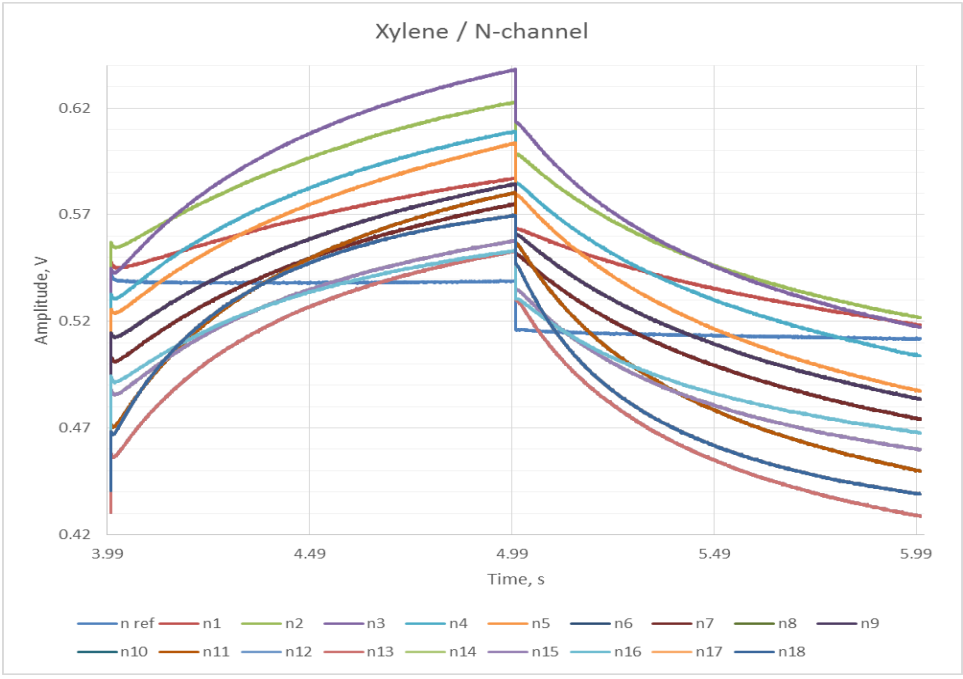

Figure 75 Full chart – Xylene measurement with N-channel MOSFET spectrometer.

Response of Spectrometer sensors for Xylene is different for N-channel MOSFET and P-channel MOSFET. Well seen from experiment is that, for Xylene, the shape of the signal for N MOSFET is changing a lot reaction is rapid and the measurement method does not allow us to see the previous stages of the signal but only already the steady state. For P-

channel MOSFET response is much slower, we observe an offset, signal is going down slowly and then there is change in shape of the signal. Process is not as rapid as the one for N-channel MOSFET.

Chlorbenzol measurement.

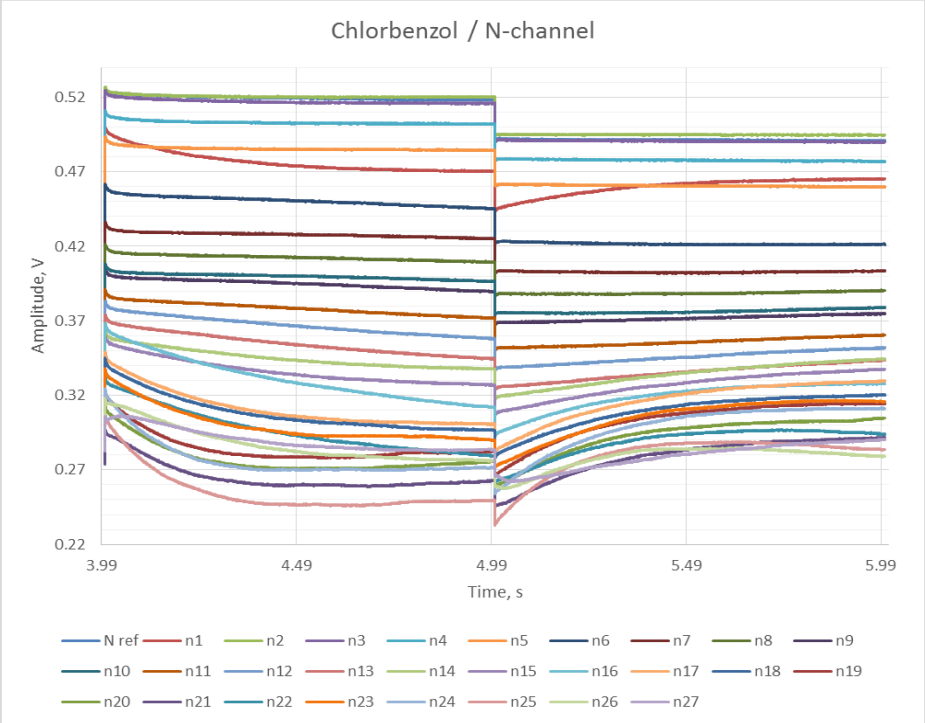

Figure 76 Chlorbenzol measurement with N-channel MOSFET spectrometer.

Results of Chlorbenzol measurement show very different behavior of both sensor in comparison with Xylene measurement. Reaction of N-channel MOSFET is very slow, first we observe offset, but no change in the amplitude. Later, some change in the shape of the signal occur but in fact the pk-pk Amplitude does not differ some much from the reference signal. Reaction of P-channel MOSFET spectrometer on the other hand is like the reaction of N-channel MOSFET for this substance, but with more significant change in signal shape.

Toluene measurement.

Spectrometer response for Toluene is very similar to response of Xylene. This can be explained with the structure of the molecule – quite similar for both compounds. If we have a look on N-channel MOSFET response we cannot see almost any difference, but P-channel MOSFET spectrometer has different behavior. Reaction is faster and the change in the amplitude is bigger. Slopes are steeper. Additional measurements are done after the end of Toluene measurement to see if sensor is recovering after the experiment with Toluene. This is shown in figures 61 and 78. Small offset is observed for both sensors, but this can be considered as normal. We are not sure about the exact room conditions and this offset can be caused by temperature or different composition of air.

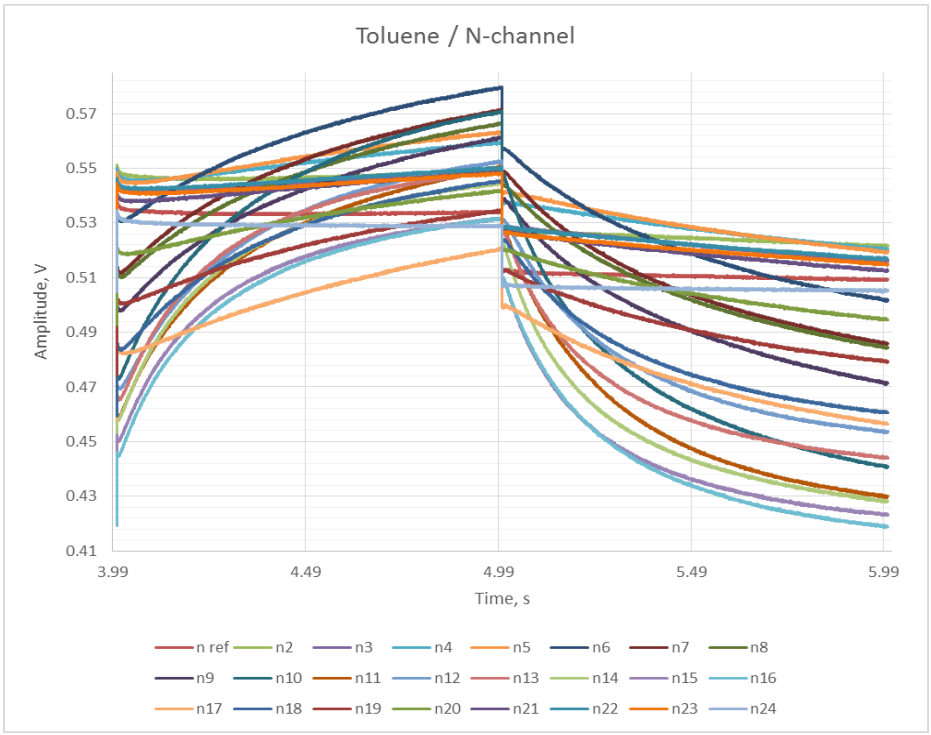

Figure 77 Full chart – Toluene measurement with N-channel MOSFET spectrometer.

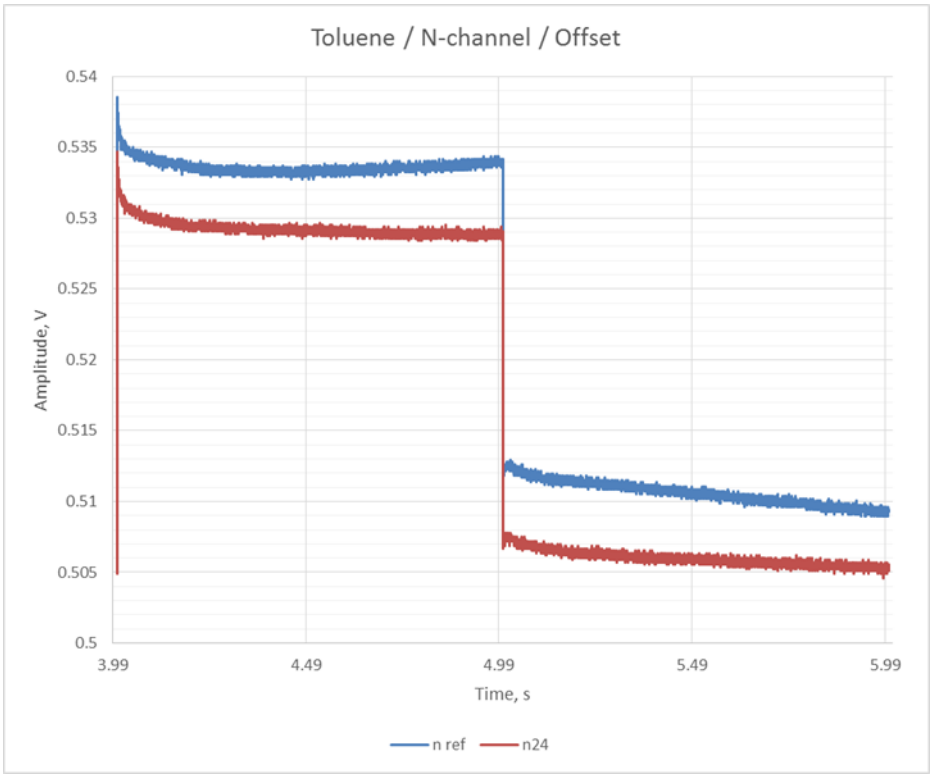

Figure 78 Toluene measurement – N-channel MOSFET Offset.

Butyl acetate measurement.

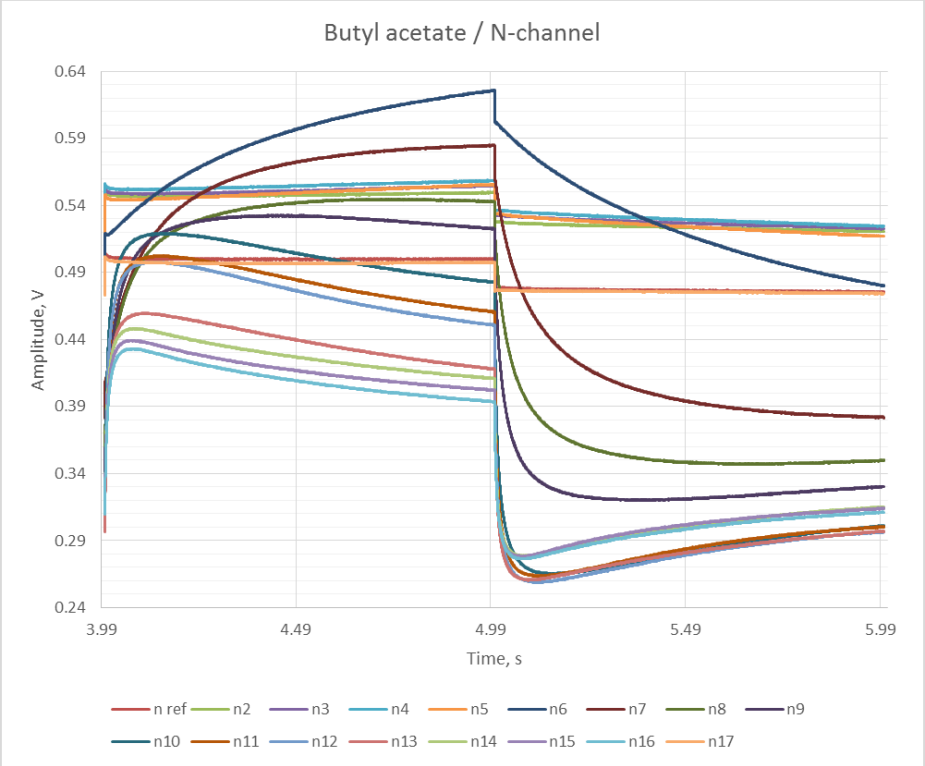

Figure 79 Full chart – Butyl acetate measurement with N-channel MOSFET spectrometer.

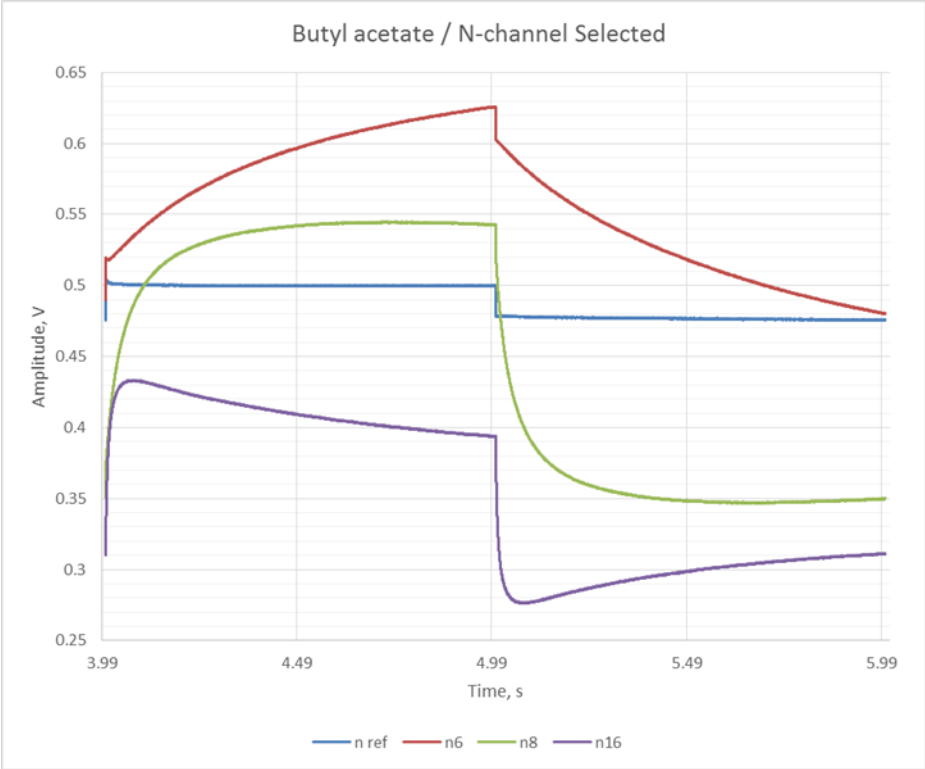

Figure 80 Selected signals – Butyl acetate measurement with N-channel MOSFET spectrometer.

Both P-channel and N-channel spectrometer MOSFET sensors react to Butyl acetate. In figure 80 are selected 4 of the most significant shapes of the drain current during the change in the concentration of the substance inside the chamber.

Methyl isobutyl ketone measurement.

MIBK measurements were performed first and although we know very well that the Spectrometer detects very good Acetone vapors, we did not expected so rapid and long reaction. Process of detection was very strong for both N-channel MOSFET and P-channel MOSFET.

The big number of measurement imposed dividing the full chart on 5 small charts, registered as a family of characteristics. Some of the most significant charts are illustrated below.

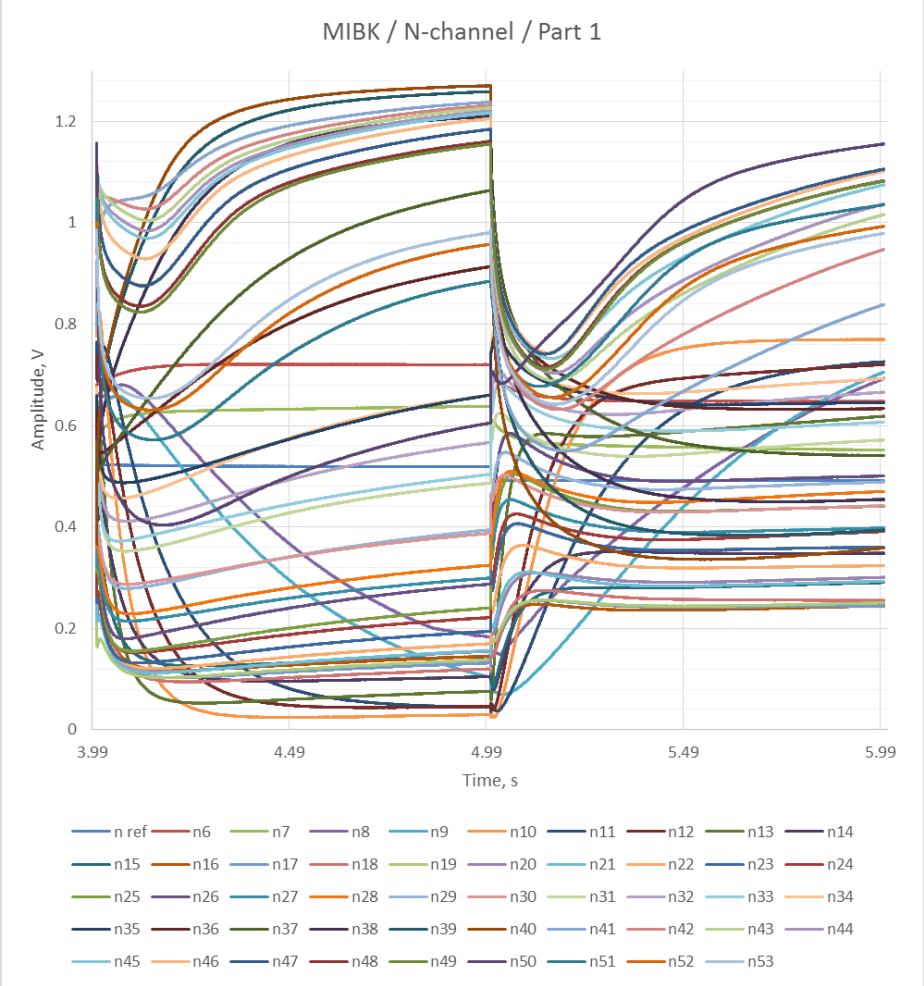

Figure 81 MIBK measurement with N-channel MOSFET spectrometer.

Results of MIBK measurement are the most significant and strongest of all five presented in this document. Amplitude of the signal is much bigger than reference signal for both – N MOSFET and P MOSFET. The most interesting is that for N MOSFET spectrometer first we observe negative offset, then the offset becomes positive. As expected, commonalities are observed between Butyl acetate measurement and MIBK measurement. For all substances is observed response. For some chemical compounds, we can see common behavior of the sensors. Combination of P-channel and N-channel MOSFET spectrometer is important from point of selectivity. The two types of sensors are complementary. The concentrations measured for this experiment are unknown, but is evident that response time is different for different substances.

Ionization measurements.

According to the principle of operation of the MOSFET spectrometer Ions have to reach the surface of a collective layer of Tin oxide that plays the role of gate of a MOSFET transistor. Modulating the drain current with a certain frequency brings the charges attached to the surface of the collective layer to move and to modify the field of the channel locally. Theoretically the ionised molecules attracted to the Tin oxide layer would acquire a negative or positive charge by gaining or losing electrons to form ions, often in conjunction with other chemical changes. This leads to change in the behaviour of the sensor.
To prove this experiment with LED Ionizer were conducted. The test setup is shown on figure 85. The LED is installed in a way that it influences only the N-channel spectrometer.

Figure 82 LED Ionizer.

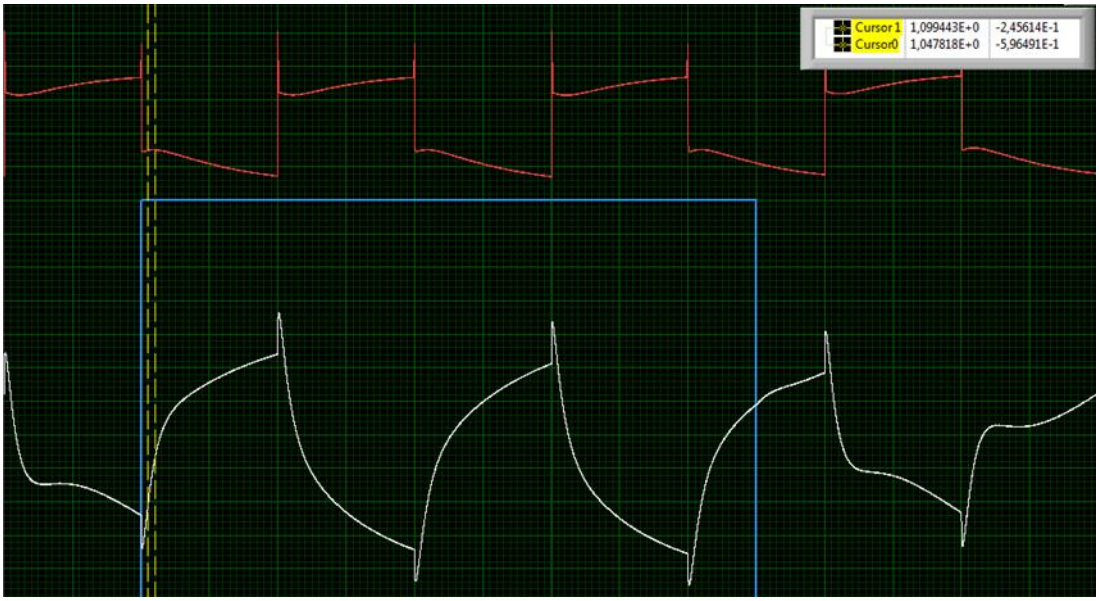

Figure 83 Measurement of Ammonium hydroxide with N-channel spectrometer plus Ion and P-channel without Ion.

Figure 84 Measurement of water vapours with N-channel spectrometer plus Ion and P-channel spectrometer without Ion.

In figure 83 and figure 84 are presented the results of the measurement of 2 different substances with MOSFET spectrometer transistors in the same measurement condition. The blue line shows the time interval of LED Ion operation. The current via N-channel MOSFET spectrometer is in white colour and the current via P-channel MOSFET spectrometer is in red colour.
The measurement illustrated in figure 83 has been conducted with NH_3. Both N and P spectrometers respond to the substance but LED is spotted only over the N spectrometer. In a result, it is observed significant difference in falling slope of the current via N spectrometer when the LED is ON and when it is OFF. The same experiment is performed with water vapours (figure 84). The result of the second experiment approves the influence of the Ionizer to the N-channel spectrometer.

Measurement laboratory setups.

The manufactured samples were tested in three laboratories. In the laboratory in Ilmenau, a test setup (figure 85) build by NANO was used for sensor pre-characterisation. The main focus of these measurement was to preselect sensor for the other project partners.

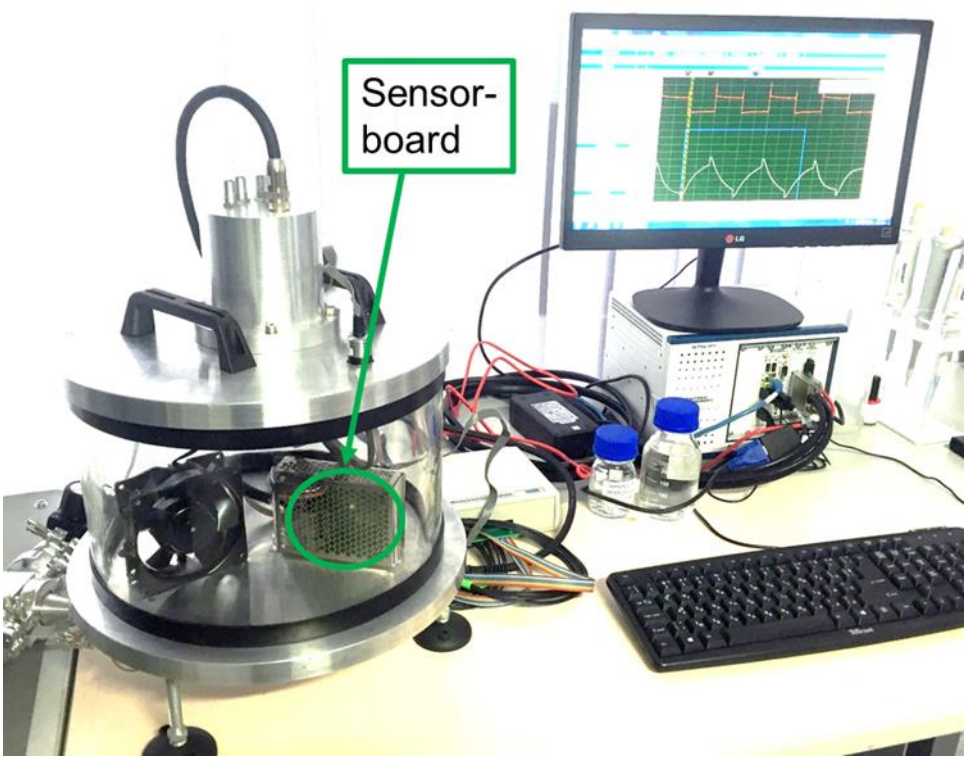

Figure 85 Measurement setup in nano analytik GmbH labs.

The characterization platform with software console for the setup was developed by FACET Bulgaria. For the purpose of gas characterisation measurements NANO has built a hermetic chamber that allowed experiments with volatile substances.

A second measurement setup delivered from FACET was installed in the labs of ISL. The focus of their work was concentrated in testing the spectrometer samples with hazardous substances.

A third measurement setup has been installed in SOFIA LABS (figure 86), where team led by professor Stefan Andreev made series of measurements to investigate the sensor behaviour.

Figure 86 SOFIA LABS - Owlstone setup on the left and FACET measurement console on the right.

A table with the possible measurement targets in SOFIA LAB in shown below.

Target	Molar mass	Formula	Permeation rate	Calibration temperature	Concentration at sample flow 125 ml/min
	g/mol		ng/min	°C	ppm *
Acetaldehyde	44,05	C_2H_4O	2839	50	12,63
Ammonia	17,03	NH_3	1098	50	12,63
Benzene	78,11	C_6H_6	1130,82	50	2,83
Formaldehyde	30,03	CH_2O	1048,87	90	6,84
Toluene	92,14	C_7H_8	831,21	50	1,76

The laboratory is Sofia lead my professor Andreev was supported by MICRO with a *OWLSTONE GEN-SYS* is a modular system for generating precise, traceable calibrated gas standards or relative humidity. The measurements were performed in strong collaboration between the partners that allowed discovering of a few strong effect and improvement of the MOSFET based spectrometer sensor.

Summary

- We have found out that the sensor response similarly decreased with an increase of the oxygen content in the film, while the response was found to be almost dependent of the film resistivity.
- The relationship between gas sensing properties and film stoichiometry was observed based on diffusivity and reactivity of the gases inside the Sn-oxide films.
- Further investigation on this phenomenon is highly recommended.
- Measurement set-up become to be a universal solution applicable and assessable for other European Users.
- We redesigned completely the measurement chamber.
- The packaging issue was solved in collaboration with FACET.

- The measured procedure was established in collaboration with Eff. Marketing.
- ISL developed successfully two sophisticated measurement chambers for each sensor.
- The obtained result is showing the operationally and performance of the transistor-spectrometer **confirming** the measurements and conclusions done during the meeting at NANO on 6-7.07.2015.
- NANO developed a set-up where rough calibration of the transistor-spectrometer is possible. Measurements in the range of 30 to 100ppm of Ammonia were successfully done.
- The experimentally observed dependence of the sheet resistance on the grain size and grain orientation of SnxOy films is correlated to the dependence of the electron mobility on grain boundary scattering.
- The electrical resistance of gate-thin film depends on the film stoichiometry.
- All theoretical predictions about the principle of operation and reproducibility are confirmed.
- The transistor-spectrometer selectivity for different species is evident.
- Further investigation should be focused on stoichiometry of the SnO_2-film with respect to grain size, thickness and doping.
- SnO_2 Layer deposited at high O_2 concentration, the SnO_2 dramatically influences the defect chemistry and the sintering behavior of tin oxide.
- More oxygen vacancies in the SnO_2-material, leading to a decrease in the free electron concentration and an increase in sensitivity of the material.
- Since film morphology has porous structure offer effectively more surface area for the sensing gas molecules to interact, SnO_2 thin films deposited at different sputtering conditions have been investigated.

Technology-Type 2: Tip-Field effect transistor

The second type of sensor is based on the patent of Prof. Ivo Rangelow – "Field effect transistor sensor" (TIP FET sensor). NANO owns the patent on this technology and this plays a key role in the protection of this sensor-technology and it is of strategic importance for this project, as well the future of this unique innovation. The technology type 2 is dedicated to specific species by its functionalization layer. The realization of the functionalization coating and its adsorption and desorption mechanics was investigated within this project.
The sensing principle has similarities with the sensor type 1, based on change of an electric field due to the adsorption of certain species on a porous layer but works in static regime only. The basic principle of this sensor is a FET placed on a micro-scale tip to enhance the overall sensing sensitivity, operated in constant voltage mode and with the source-drain current changing with the number of adsorbed species. The species are adsorbed by special functionalization coating which ensures selectivity. A sketch of this sensor-type is demonstrated (figure 87). The target operation of this sensor is the detection of hazardous species such as fungus (mold).

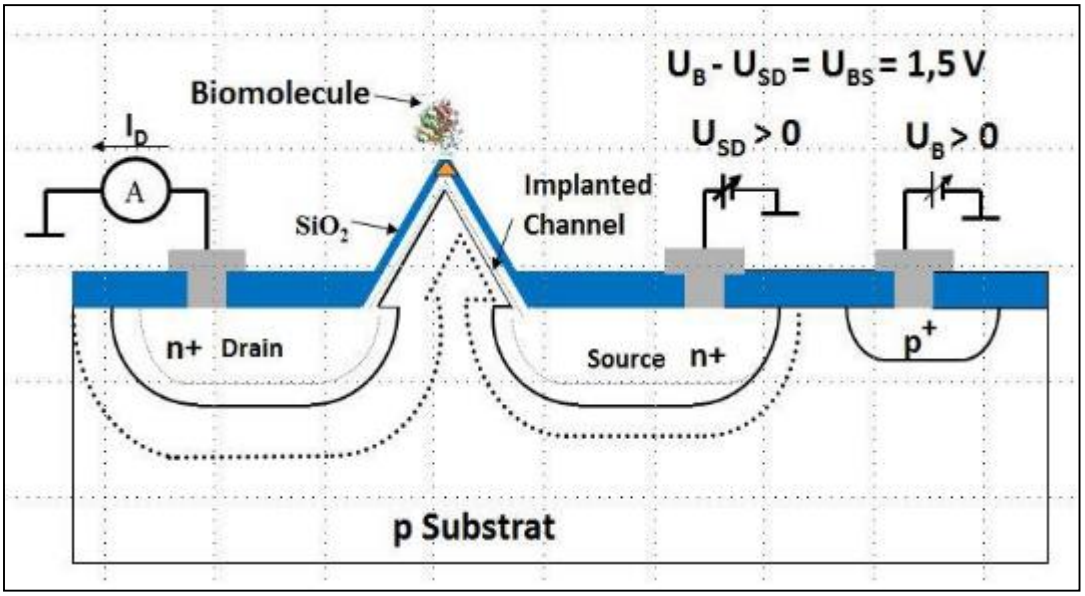

Figure 87 TIP FET transistor illustration.

TIP FET sensor was realized on 4" wafer in 16 designs in total. There are 4 layouts, and each one with 2 different dimensions. For each layout exist version with and without gate. The dimensions of all variations are listed below:

		V1 - L/W µm	V2 - L/W µm	V3 - L/W µm	V4 - L/W µm
SnO-Gate (G)	1.	40 / 4	40 / 40	40 / 4 D	40 / 8
	2.	100 / 10	100 / 100	100 / 10 D	100 / 20
- None - (nG)	1.	40 / 4	40 / 40	40 / 4 D	40 / 8
	2.	100 / 10	100 / 100	100 / 10 D	100 / 20

The layout includes a heater and a diode for temperature measurement and control.

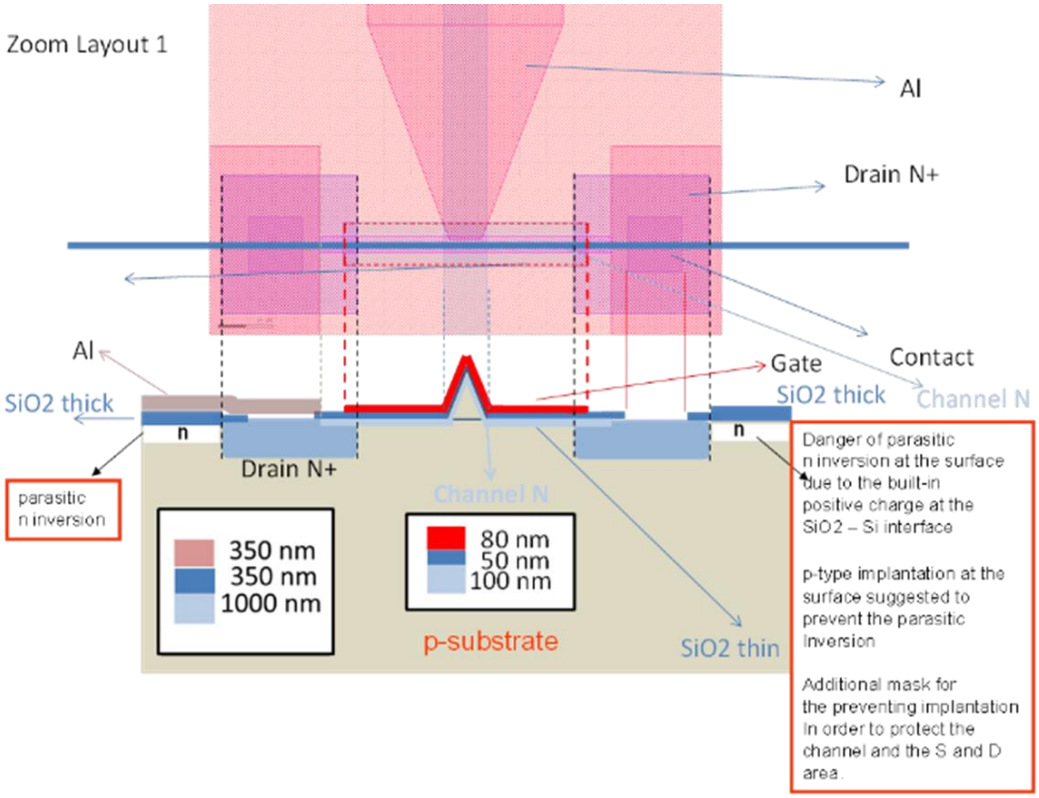

Figure 88 TIP FET mask layout and cross-section.

Detailed layout of the TIP FET sensor is shown in figure 88. Below the mask is illustrated the cross-section of the sensor. On a P substrate are implanted 1μm N+ source and drain regions and the channel between them with thickness of 100nm decreasing to the tip of the transistor. The channel is isolated with 50nm SiO_2 and covered with 80nm gate layer.

One of the biggest challenges in the process of developing this technology is the parasitic N inversion at the surface due to the built-in positive charge at the SiO_2 – Si interface. To prevent this additional p-type implantation was performed at the surface in order to eliminate the parasitic inversion. For this purpose, extra mask was used to protect already implanted source, drain and channel.

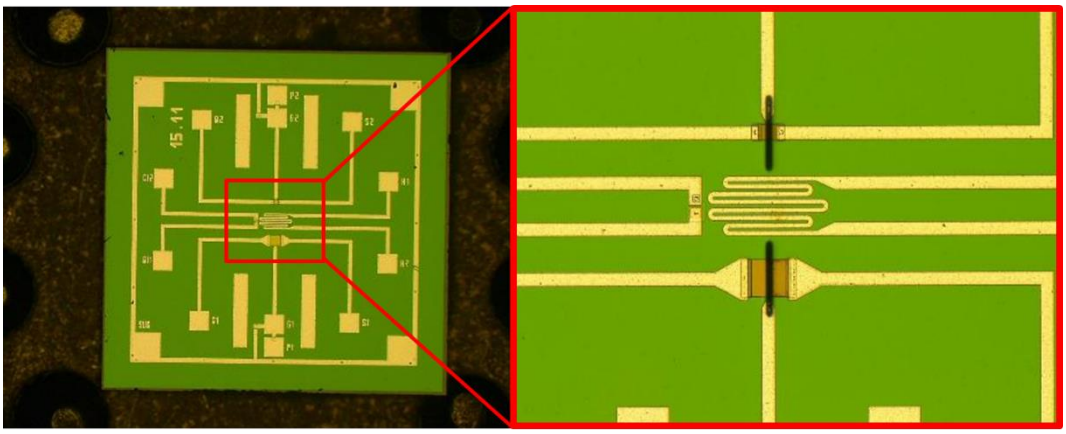

Figure 89 Tip field-effect transistor - optical image.

Tip field effect transistors were investigated with SEM. Images of the manufactured sensors are shown in figure 90.

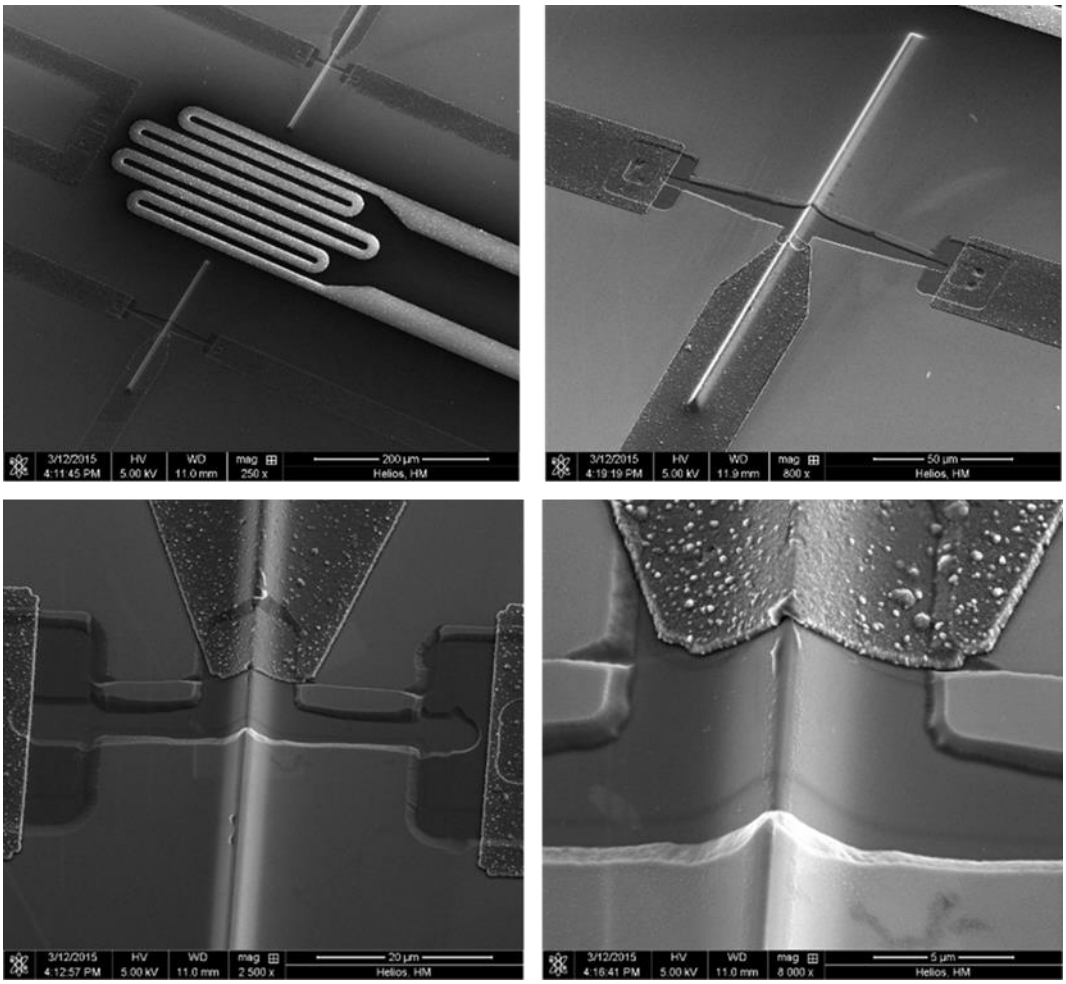

Figure 90 Tip field-effect transistor - SEM images.

Further investigations of the Tip field-effect sensors have reviled complex issues. Detailed measurement of the "Tip" showed sharpness in the range of 1 µm. This is quite large value that decreases or eliminates external influence to the transistor channel conductivity. Tip field-effect transistor conducts electrical current without gate voltage because of its implanted channel, but should not be completely saturated. To achieve manufacturing working device, NANO has developed technology for forming "Tip" transistors with sharpness in range of a few nanometers.

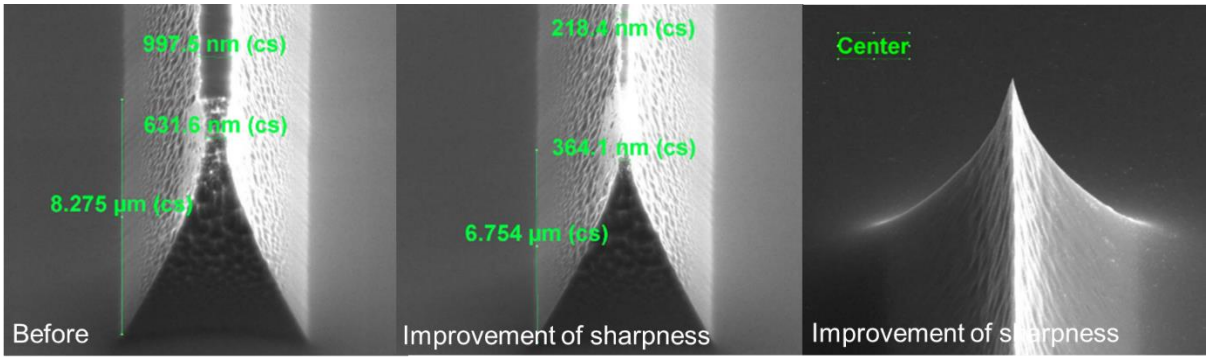

Figure 91 Tip sharpness development.

Big challenge for NANO during the establishment of the technology for Tip field-effect transistor was the “tip” height. This is another important parameter of the sensor characteristics.

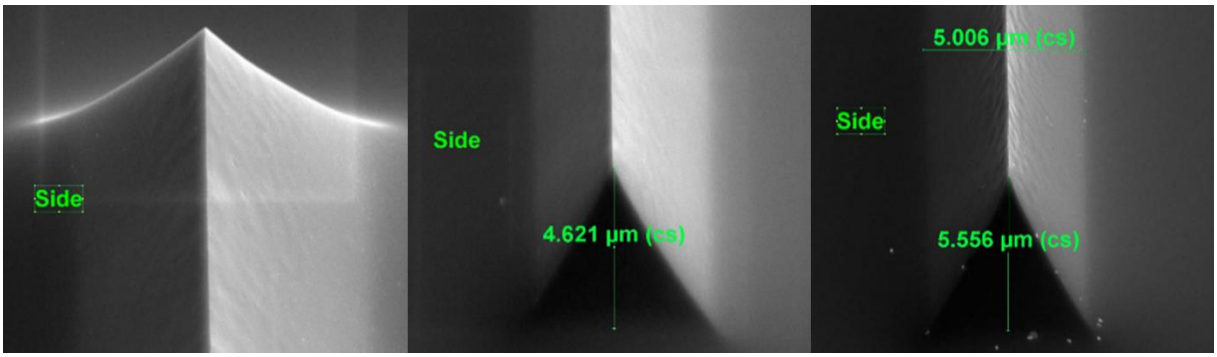

Figure 92 Tip field-effect transistor -SEM investigation of the "tip" height.

First runs of manufacturing tip transistor samples showed that the “tip” height is undefined. This has been proved by the electrical measurements – the channel of the transistor had to be modulated with external electrical field (see figure 93). Further runs allowed improving the technology for the forming of the “tip”.

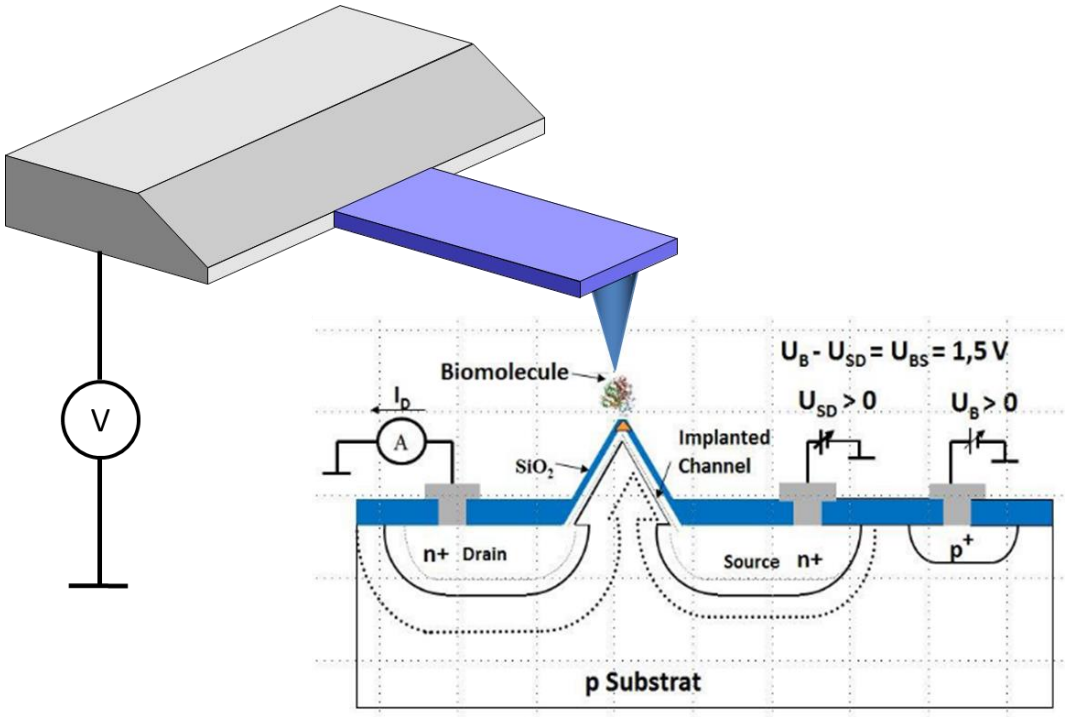

Figure 93 Tip field-effect transistor experimental measurement setup.

With a decision of the consortium, the development of this sensor type technology was stop in order to switch all resources for developing of other two technologies.

Technology -Type 3 (TT3): Nanostructured collectors on cantilevers for trace and ultra-trace sensing.

Technology description

The sensor works as nano-balance. The cantilever is an oscillating and capable of detecting atto mass-changes sensor.
The detection is based on reference, non-adsorbing device to be compared to the adsorbing one in terms of oscillating frequency. This way one chip should be composed of multiple different active layers/cantilevers and one reference using 4 places on the chip.
This principle is widely used in gas and mass sensing for example of "artificial noses".
The key aspects of this technology are: (a) sensor design, (b) sensor fabrication, (c) mass-detection readout technique (piezo-resistive), and (d) special functional coating to adsorb the species (nano-rods). NANO and ISL are the key partners in the development of this technology – are in the possession of unique knowhow on these key aspects.

Cantilever theory and modes of operation

The microcantilever is widely used component in the microsystem devices. Its flexibility and versatility make it a popular component for a variety of applications.

Cantilever static bending mode

This section is aimed at theoretical background of adsorption-induced stresses and definition of cantilever's spring constant, which will be widely used for further explanations. Figure 94 introduces a cross sectional drawing of a cantilever along with some designations. The most general relationship between the force exerted normally on the cantilever apex (F) and its displacement (Δz) can be defined using Hook's law:

$$F = -k \cdot \Delta z$$

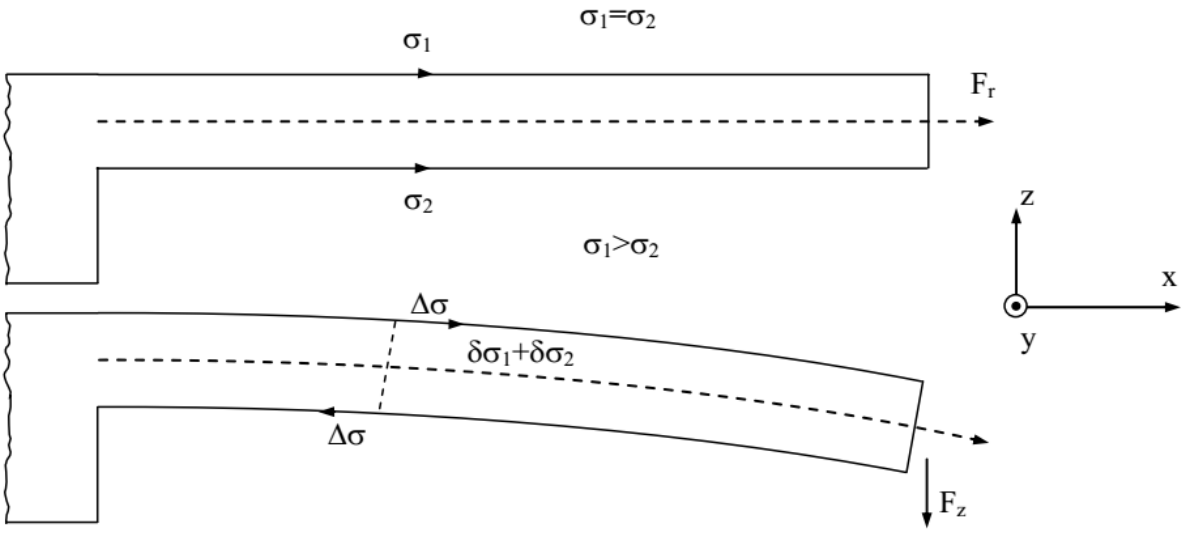

Figure 94 Cross sectional drawing of a rectangular cantilever. σ1 and σ2 – induced stresses on the top (σ1) and bottom (σ2) of the cantilever.

where *k* is spring constant of the cantilever beam, which denotes its elastic properties. This is a very important parameter for cantilever as a chemical sensor, because *k* is a subject to change when functionalized cantilever interacts with some media. In the absence of external gravitational, magnetic, and electrostatic forces, cantilever deformation is unambiguously related to a gradient of mechanical stress generated in the device.

Differential surface stress:

$$\Delta\sigma = \frac{d\sigma_1}{dz} + \frac{d\sigma_2}{dz}$$

Differential surface stress causes the cantilever with length *l*, width *w*, and thickness *h* to bend with the radius of bending *R*. A geometrical relation for *R* is:

$$\frac{1}{R} = \frac{d^2z/dx^2}{[1 + (\frac{dz}{dx})^2]^{3/2}} \approx \frac{3\Delta z}{2l^2}$$

which for a small amount of bending may be simplified to:

$$\frac{1}{R} \approx \frac{d^2z}{dx^2} \approx \frac{2\Delta z}{l^2} \approx \frac{M}{Y \cdot I}$$

Where R is furthermore related to the moment of the bent body (M), the moment of inertia (I) and the effective modulus of isotropic elasticity (Y):

$$Y = \frac{E}{1 - v^2}$$

Where E is Young's modulus and v is Poisson's ratio for the substrate (for silicon v=0.27). The area moment of inertia for a rectangular cantilever can be calculated as:

$$I = \int_0^w \int_{-h/2}^{h/2} z^2 dz dy = \frac{wh^3}{12}$$

Where w is the width and h is the thickness of the cantilever. If the bending moment is:

$$M = \Delta\sigma \cdot w \cdot h/2$$

Then if cantilever length l>>w, Hooke's law for small displacements can be re-written as:

$$\frac{1}{R} \approx \frac{d^2z}{dx^2} = \frac{M}{Y \cdot I} = \frac{\Delta\sigma \cdot w \cdot h \cdot (1 - v^2) \cdot 12}{2 \cdot E \cdot w \cdot h^3}$$

And finally, we obtain "Stoney's equation", originally derived by Stoney and von Preissig, which can in many cases accurately predict adsorbate-induced deformations of thin plates:

$$\frac{1}{R} = \frac{6(1 - v^2)}{Eh^2}\Delta\sigma$$

where R is the radius of microcantilever curvature, ν and E are Poisson's ratio and Young's modulus for the substrate, respectively, h is the thickness of the cantilever, and $\Delta\sigma$ is the differential surface stress. Knowledge of the radius of curvature R allows the tip displacement of a microcantilever with length l to be determined by:

$$\Delta z = \frac{1}{2}\frac{l^2}{R} = \frac{3l^2(1-v)}{Eh^2}\Delta\sigma$$

The Stoney's equation can be also equivalently presented as:

$$\Delta\sigma = \frac{Eh^2}{3l^2(1-v)}\Delta z$$

So, measuring the tip deflection like in AFM, one can derive the differential surface stress. The cantilever is rigidly clamped on one side and is free on the other. It has a length, l, and a concentrated force, F, acting on the cantilever at a distance a from the clamped side. The moment, which is produced by the force acting on the cantilever, is given by:

$$M = F(x-a)$$

Then the displacement Δz can be derived. Furthermore, by then setting $x=a=l$ we obtain:

$$\Delta z = -\frac{l^3}{3YI}F$$

Inserting this in Hook's law, given before and solve for k:

$$k = 3\frac{YI}{l^3}$$

Finally, assuming that $1-\nu^2 \cong 1$, the spring constant of a cantilever is calculated according to:

$$k = \frac{Eh^3w}{4l^3}$$

This interrelates the cantilever's spring constant and its geometry along with its material properties. Hereafter, this equation will be used for calculation of spring constant k as
measure of cantilever stiffness.
Such the way, the static mode considers bending of the cantilever through modulation of mechanical stresses due to either direct influence of the environment or thermal effects caused
by this influence. In the latter case, the presence of analyte species can be detected due to the
following phenomena:

- the heat associated with their adsorption on the transducer;
- the heat produced in the course of a subsequent chemical reaction on the cantilever
  surface.

Cantilever bending can also be driven by external gravitational, electrical or magnetic fields.
If the conversion of chemical energy into mechanical energy takes place directly, i.e. independently on the thermal effects, then the surface stress σ can be expressed by using the
Shuttleworth equation:

$$\sigma = \gamma + \frac{\partial \gamma}{\partial \varepsilon}$$

Where γ is the surface free energy. The surface strain $d\varepsilon$ is defined as the relative change in
surface area $d\varepsilon = dA/A$. In many cases, the contribution from the surface strain term can be
neglected and the free energy change approximately equals the change in surface stress. In its own turn, the surface free energy γ (or interfacial tension) is interrelated with the amount of adsorbed molecules on the cantilever surface by the Gibbs adsorption equation:

$$\Gamma = -\frac{C}{RT}\left(\frac{d\gamma}{dC}\right)$$

where Γ is excess of adsorption at an interface in a two-phase system, $d\gamma$ is the change in surface free energy and C is the concentration of the solute.

Previous two equations are appropriate to describe molecular adsorption processes at different
interfaces. Therefore, cantilever bending mechanism is compatible with many responsive phases and can function in both gas and liquid environments. Despite the static cantilever bending is a result of direct adsorbate influence, it is rather difficult to estimate the adsorbed mass quantitatively because the surface coverage is basically not known. However, cantilever operation at its eigenfrequency, enables accurate calculation of the amount of molecules adsorbed.

Cantilever dynamic resonant mode

The dynamic mode of the cantilever operation considers motion of the cantilever beam, which can take place either with or without forced excitation. The forced excitation can be realised by alternated fields of electric, electromagnetic, thermal, or acoustic origin. Furthermore, minute sizes and mass of microfabricated cantilevers makes them susceptible to thermally induced noise, which has the same origin as Brownian motion of small particles in liquids. Therefore, cantilever sensors may operate in the resonant mode with or without external excitation. The mechanically excited cantilevers require the presence of actuator, which causes the cantilever to vibrate. Practically, it can be achieved by either oscillating quartz crystal, which is in firm mechanical contact with the cantilever, or by integrated actuator employing bimorph effect. Normally, the actuator provides with periodic oscillations of the cantilever beam over certain frequency range near its natural or higher resonances.
Alternatively, pulsed excitation of the cantilever or amplification of the Brownian

motion of the cantilever beam (i.e. without forced excitation) gives also information on its frequency spectrum. Gain-frequency or phase-frequency responses of the functionalized cantilever gathered over a time interval reflect chemical or biological stimuli exerted on the cantilever. Resonance frequency shift of the cantilever under analyte exposition is mostly due to the additional mass loading, which is considered in the effective mass of a harmonic oscillator m_{eff}:

$$\omega = \sqrt{\frac{k}{m_{eff}}}$$

However, adsorption-induced changes in the elasticity of the cantilever beam and damping of the cantilever (its Q-factor modulation) are other two significant mechanisms for resonance frequency modulation.

Main objective

Development of nanostructured cantilever sensors permits to lower the detection limit of VOCs. The adsorption of VOCs molecules on the surface of an AFM cantilever modifies its resonant frequency by changing the mass of the oscillation sensor.

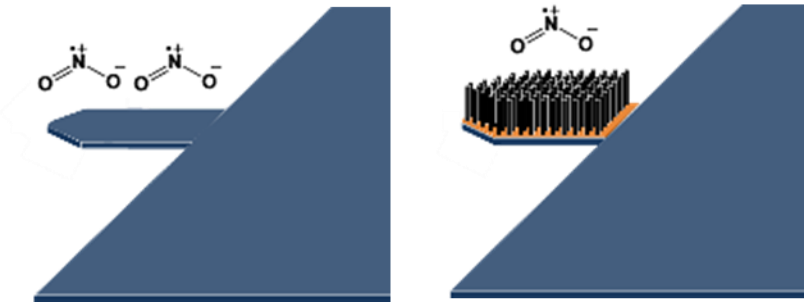

Figure 95 Development of nanostructured AFM cantilever.

Modification of the raw AFM cantilever with nanostructure (nanotubes) brings selectivity of the measurement sensing construction, and in the same time increase the sensitivity of the cantilever due to larger total surface of nanostructured cantilever.

A special designed electronic equipment and PC software for PLL (Phase-Locked Loop) detection allows continuous monitoring and recording of the cantilever resonance frequency and phase signal.

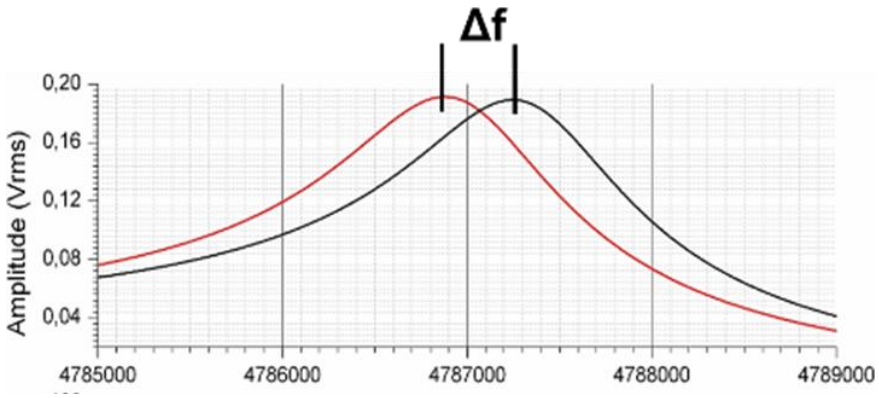

Figure 96 Cantilever resonance detection plots.

Any change in the cantilever measurement system leads to resonance frequency shift according to the theory described in "***Cantilever dynamic resonant mode***". The deviation in the resonance frequency can be calculated with the following equation:

$$\Delta f = -\frac{f_r}{2m_0}\Delta m$$

Where Δm is the difference in the mass of the cantilever sensor, m0 is the initial mass and f_r is the resonant frequency that can be presented as:

$$f_r = \frac{1}{2\pi}\left(\frac{1.875}{l}\right)^2\sqrt{\frac{EI}{\rho A}}$$

where ρ and E are the mass density and the elastic modulus of the material of the lever, respectively, I is its moment of inertia, A is its cross-sectional area and l is the cantilever length.

The material chosen for nanostructuring of the cantilevers is Cupric oxide (CuO) because it is commonly used for VOCs detection. It is popular material for sensing toluene[1], xylene[1], NO_2 [2,3], CO_3 …

[1] C. Yang, X. Su, F. Xiao, J. Jian and J. Wang, *Sensors and Actuators B:Chemical*, 2011, **158**, 299
[2] J. Park, B. Y. Yoon, C. O. Park, W.-J. Lee, C. B. Lee, *Sensors and Actuators B : Chemical*, 2009, **135**, 516
[3] W. J. Park, M. H. Kim, B. H. Koo, W. J. Choi, J.-L. Lee, J. M. Baik, *Sensors and Actuators B : Chemical*, 2013, **185**, 10

Development

The processing technology for this sensor-type is known by NANO. The coating process was transferred to NANO by ISL, to produce the entire sensor unit with one micro-machining process plan. There are variation parameters for the sensor design in terms of coating. The greatest challenge was to develop a straight-forward processing technology.

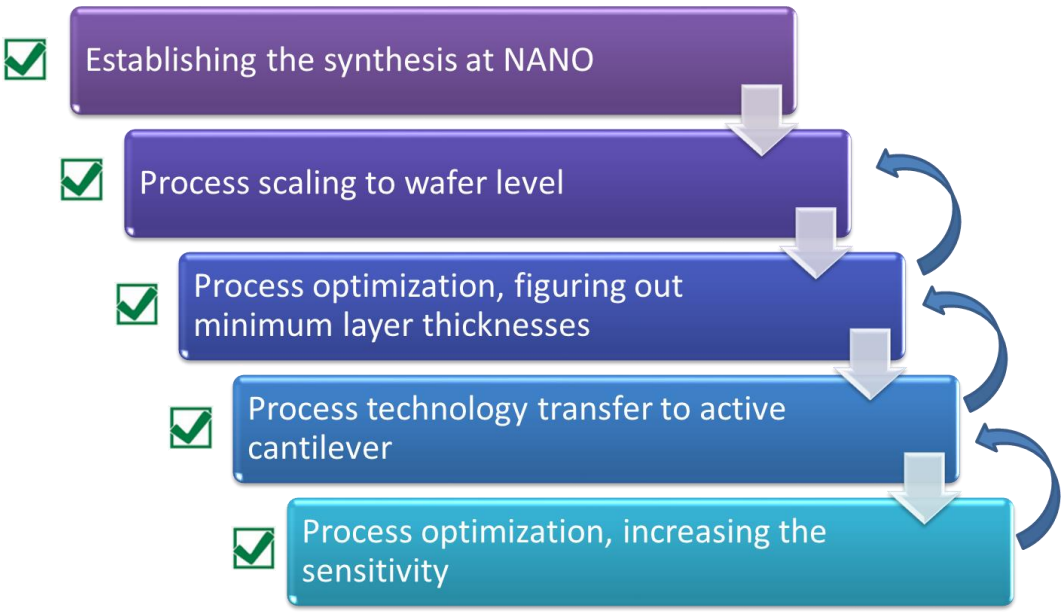

Figure 97 Roadmap for the objective wafer level transfer.

First important step of the realization of active piezo-resistive cantilevers with CuO coating was the synthesis of the cupric oxide nanotubes at NANO laboratories. With the support from ISL, the technology algorithm was transferred successfully.

Establishing of the synthesis of CuO nanatubes on silicon:

Step1 Evaporation under vacuum of a dense layer of copper.

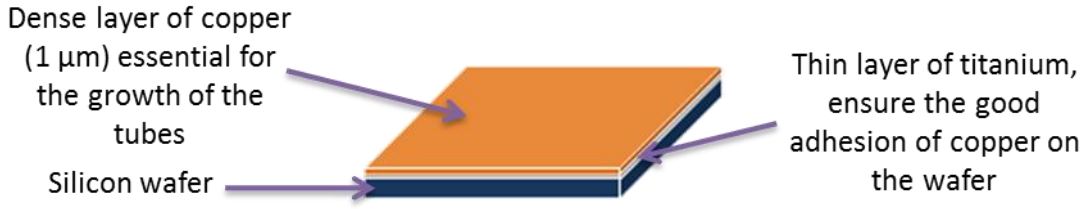

Figure 98 Preparation of silicon wafer for synthesis of CuO nanotubes.

Step 2 Growth of $Cu(OH)_2$ tubes with 2 successive reactions.

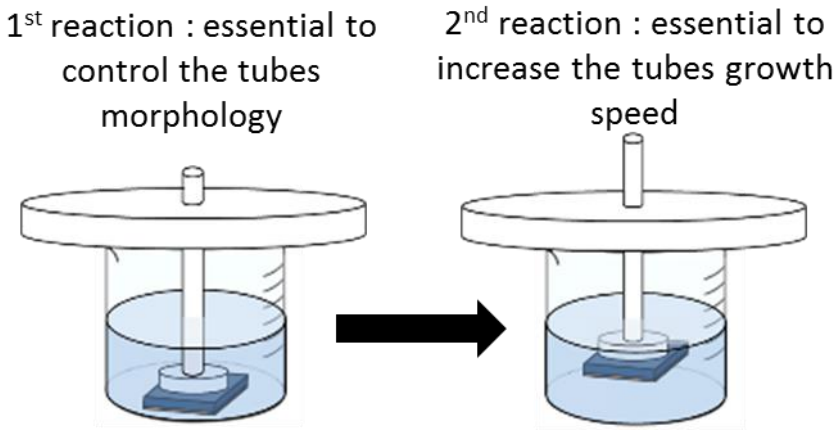

Figure 99 CuO nanotubes synthesis - wafer suspended upside-down very close to the bottom (100microns) on the left wafer upside-down, hight over the bottom on the right.

Both processes are running for 15 minutes each at room temperature. Diluted solutions are:

- Aqueous solution of sodium hydroxide (NaOH)
- Aqueous solution of ammonium persulfate ($(NH_4)_2S_2O_8$)
- Distilled water

Reaction : $Cu + 4NaOH + (NH_4)_2S_2O_8 \rightarrow Cu(OH)_2 + 2NH_3\uparrow + 2Na_2SO_4 + 2H_2O$

Step 3 Synthesis of CuO tubes by dehydration of $Cu(OH)_2$ tubes.

Sample annealed at 200°C during 1 hour under air

After the process of thermal dehydration of the Cu(OH)2 nanotubes, they are transformed into CuO nanotubes. SEM investigation of the nanostructured layer was performed to identify any morphological and dimensional in result of the annealing process.

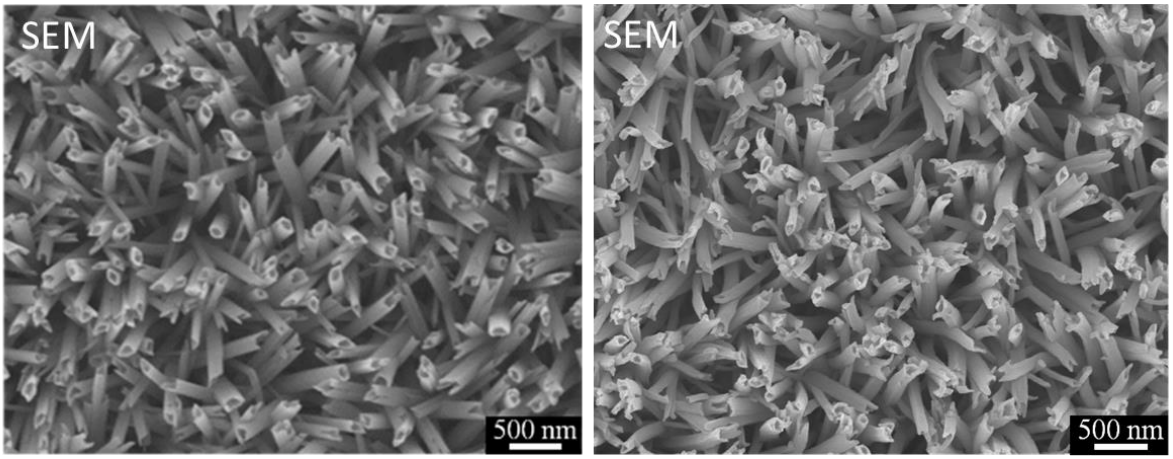

Figure 100 SEM images of copper oxide nanotubes before (on the left) and after (on the right) annealing.

The results of the measurement show that the morphology and the dimensions of the nano tubes are almost identical before and after annealing.

Growth of CuO nanotubes on a cantilever with optical readout.

The process of nanostructuring was applied first on a single passive cantilever.

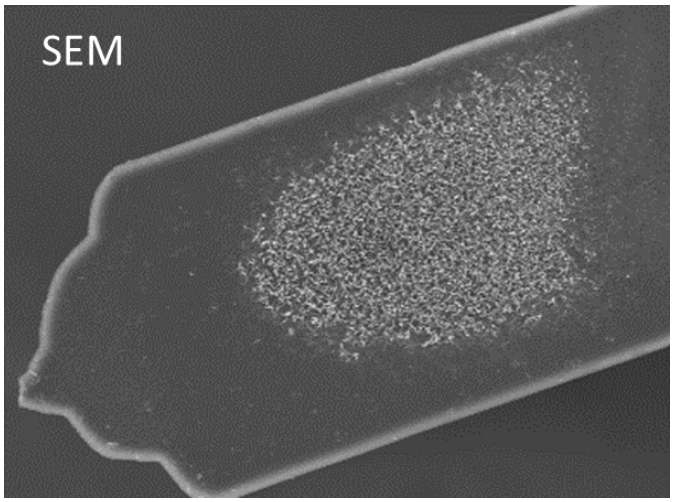

Figure 101 SEM image of nanostructured single passive cantilever.

The experiment was unsuccessful. The SEM investigation of the used sample showed no growth of tubes at the border of the cantilever.

A special procedure was developed for solving the “Boundary problem”. The whole cantilever chip was introduced in resin.

Figure 102 Procedure developed to overcome the border effect.

In figure 102 is illustrated the mechanism to overcome the border effect.

The cantilever chip is covered with layer of resin (a). The second step of the procedure is evaporation of a titanium/copper layer and growth of CuO nanotubes (b), followed by dissolution of the resin(c).

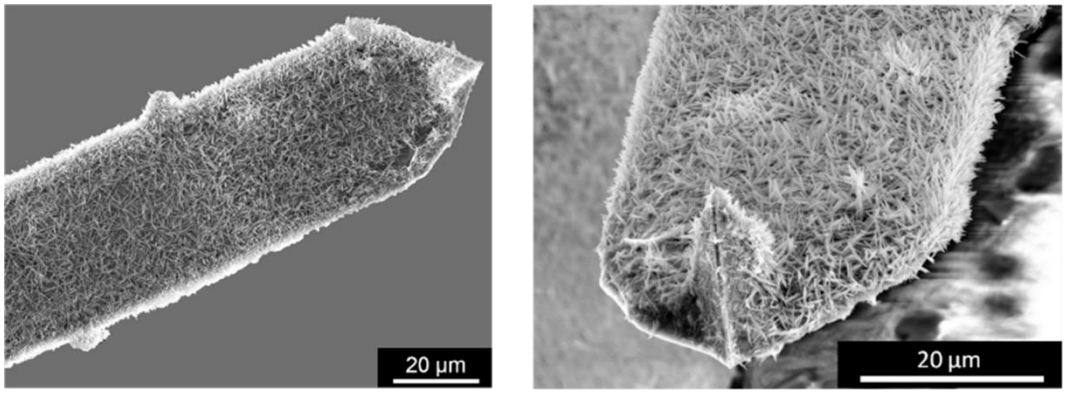

Figure 103 SEM images of nanostructured passive cantilever.

Result obtained with the procedure is shown in figure 103. No border effect observed.

Production

The production of the sensor is based on standard SOI-technology. The realization requires only a few standard micro-fabrication steps, such as lithography and oxide etch. The functionalization coating was done with collaboration with ISL at NANO laboratories.

With a decision taken after discussion between NANO and ISL the synthesis of nanotubes was transferred directly on a wafer level piezo-resistive cantilevers. The active cantilevers have one side “busy” with the integrated thermos-mechanical actuator for the excitation of the cantilever and Wheatstone bridge for measuring the cantilever deflection. For this reason, the CuO had to cover only the opposite side of the cantilever beam.

The process of growth of CuO nanotubes includes usage of NaOH, so the synthesis of nanotubes on a ready silicon wafer (Membrane) before the final etching procedure that allows the formation of the cantilever was challenging.

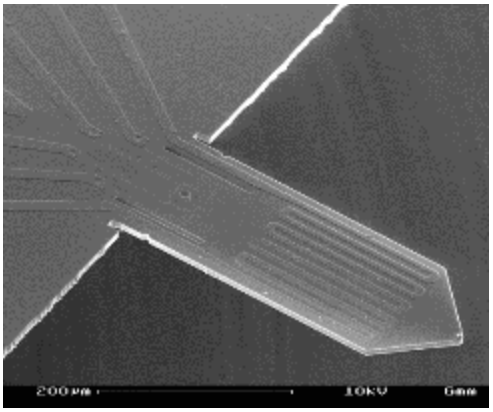

Figure 104 SEM image of an active piezo-resistive cantilever. Side with electrical circuits.

Nano found a resin able to protect the electrical circuits composed with aluminum, because aluminum is immediately dissolved in the nanotubes reaction solution.

The synthesis of CuO before final etching of the cantilevers was performed the SEM investigation showed that the achieved result is much different than the expected one. The morphology and the number of tubes for a given surface have been changed (See image 105).

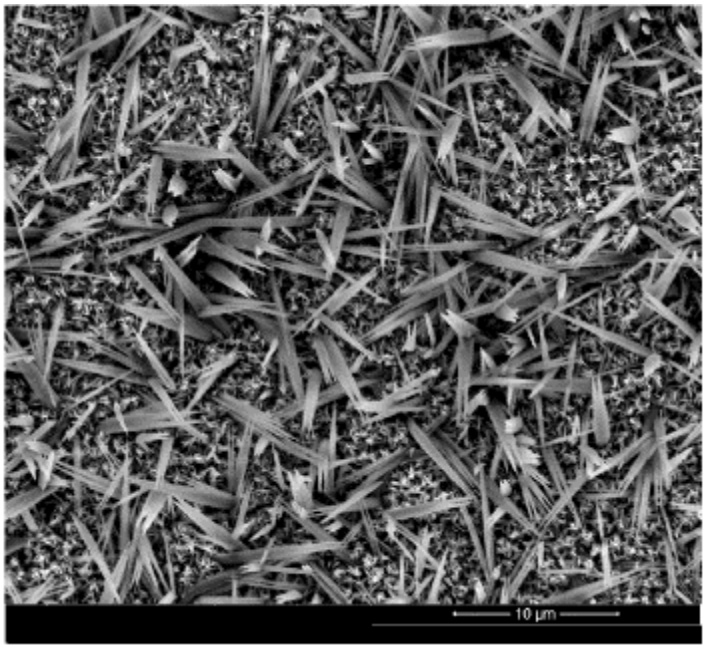

Figure 105 SEM image of CuO nanotubes synthesized on a cantilever membrane before final etching procedure.

The solution of the problem was shifting the synthesis of nanotubes as a final step of the sensor manufacturing. The ready cantilevers were protected with special resist to protect the electrical circuits integrated on the cantilever and to prevent growth of nanotubes on the sides.

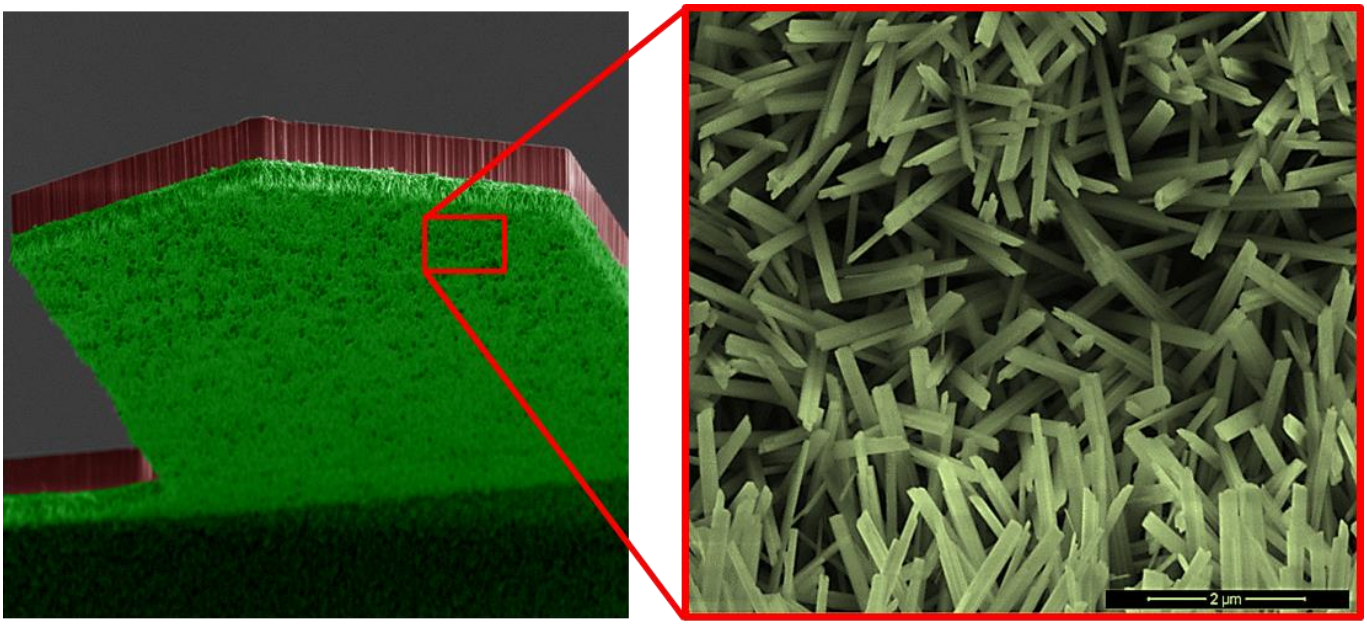

Figure 106 SEM image showing the top side of piezo-resistive cantilever with CuO nanorods.

In figure 106 is presented SEM image of ready active cantilever with piezo-resistive readout, functionalized with CuO nanorods. The technology was established and ready for mass production on wafer scale.

High-frequency active piezo-resistive cantilever

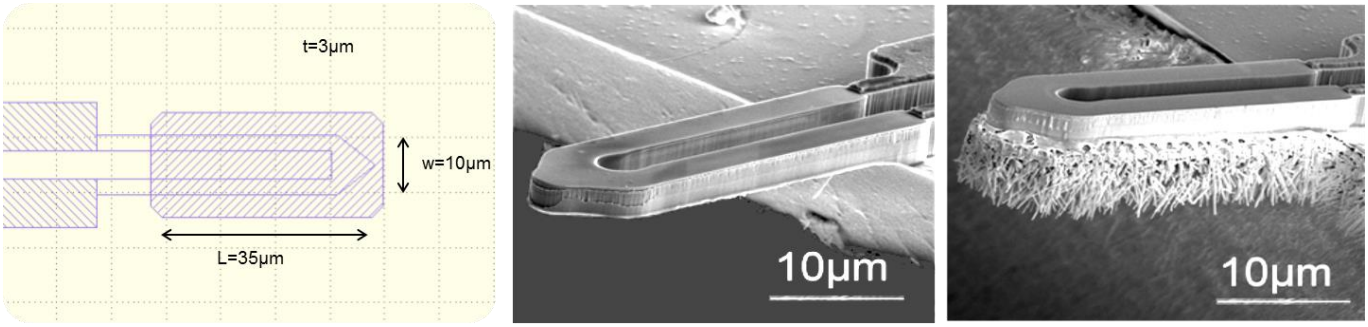

This is the smallest cantilever in the world with integrated read-out. The activation of this type of cantilevers is realized with external piezo crystal because the resonant frequency of the samples is too high for thermos-mechanical actuation technology, which is reaching the limits around 1MHz.

The functionalization available for this type of cantilever sensors is $Cu(OH)_2$ and CuO.

The technology is processed on wafer scale and it is ready for mass production.

Development of the detection device. Principle of operation.

The measurement setup was developed by ISL, where all characterization measurements with functionalized cantilevers have been performed.

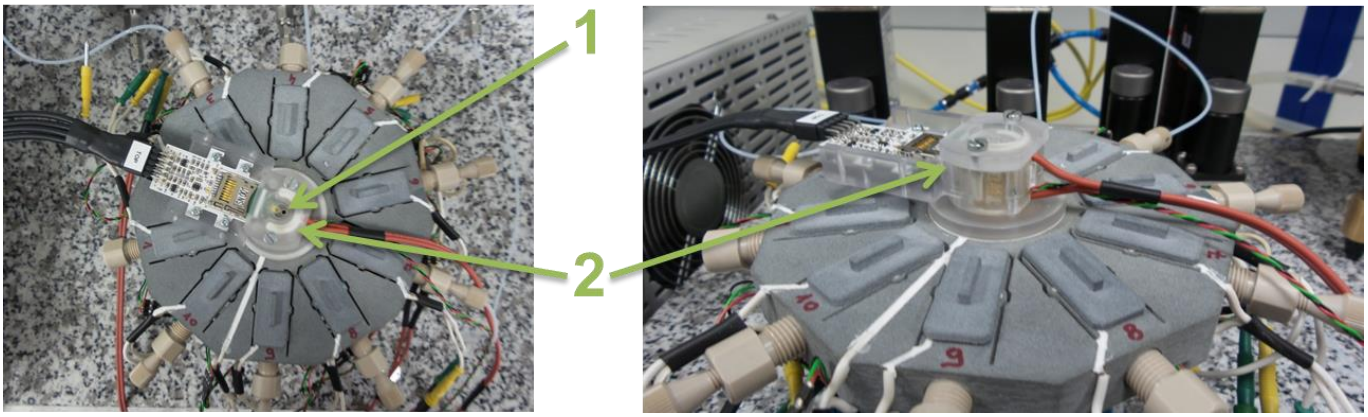

Figure 107 Test setup for characterization of active piezo-resistive cantilevers.

In figure 107 are shown images of the measurement setup for cantilever sensor gas characterization. The setup has 10 capsules that allow measurement with 10 different substances. In the center of the chamber is mounted the cantilever sensor covered with chamber lid (2). Presence of 2 holes (1) allowing the elimination of the gases ➔ dynamic detection.

Cantilever sensor is bonded on a green PCB holder that is connected in a white board, that produces the sensor supply voltage and amplifies the sensor signal. Via coaxial cable the sensor signal is delivered to the input of system controller, where the signal is processed and the frequency shit is measured.

Improvement of the detection device

A modification of the gas temperature and of the air flow allow to control the gas concentration. This allows measurement of the real concentration of the pollutant.

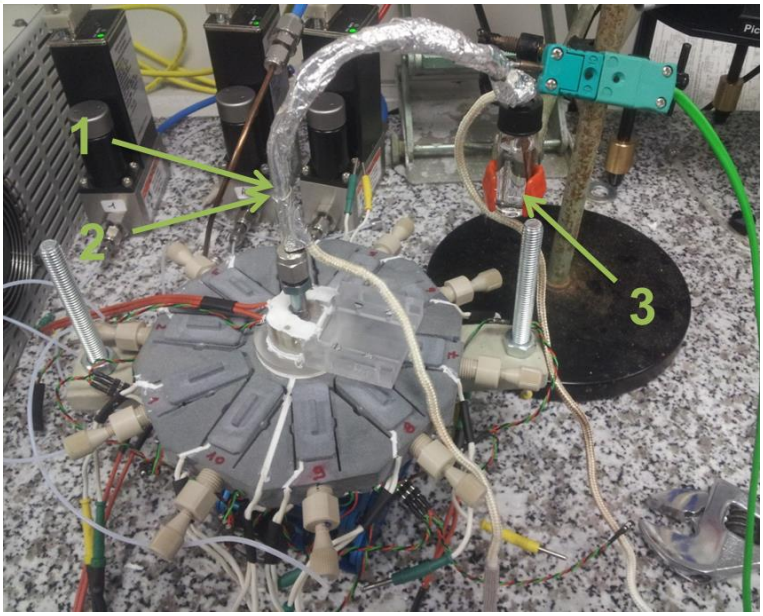

1. The air flow containing the pollutant goes through an inert tube
2. The tube is surrounded by a heater and by a thermocouple in order to avoid possible condensation
3. Methanol solution. The flow containing the pollutant is bubbled in this solution to dissolve the pollutant in the solution.

After dissolution of the pollutant in the methanol solution, the concentration is measured by HPLC (with a calibration curve)
➔ After measurement the real concentrations are relatively close to the theoretical ones

Improvement step - Addition of a bubbler to avoid external contamination.

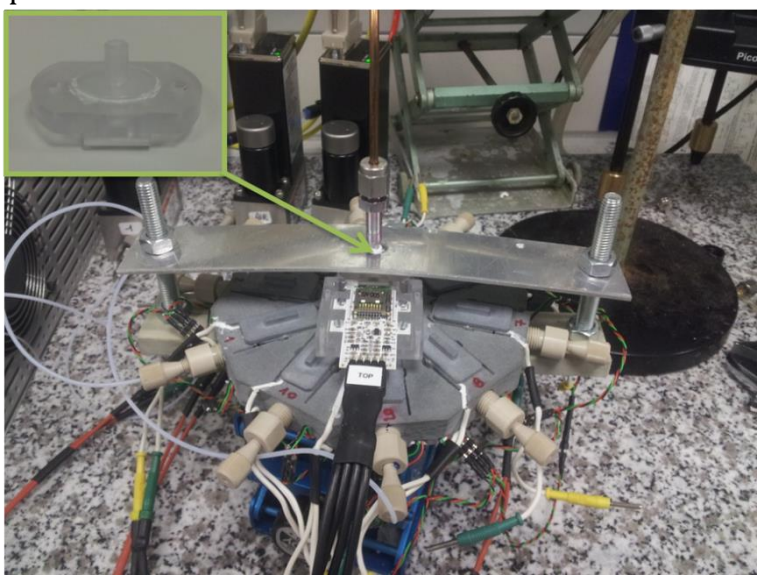

Figure 108 Image of the measurement setup for active piezo-resistive cantilevers - improved.

3Modification of the lid - a top part is added to fix a tube which can be connected to a bubbler to avoid possible contamination coming from outside. There is possibility to measure the value of the flow and to detect possible leakages.

Measurement results achieved with piezo-resistive cantilevers functionalized with CuO nanorods.

Explosive detection results.

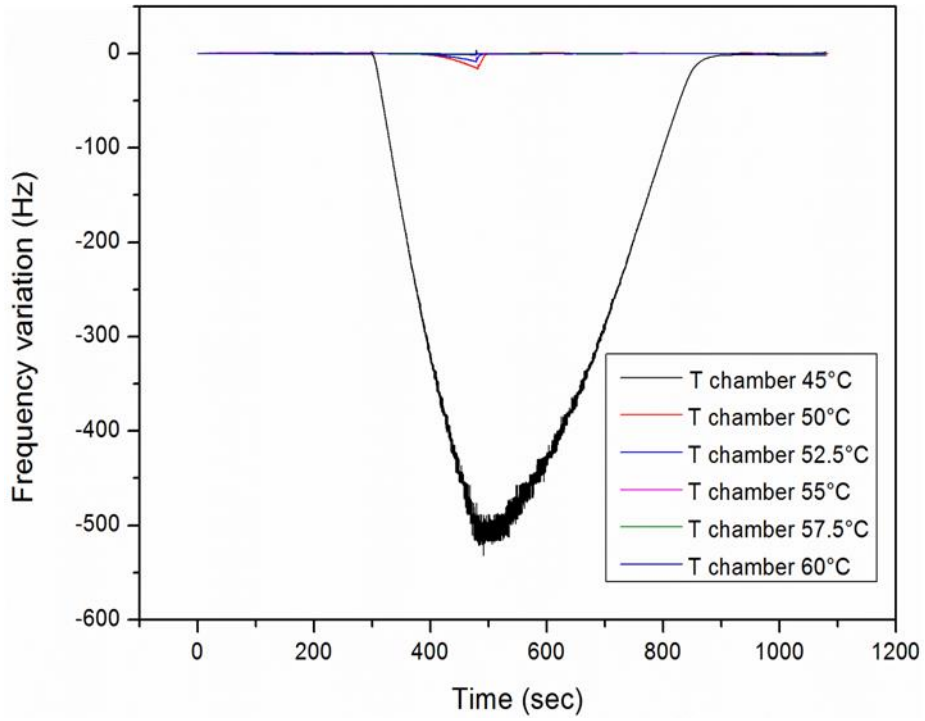

Figure 109 Concentration: 830 ppb of explosive.

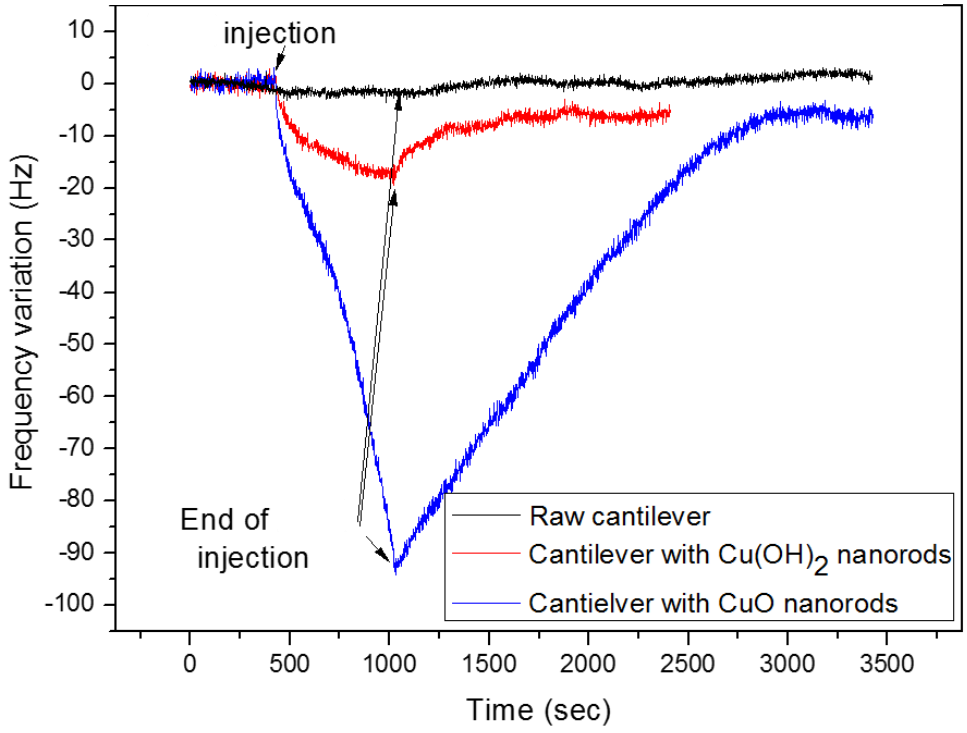

Figure 110 Concentration: 15 ppb of explosive.

In figure 109 and 110 are presented the results of explosive gas measurements performed with 3 different type of cantilevers. Sensors without functionalization do not show sensitivity to the measurement substances, or at least no frequency deviation is observed (figure 110 black line). The second type of sensor used in the characterisation

measurement is active cantilever with $Cu(OH)_2$ nanorods (figure 110 red line). At the moment of the injection of the explosive (concentration 15 ppb) is observed frequency shift of 20Hz. The result of the measurement with piezo-resistive cantilever with CuO nanorods (figure 110 blue) is the most significant. The deviation of the frequency is more than 90Hz for concentration of 15ppb.

At the moment when the gas emission is stopped the functionalized sensors slowly start to recover, and return to the initial state.

NO_2 detection results

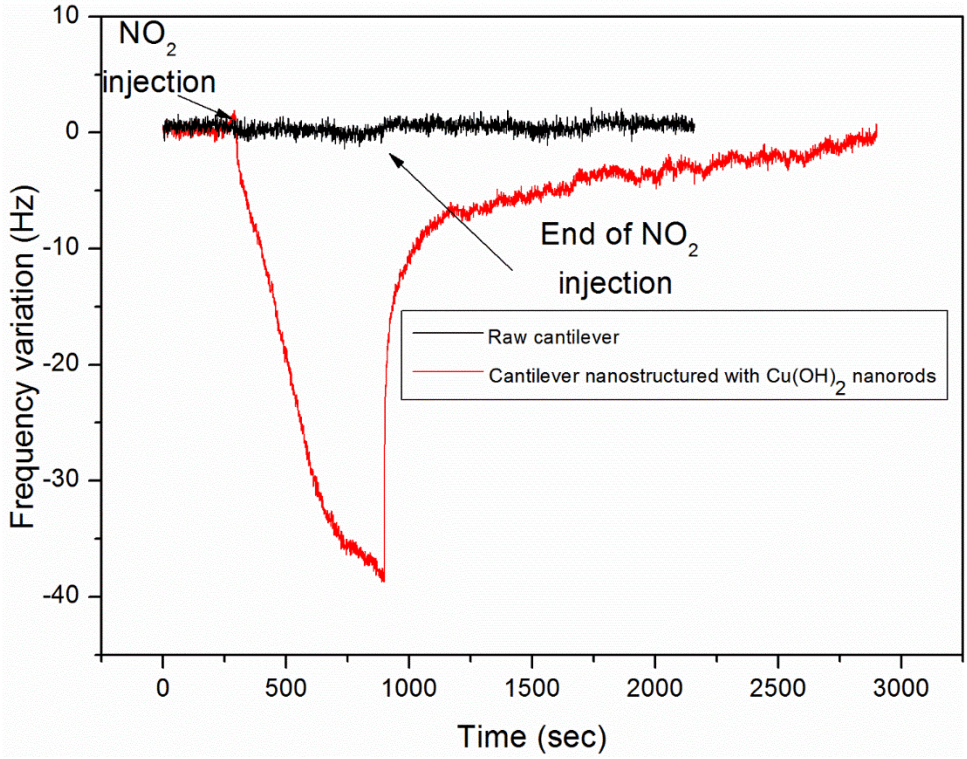

Figure 111 Active piezo-resistive cantilever - Nitrogen dioxide measurement.

Baseline: Air flow of 125 mL/min NO_2 flow 125 mL/min

Cantilever temperature: 55°C NO_2 temperature: 40°C

The result of the NO_2 measurement presented in figure 111 compare the response of a raw cantilever sensor to the response of nanostructured cantilever with $Cu(OH)_2$ nanorods. After injection of the substance no change in the resonance frequency of the raw cantilever (figure 111 black) is observed. The nanostructured cantilever (figure 111 red) result is very significant. Frequency shift is almost 40Hz.

Summary

- Modelling, development, fabrication and demonstration of small mass-sensitive cantilever-resonators have been realized
- The measurement time are a few seconds and is based on the transduction of chemical or physical processes into a mechanical response.
- The fabrication technology of small cantilever-resonators (fc>1MHz) functionalized with Metal-Oxide-Nanotubes (MOxNT) and Metal-Oxide-Nanorods (MOxNR), equipped with actuation have been shown. It allows the simultaneous detection of cantilever oscillation and bending by means of nano-electronic piezo resistive 1(2) DEG circuity.
- A novel Chemical - "lock-in" due to post-functionalization of the cantilever-resonators for ultimate chemical selectivity and sensitivity have been shown. Further investigation employing Chemically Modified Metal-Oxide Nanotubes (ChMMOxNT) and Chemically Modified Metal-Oxide Nanorods (ChMMOxNR) are needed.
- The development and realization of a portable, low-power device allowing network operations is in place.
- Specialized characterization chamber for cantilever characterization is in place.

Preparation of the test environment and the platform for system integration (sensors + MEMS + IC) and preparation of the test environment (hardware and software) for the sensing heads and follow-up of the test results.

Subtask – Detection system for nano-functionalized cantilevers.

Objectives

- To ensure the electrical test of the different components (technologies) and sub-components of the sensing head to release working heads for further characterization,
- To provide the characterization platform to the different actors of the characterization step. It will provide datalogging of the responses to different gases or molecules,
- The platform should also provide the necessary flexibility to install signal processing of the data logs (batch processing) to prepare the future integrated real time algorithms.

Results

Cantilever based mass detection system

Status and the end of period 1, reported Feb 2015

Two-channel system developed by MICRO and provided to WP3 partners. The system consists of mass detection controller and control and data processing software.

The plan for further development was oriented in following directions:

- Decreasing the size and cost of the hardware;
- Adding wireless connectivity;
- Increasing the number of channels to eight;
- Performing experiments with functionalized cantilevers, proving the sensitivity of the system to be same or better compared to one developed in Period 1.

System miniaturization

The first step towards the decreasing the system size was to develop an intermediate prototype having two channels, but smaller size and cost. The system re-design done by MICRO was based on Red Pitaya™ platform. The system fully covers the functionality of the platform designed in Period 2. In addition:

- It has smaller size (credit-card footprint);
- Ethernet connectivity channel was added.

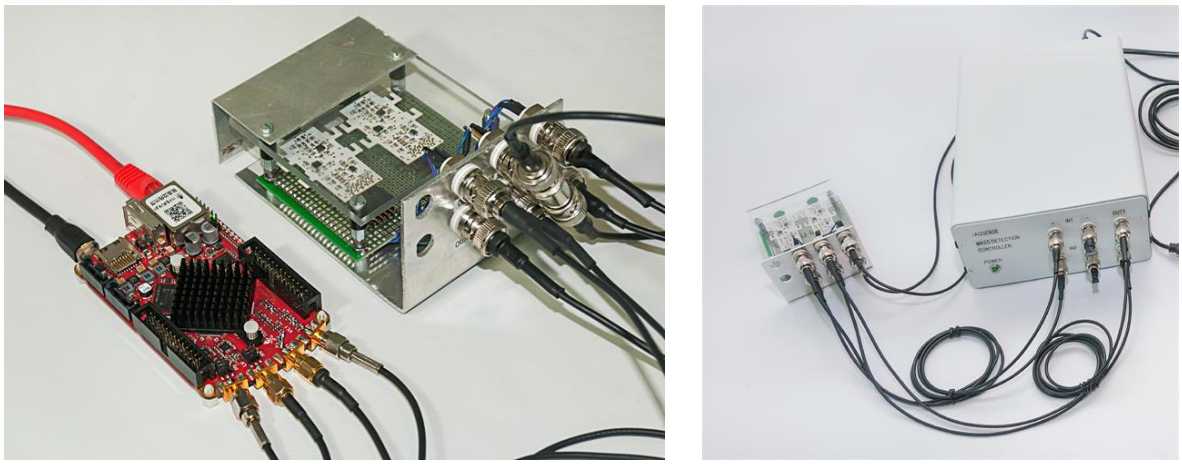

Figure 112 Comparison between two platforms. Same preamplifier head with two cantilevers used as a reference. New system based on Red Pitaya platform (on the left) and two channel system developed in Period 1 (on the right).

Figure 112 shows the comparison in size between two system which have identical functionality.

Eight channel system for sensor networks

The next step was to develop the eight-channel system with added wireless connectivity. The new system is intended to serve also as an engineering / pre-production prototype for further commercialization.

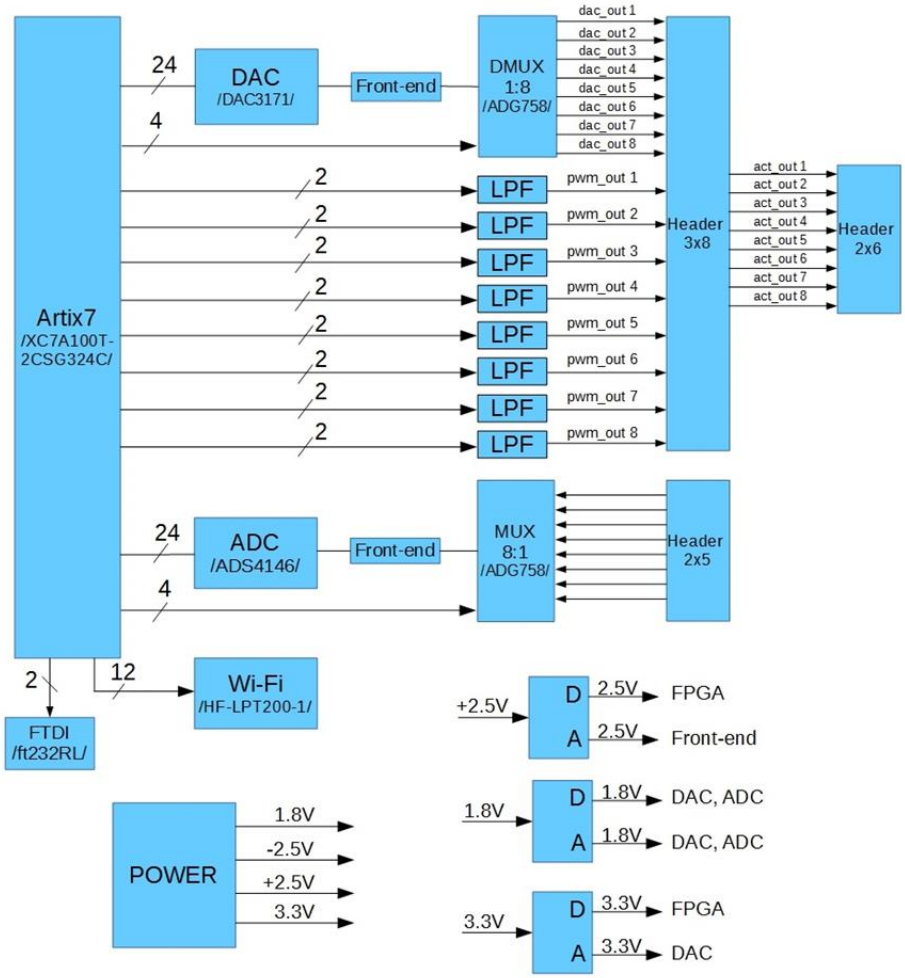

Figure 113 Functional diagram of eight channel system.

The system architecture (Fig. 113) allows different actuation modes to be combined,

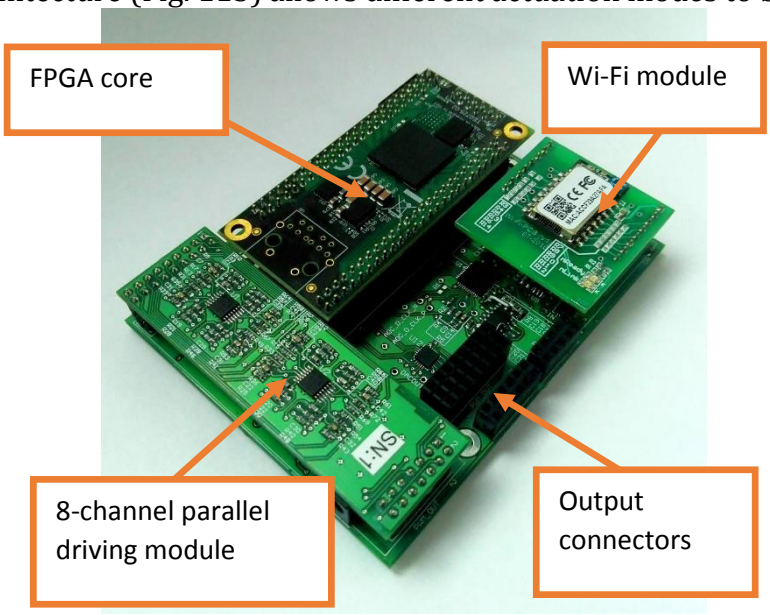

Figure 114 Eight channel hardware platform for cantilever sensor networks.

namely full parallel actuation using PWM DACs (up to 500 kHz) or subsequent channel actuation using high resolution DAC (up to 2MHz).

The new system, designed by MICRO is based on newer Xilinx™ Artix device. It has following main features:

- Eight full channels, cover the functionality of previous system;
- Additional eight PWM DAC outputs allowing full parallel work;
- Added PLL functionality;
- USB and Wi-Fi connectivity;
- Compact design (10cm x 8cm x 2cm, smaller than 1st system)

The system architecture allows different actuation modes to be combined, namely full parallel actuation using PWM DACs (up to 500 kHz) or subsequent channel actuation using high resolution DAC (up to 2MHz).

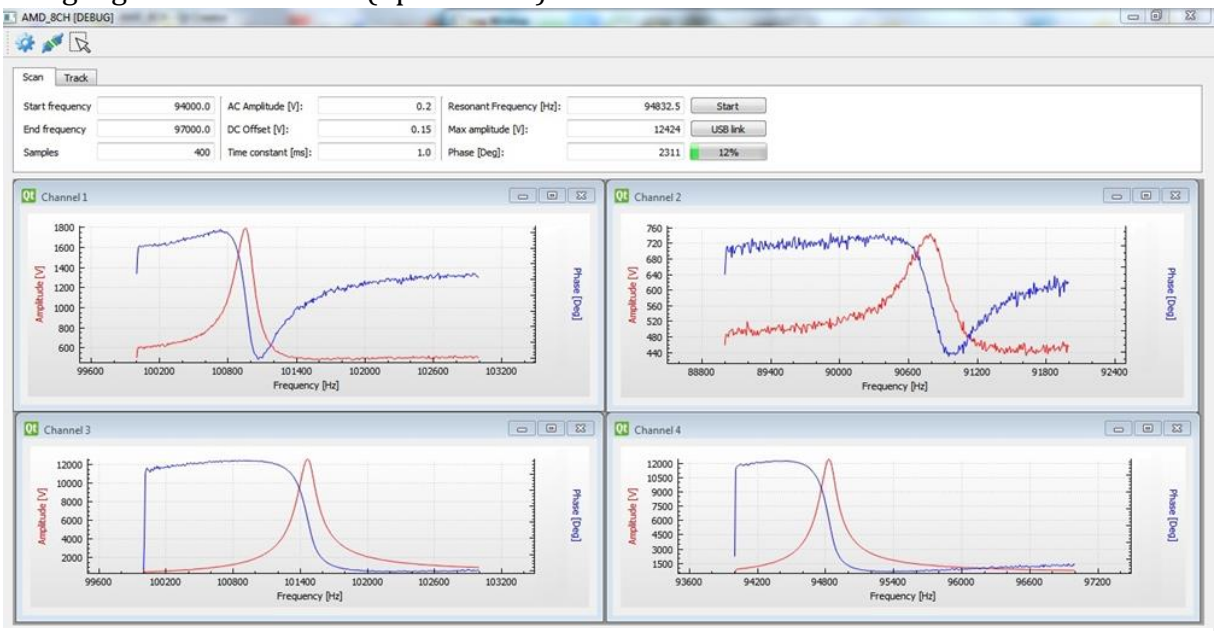

Figure 115 Frequency sweep mode, four cantilevers connected (second channel not amplified).

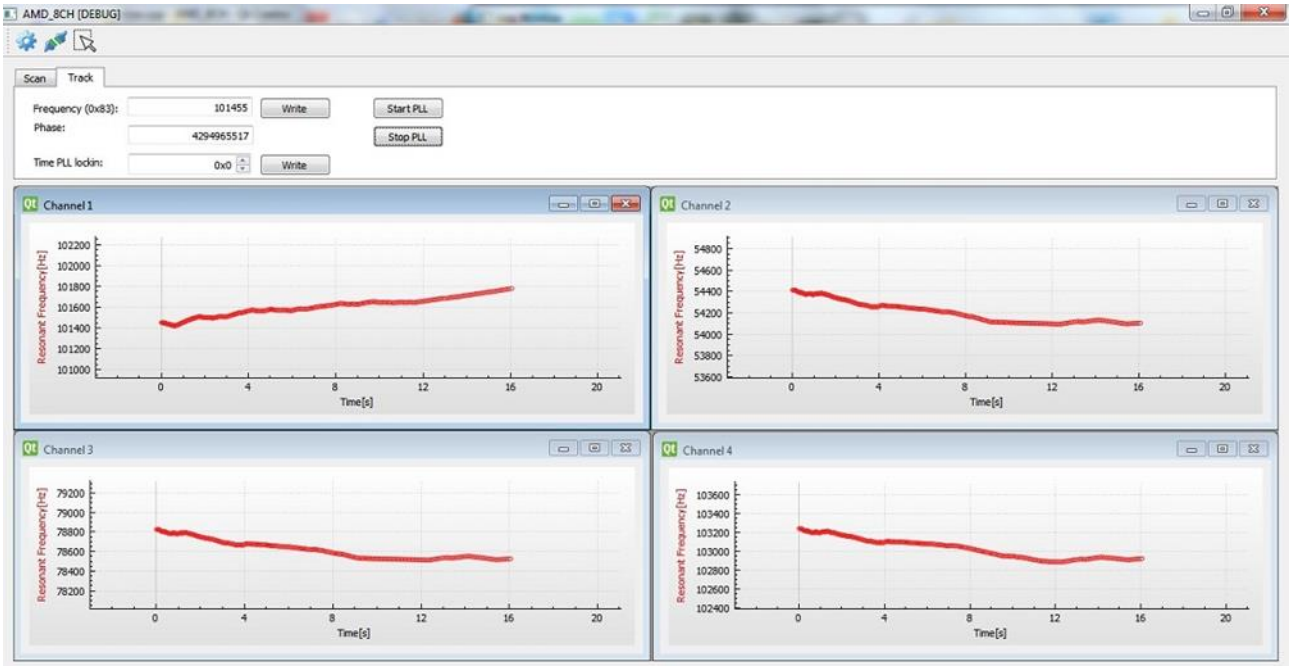

Figure 116 Screenshot from client software window with four cantilevers connected, showing frequency tracking (PLL) mode.

Both amplitude modulation and PLL tracking mode can be used for detection of the frequency change.

The hardware platform passed full electrical tests. The final tests were performed by connecting four cantilevers combining two x two preamplifier heads to different sets of four selected channels. The screenshots from the control and data recording software are shown in figures 115 and 116.

The wireless functionality was tested by a dedicated test design as follows: ASCII string was send from serial terminal over USB cable to the eight-channel system. Then, the received string was send from FPGA to the Wi-Fi module. A PC with TCP client software was connected to the Wi-Fi module of the system, and the same string was observed on the TCP client terminal. Finally, the analysis of the performance the eight-channel system show that it covers the criteria “same or better”, compared to the two-channel platform, developed in Period 2.

Deviations

No deviations from the planned work for this subtask.

Outcomes

Cantilever based mass detection system

MICRO developed a compact, eight-channel, very high-sensitive detection system for nano-functionalized cantilevers. The performance of the system was checked against the two-channel system, developed in Period 1 and already proven for very high sensitivity detection of for explosive materials. The system design level corresponds to the pre-production prototype; the technology is proven and the design is ready for production implementation.

This result allows direct practical exploitation in a commercial product.

Process porting package reporting for mass production

All three sensor technologies were developed and implemented on 4" silicon wafers due to cost savings.

The second type of sensor technology based on the patent of Prof. Ivo Rangelow – "Field effect transistor sensor" (TIP FET sensor) was stopped after first runs of manufacturing. TIP FET sensor was pretested and the results were reported. With a decision of the consortium for relocation of resources further development of TIP field-effect sensors was suspended and all resources were relocated to the other sensor technologies.

Spectrometer MOSFET sensor and active piezo-resistive nanostructured cantilever technologies are CMOS based sensors with a not CMOS compatible sensing layer – SnO_2 collective gate layer for spectrometer MOSFET sensor and nanostructured $Cu(OH)_2$/CuO layer for active piezo-resistive cantilever.
The sensing layer for both sensor technologies plays crucial role in the sensor selectivity and sensitivity. For that reason, NANO concentrated on the establishment of sensing layer manufacturing parameters.

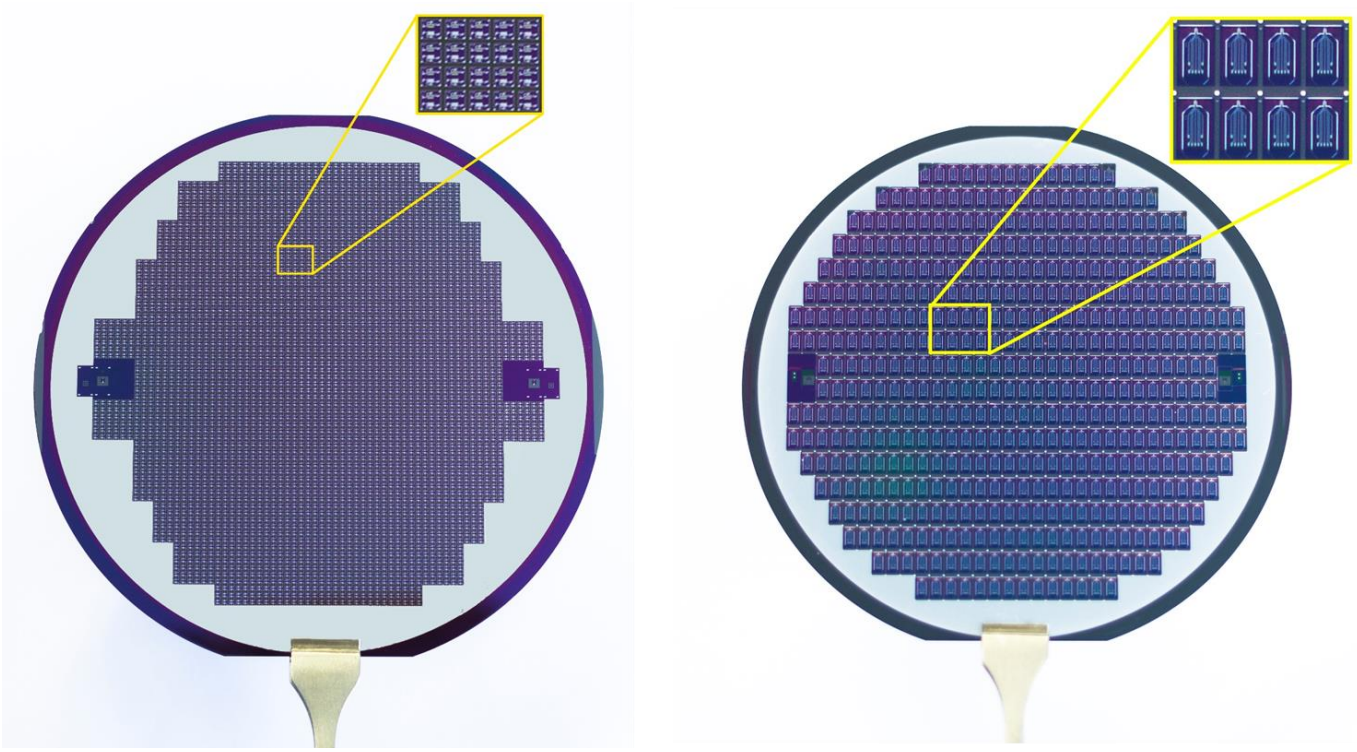

Figure 117 A silicon 4" wafer with MOSFET spectrometer sensors (on the left) and a silicon 4" wafer with active piezo-resistive cantilevers (on the right).

In figure 117 are shown images of silicon substrates with spectrometer sensors and cantilevers manufactured by NANO in their facilities.

All process steps for manufacturing MOSFET spectrometers and active cantilevers with CuO nanorods are documented. The production technology is fully established and ready for mass production.

Achieved results

- Process is fully documented;
- One FAB placed an offer for part of the process for spectrometer fabrication;
- Negotiations with two other FAB's are in progress;

No deviations

- Functional material cannot be covered from the FAB – external process in Ilmenau or other clean-room must be excepted;
- 4"-6" wafer production due to the functionalization and customization;
- Several potential FAB have been identified;
- The process identification according to the FAB-standards are in progress;
- Spectrometer and Cantilever fabrication for gas sensing are not CMOS compatible;
- A combination of FAB and external production steps will be always required;
- 4" and 6" will be needed for mass production due to the process opportunities in Ilmenau;

List of figure:

Figure 1 The 3 groundbreaking sensor concepts of IAQSense. 2
Figure 2 2D model of the MOSFET spectrometer sensor. 3
Figure 3 Batch 1 – layout 1, 100x10. 4
Figure 4 Batch 1 – layout 1, 40x4. 5
Figure 5 Batch 1 - layout 2, 40x4. 5
Figure 6 Batch1 - layout 2, 100x10. 5
Figure 7 Batch 1 - layout 3, 40x10. 6
Figure 8 Batch 1 - layout 3, 100x25. 6
Figure 9 Batch 1 - layout 4, 40x40. 6
Figure 10 Batch 1 - layout 4, 100x100. 7
Figure 11 Batch 1 - layout modification. 7
Figure 12 Batch 1 - Chip block diagram. 8
Figure 13 Batch 1 - Chip layout with ESD protection. 8
Figure 14 Batch 1 - Chip layout with addresses. 9
Figure 15 TO12 package. 9
Figure 16 Spectrometer sensors, bonded in TO12 packages. 10
Figure 17 Batch 1 - all 8 designs realized on 4" wafer. 11
Figure 18 SEM images of MOSFET spectrometer T1:40x40, T2:100x100. 11
Figure 19 SEM images of the Tin oxide layer. 12
Figure 20 Batch 1 - ESD layout. 12
Figure 21 SEM image of the ESD diode. 12
Figure 22 Batch 1 - wafer map. 13
Figure 23 Dual Channel System Source Meter Keithley 2602A. 13
Figure 24 Sample pinout with electrical schematics of structures within 13
Figure 25 MOSFET output and transfer characteristics equivalent measurement setup. 14
Figure 26 Output characteristics – Chip 05.04 T1(100 µm). 14
Figure 27 Output characteristics – Chip 05.04 T2(40 µm). 15
Figure 28 Output characteristics – Chip 07.04 T2(40 µm). 15
Figure 29 Output characteristics – Chip 07.04 T1(100 µm). 16
Figure 30 Transfer characteristics – Chip 05.04 T2(40 µm). 16
Figure 31 Transfer characteristics – Chip 05.04 T1(100 µm). 17
Figure 32 Transfer characteristics – Chip 07.04 T1(100 µm). 17
Figure 33 Transfer characteristics – Chip 07.04 T2(40 µm). 18
Figure 34 Test setup for MOSFET breakdown voltage measurements. 18
Figure 35 Batch 1 - Breakdown voltage measurement result. 19
Figure 36 Break-down voltage - Doping concentration relation. 20
Figure 37 Left: New set of manufacturing steps for ESD-protection. Right: image of the ESD-protection diode taken with digital microscope. 20
Figure 38 Left: The picture of SoC sample bonded to TO-housing (no cap), Right: Geometry of measured transistor with square geometry of the channel. 21
Figure 39 Left: The layout of the mask for N-channel MOSFET spectrometer on membrane (Batch 2), Right: SEM image of a MOSFET is rectangular geometry. 22
Figure 40 Batch 2, output characteristics – Chip 14.11 T1(100 µm). 22
Figure 41 Batch 2, output characteristics – Chip 13.09 T1(100 µm). 23
Figure 42 Batch 2, output characteristics – Chip 21.06 T1(100 µm). 23
Figure 43 Averaged transfer characteristics of 25% of total amount of V2.2 transistors. 23

Figure 44 Output characteristics symmetry test. 24
Figure 45 Test setup with NI platform and measurement realized by FACET and delivered on 7th July 2015 for dynamic characterization of spectrometer on chip sensors. 25
Figure 46 Spectrometer chip 9.08 N-channel MOSFET, L:100 W:10 – response in air. 26
Figure 47 Spectrometer chip 9.08 N-channel MOSFET, L:100 W:10 – response in acetone vapours in progress. 26
Figure 48 Spectrometer chip 9.08 N-channel MOSFET, L:100 W:10 – response in air after acetone. . 27
Figure 49 Spectrometer chip 9.08 N-channel MOSFET, L:100 W:10 – response in acetone vapours. . 27
Figure 50 Spectrometer chip 9.08 N-channel MOSFET, L:100 W:10 – response in isopropyl alcohol vapours. 28
Figure 51 P-channel spectrometer MOSFET, batch 3. 28
Figure 52 Batch 3 - P-channel MOSFET spectrometer output characteristics. 29
Figure 53 Tested substances. 30
Figure 54 Full chart – Xylene measurement with P-channel MOSFET spectrometer. 30
Figure 55 Xylene measurement with P-channel MOSFET spectrometer - part 2. 31
Figure 56 Xylene measurement with P-channel MOSFET spectrometer - part 1. 31
Figure 57 Xylene measurement with P-channel MOSFET spectrometer - part 3. 32
Figure 58 Chlorbenzol measured with P-channel MOSFET spectrometer. 32
Figure 59 Selected signal – Chlorbenzol measurement with P-channel MOSFET spectrometer. 33
Figure 60 Full chart – Toluene measurement with P-channel MOSFET spectrometer. 33
Figure 61 Toluene measurement – P-channel MOSFET Offset. 34
Figure 62 Toluene measurement – P MOSFET Offset. 34
Figure 63 Full chart – Butyl acetate measurement with P-channel MOSFET spectrometer. 34
Figure 64 Selected signal – Butyl acetate measurement with P-channel MOSFET spectrometer. 35
Figure 65 Butyl acetate measurement – P-channel MOSFET Offset. 35
Figure 66 MIBK measurement with P-channel MOSFET spectrometer. 36
Figure 67 MIBK measurement with P-channel MOSFET spectrometer - part 1. 36
Figure 68 MIBK measurement with P-channel MOSFET spectrometer - part 3. 37
Figure 69 N-channel spectrometer MOSFET, batch 4. 37
Figure 70 Batch 4 - N-channel MOSFET spectrometer output characteristics. 38
Figure 71 Tin oxide gate layer of the MOSFET spectrometer investigated with Atomic-Force Microscope. 38
Figure 72 The interface spectrometer PCB for gas measurements. 39
Figure 73 Microscope image of N-channel spectrometer Batch 4(on the left)) and P channel-spectrometer Batch 3 (on the right). 39
Figure 74 Image of the IAQSense software console developed by FACET. 40
Figure 75 Full chart – Xylene measurement with N-channel MOSFET spectrometer. 40
Figure 76 Chlorbenzol measurement with N-channel MOSFET spectrometer. 41
Figure 77 Full chart – Toluene measurement with N-channel MOSFET spectrometer. 42
Figure 78 Toluene measurement – N-channel MOSFET Offset. 42
Figure 79 Full chart – Butyl acetate measurement with N-channel MOSFET spectrometer. 43
Figure 80 Selected signals – Butyl acetate measurement with N-channel MOSFET spectrometer. 43
Figure 81 MIBK measurement with N-channel MOSFET spectrometer. 44
Figure 82 LED Ionizer. 45
Figure 83 Measurement of Ammonium hydroxide with N-channel spectrometer plus Ion and P-channel without Ion. 45
Figure 84 Measurement of water vapours with N-channel spectrometer plus Ion and P-channel spectrometer without Ion. 45

Figure 85 Measurement setup in nano analytik GmbH labs. 46
Figure 86 SOFIA LABS - Owlstone setup on the left and FACET measurement console on the right. .. 47
Figure 87 TIP FET transistor illustration. 49
Figure 88 TIP FET mask layout and cross-section. 50
Figure 89 Tip field-effect transistor - optical image. 50
Figure 90 Tip field-effect transistor - SEM images. 51
Figure 91 Tip sharpness development. 51
Figure 92 Tip field-effect transistor -SEM investigation of the "tip" height. 52
Figure 93 Tip field-effect transistor experimental measurement setup. 52
Figure 94 Cross sectional drawing of a rectangular cantilever. σ1 and σ2 – induced stresses on the top (σ1) and bottom (σ2) of the cantilever. 53
Figure 95 Development of nanostructured AFM cantilever. 57
Figure 96 Cantilever resonance detection plots. 57
Figure 97 Roadmap for the objective wafer level transfer. 58
Figure 98 Preparation of silicon wafer for synthesis of CuO nanotubes. 59
Figure 99 CuO nanotubes synthesis - wafer suspended upside-down very close to the bottom (100microns) on the left wafer upside-down, hight over the bottom on the right. 59
Figure 100 SEM images of copper oxide nanotubes before (on the left) and after (on the right) annealing. 60
Figure 101 SEM image of nanostructured single passive cantilever. 60
Figure 102 Procedure developed to overcome the border effect. 60
Figure 103 SEM images of nanostructured passive cantilever. 61
Figure 104 SEM image of an active piezo-resistive cantilever. Side with electrical circuits. 61
Figure 105 SEM image of CuO nanotubes synthesized on a cantilever membrane before final etching procedure. 62
Figure 106 SEM image showing the top side of piezo-resistive cantilever with CuO nanorods. 62
Figure 107 Test setup for characterization of active piezo-resistive cantilevers. 63
Figure 108 Image of the measurement setup for active piezo-resistive cantilevers - improved. 64
Figure 109 Concentration: 830 ppb of explosive. 64
Figure 110 Concentration: 15 ppb of explosive. 64
Figure 111 Active piezo-resistive cantilever - Nitrogen dioxide measurement. 64
Figure 112 Comparison between two platforms. Same preamplifier head with two cantilevers used as a reference. New system based on Red Pitaya platform (on the left) and two channel system developed in Period 1 (on the right). 64
Figure 113 Functional diagram of eight channel system. 64
Figure 114 Eight channel hardware platform for cantilever sensor networks. 64
Figure 115 Frequency sweep mode, four cantilevers connected (second channel not amplified). 64
Figure 116 Screenshot from client software window with four cantilevers connected, showing frequency tracking (PLL) mode. 64
Figure 117 A silicon 4" wafer with MOSFET spectrometer sensors (on the left) and a silicon 4" wafer with active piezo-resistive cantilevers (on the right). 64